SUBJECT ISOLATION AND NON STATIONARY CLUTTER REJECTION USING RF BACKSCATTER – TAG RADAR

A DISSERTATION SUBMITTED TO THE GRADUATE DIVISION OF THE UNIVERSITY OF HAWAIʻI AT MĀNOA IN PARTIAL FULFILLMENT OF THE REQUIREMENTS FOR THE DEGREE OF

DOCTOR OF PHILOSOPHY

IN

ELECTRICAL ENGINEERING

DECEMBER 2012

By

Aditya Singh

Dissertation committee:

Victor M. Lubecke, Chairperson
Olga Boric-Lubecke
Aaron Ohta
David Garmire
Flavio Pardo
Marguerite Butler

Keywords: radar, passive RF tags, physiological monitoring, motion detection

To my parents –

Dr. Vishwakarma Singh and Premlata Singh

Acknowledgements

First and foremost, I would like to express my gratitude to Dr. Victor Lubecke who has been a true guide in every sense of the word. His guidance and support as an advisor has been instrumental in shaping my research and thought process. I am greatly indebted to Dr. Olga Boric-Lubecke for her mentorship, support and encouragement throughout the course of my research. I also want to thank the members of my committee for their advice, input, and for being generously accommodating.

I would also like to thank my colleagues and friends who have assisted my development as a researcher over the past six years. They include Alex, Bryson, Byung-Kwon, Ehsaneh, John, Isar, Michelle, Navtej, Noah, Scott, Shuhei, Wansuree, Wenqi and Xi. I would also like to thank Xiaomeng Gao, Ehsan Yavari and Mari Zakrzewski for collaborating on work presented in chapter six of this dissertation.

I would not be writing this if it weren't for the encouragement of my parents, Dr. Vishwakarma Singh and Premlata Singh, who have always taught me to work hard, be sincere and live life without worries. I am also grateful to my brother, Anand Singh for his constant support and help to get accustomed to the new environment. Special thanks to Pradeep Ramadoss and Siddharth Gujral for helping me since day one in Hawai'i. Special thanks are also due, to my dear friend and now my wife Hsiang-Yin Wu who has been with me throughout the difficult but ultimately rewarding journey of graduate school, even as the pursuit occurred at the expense of valuable time together.

Abstract

Microwave Doppler radar can be used for remote monitoring of physiological motion for humans or animals, but suffers from limitations in selectivity, clutter rejection, subject isolation and identification. The research presented in this dissertation proposes a solution to this problem by placing passive radio frequency tags on the subject of interest and designing radar systems to detect backscattered information from the tags. Two types of passive radio frequency tags and radar systems were developed and tested successfully to independently track and monitor moving sources that have tag as well as sources that do not have a tag, when both the motions were occurring in front of the radar system. The contributions of this dissertation encompass innovative solutions in software and hardware including theory, simulation and design of Doppler radar compatible tags, design, implementation and analysis of radar receivers, and innovative use of signal processing techniques to extract more useful information from the radar and extend its application. The use of suggested approaches has created a Doppler radar system that would improve detection rate by as much as 100% as compared to a regular quadrature Doppler radar. In addition to tracking motion of one or more tagged objects in presence of untagged motion (clutter), the system can reliably provide information about the clutter. The designed radar systems are shown to provide the required selectivity, subject isolation, identification and multiple subject detection that brings Doppler radar one step closer to its commercial feasibility for a wide range of applications that include remote health monitoring, activity monitoring and search and rescue operations.

Table of Contents

List of Tables

List of Figures

Chapter 1. Introduction

Non invasive physiological monitoring can open the door to new methods in research and treatment. Vital signs and statistics taken over long periods of normal activity can provide insights into health and energy usage, which can be used to diagnose conditions from SIDS to cardiopulmonary disease. The key to facilitating this approach is practical technology which provides an automated assessment of vital signs without impacting the monitored subject. The application of microwave Doppler radar techniques the measurement of physiological motion is very promising to this end. However, shortcomings in this method, including noise reductions and positive subject identification, must be addressed for this approach to become practical and effective.

Radio detection and ranging (RADAR) refers to the technique and system for remote detection of reflecting objects using electromagnetic (EM) waves. Radar can detect an object by measuring its location, range and/or velocity. A radar system typically operates by transmitting electromagnetic waves into space and detecting the reflected electromagnetic waves from objects in its field of view. The received echo can be processed to give information regarding the range, velocity and location of the objects that include but are not limited to ships, aircrafts, vehicles, and people. An important advantage of radar is its ability to operate under conditions where optical and infrared sensors would fail. For example, the radar can operate at night and in extreme weather conditions. An interesting review on radar history has been given in (Skolnik, 2001).

Doppler radars are a class of radars that detect the Doppler shift in the return signal to provide information about moving objects at a distance. Doppler effect

describes the apparent change in the frequency of sound or an EM wave between the source of the wave and the receiver due to relative motion between them. Fig. 1.1 and Fig. 1.2 illustrate the Doppler effect for two different situations. When an EM wave is transmitted towards a car moving at a constant radial velocity of v_r, the received signal will be shifted by a frequency (f_d) that is related to the car's radial velocity by,

$$f_d = \frac{2 \times v_r}{\lambda} \tag{1.1}$$

where $v_r = \frac{dR}{dt}$ is the radial velocity in meters/second (Skolnik, 2001). Doppler radars are widely used for air traffic control, weather monitoring and speed detection (police radar gun).

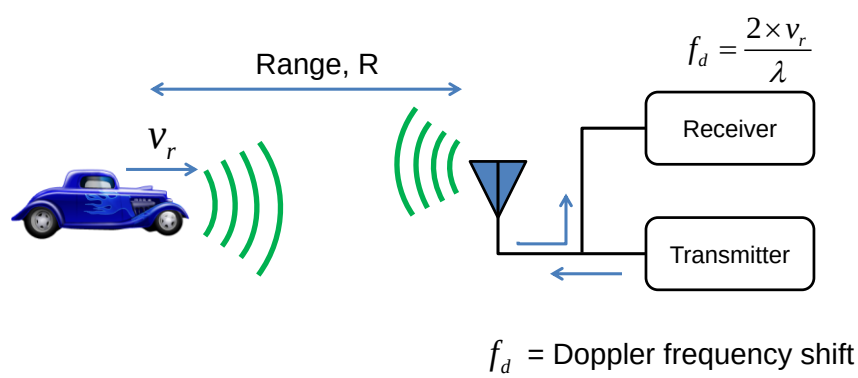

Fig. 1.1 Doppler effect for a target moving at a constant radial velocity towards the stationary transmitter and receiver.

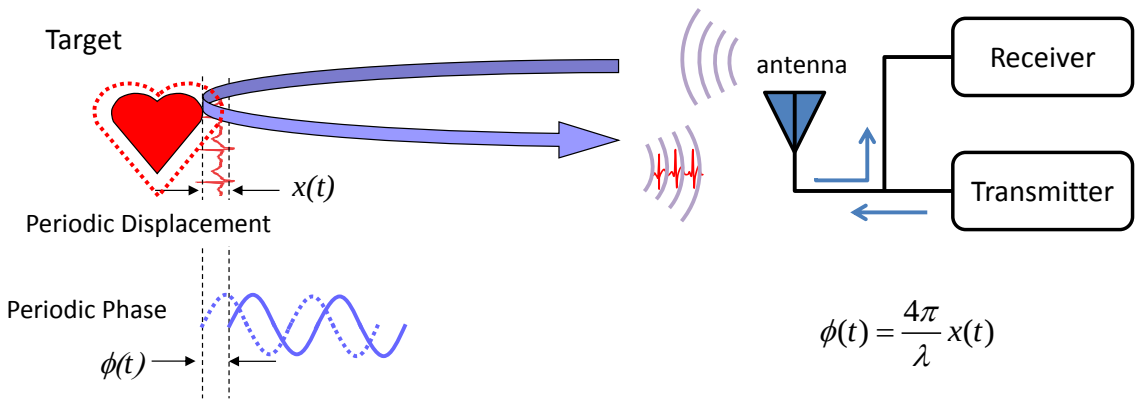

Fig. 1.2 Doppler effect for physiological signals that have periodic movement but zero net velocity.

Doppler radar has many beneficial applications in non-contact and non-invasive human health monitoring and animal monitoring. CW Doppler radar is ideal for detecting phase changes as it is immune to stationary clutter and detect only moving objects which is its biggest advantage. Doppler radars can be pulsed or continuous wave (CW). Pulsed Doppler radar signals transmit a pulse modulated RF carrier at a pulse repetition frequency (PRF). Pulse Doppler radars can have ambiguities in both range and Doppler depending on the PRF used. A high PRF corresponds to range ambiguities whereas a medium PRF corresponds to ambiguities in both range and Doppler. Continuous wave (CW) Doppler radars transmit an unmodulated signal and they transmit while they receive signals. Since they transmit continuously, CW radars are unable to measure range but can unambiguously measure velocity at any range.

The use of CW Doppler radar suffers from some limitations and challenges as well. Being a motion sensor, it detects any motion in its field of view and cannot identify the sources of motion. If the motion to be detected is small, it can get easily buried under

clutter signals. The aim of this dissertation is so develop techniques to overcome these challenges.

The following sections would talk about application areas for CW Doppler radars and its advantages; discuss the recent advancements that have taken place and discuss further about limitations and challenges that will be addressed by this dissertation.

1.1 Application areas for CW Doppler radars

1.1.1 Health monitoring

Continuous wave (CW) microwave Doppler radar could be proposed as a good cost effective solution for non-invasive and non-contact cardiovascular monitoring. Cardiopulmonary monitoring can serve as good prognostics and diagnostics tool for respiratory and cardiac ailments, which have become the leading cause of death globally, causing an estimated 17.3 million deaths (30%) in 2008 with over 80% of the deaths occurring in low and middle-income countries that do not have effective health care services in place (World Health Organization, 2011).

The use of microwave Doppler radar for non-contact detection of body motion has been demonstrated in early 1970's (Lin J.C, 1975), (Lin J.C, 1992). Based on the information provided by the motion of human body, microwaves have enabled non-invasive monitoring of several vital physiological parameters such as respiration rate (Droitcour *et al.*, 2001), (Lin J.C, 1975), arterial wall movement (Stuchly *et al.*, 1980) and heart rate (Chan and Lin, 1987), (Park, Boric-Lubecke and Lubecke, 2007).

Some of the existing techniques for respiratory health monitoring include pulse oximetry (Fearnley, 1995), spirometry (Miller *et al.*, 2005), and plethysmography (Bache *et al.*, 1969). The existing standard for cardiac health monitoring is electrocardiogram (ECG). Each measurement technique described above has advantages and disadvantages. Pulse oxymetry provides the level of oxygen saturation in the blood and can also be used to measure respiratory disturbance but does not provide respiratory rate and has a considerable lag in response. Airflow measurements (spirometry) provide the most accurate respiratory rate and tidal volume measurements, but interfere with normal respiration. The whole-body plethysmograph can be highly accurate and does not interfere with respiration, but requires immobilization of the patient. Even for the transducers (belts or electrodes), which are commonly used for ambulatory respiration monitoring, their performance significantly degrades over time with wear and tear. ECG records the electrical activity of the heart over time by measuring the electrical signals passing through the body using electrodes attached to the skin. An ECG displays the voltage between pairs of these electrodes, and the muscle activity that they measure (that depends on the location of the electrodes). The use of ECG always requires a trained personnel to correctly position the electrodes on the body. Long term monitoring of a subjects health would require the subject to spend a lot of time in hospital strapped to various wires.

The use of Doppler radar for physiological monitoring has a lot of advantages. Working as a motion sensor with a very high sensitivity, it can detect any motion at the surface of the human body and any significant motion occurring inside human body. It could be readily used in situations where contact sensors could prove inconvenient such

as long term sleep monitoring, health monitoring at home, baby monitoring and assessment of cardiovascular health of burn victims. In other cases, it could provide additional information to complement any contact sensor such as ECG without adding any complexity to the overall system.

1.1.2 Search and rescue, military

Since microwaves can pass through objects and obstacles that are otherwise opaque to light, CW Doppler radar can be used to detect the presence of people behind obstacles which makes it very attractive for reconnaissance applications in military and search and rescue operations (Arai, 2001). Successful measurement of human heart rate and respiration rate under layers of brick was shown by Chuang *et al.* (Chuang, Chen and Chen, 1990). The results from experiments performed by Chen *et al.* indicate the ability of 450 MHz signal to penetrate deep into concrete that does not have any metal and the ability of 1150 MHz to penetrate rubble with metallic wire mesh (Chen *et al.*, 2000). Use of radar technology for search and rescue operation may increase the efficiency by helping to locate the victim in a timely manner. Even if the victim is unable to move, he/she can be located by detection of their vital signs. Characterizing human dynamics such as gait and other micro-Doppler signatures is also a way to detect the presence and behavior of a human being (Bjorklund *et al.*, 2011), (Wildemeersch *et al.*, 2009).

1.1.3 Animal monitoring

Activity monitoring of animals in their natural environment can yield important information about energy expenditure, thermoregulation, behavioral patterns, and even population health (Nagy *et al.*, 1999), (Wikelski and cook, 2006). As energetics plays a

large role in ecology, behavior, and physiology, accurate methods for activity monitoring are critical for a wide range of animal studies. The standard technique for measuring Field Metabolic Rate is the doubly-labeled water technique which involved injecting animals with radio-labeled water and observing the rate of carbon dioxide (CO_2) production over several weeks (Nagy *et al.*, 1999). Because the technique relies on the biological half-life of ^{18}O, which is long relative to the duration of specific behaviors, it is not possible to measure the cost of specific activities such as foraging, mating, or locomotion. Recent advances in the miniaturization of electrical circuits have allowed measurements of activity using continuous heart-rate monitoring, but as this technique uses implantable data-loggers, it is limited to animals 1 kg or larger (Butler *et al.*, 2002). For smaller animals, the only available techniques are visual inspection or video recording. Both are extremely time-consuming, labor-intensive, and require extensive post-experiment effort in recording, transcribing, or analyzing the raw data.

Doppler radar motion sensing can provide a better tool for the automated activity monitoring in animals, as well as the detection of multiple behavioral events in real-time by classifying different states of activity, such as fidgeting, walking, or running, which differ tremendously in energetic cost and are important to distinguish in studies of activity (Heal, 1975), (Martin and Unwin, 1980), (Singh *et al.*, 2012b).

1.2 Recent advances in CW Doppler radar

Technological advances in fabrication techniques for chip and circuit design have allowed the fabrication of compact Doppler radars (Droitcour *et al.*, 2002), (Droitcour *et al.*, 2004). Although the technology is well known, a thorough understanding of its

application to physiological monitoring has been realized within the last decade. The effect of receiver architecture, antenna gain, frequency and transmit power on radar performance were studied (Droitcour, 2006). Quadrature receivers were proposed to improve the spatial detection of moving objects. The limitations of single channel receivers were mathematically and experimentally studied (Park *et al.*, 2006). Different signal processing techniques such as linear demodulation, arc-tangent demodulation with center tracking and non-linear phase modulation were introduced to extract information about the rate and displacement of the moving surface (Li and Lin, 2007), (Park, Boric-Lubecke, and Lubecke, 2007). Novel techniques were introduced to cancel out the random body movements of a human subject and extract respiration and heart rates (Li and Lin, 2008a), (Yu, Li and Lin, 2011). Detection of multiple respiration and heart rates were shown through the use of multiple input multiple output (MIMO) systems and MIMO signal processing techniques such as blind source separation (Boric-Lubecke *et al.*, 2005), (Samardzija *et al.*, 2007), (Vergara *et al.*, 2008). Innovative ideas were also introduced to cancel the motion in a handheld radar system and increase the signal to noise ratio (SNR) using a coherent low-IF receiver (Mostafanezhad *et al.*, 2008), (Mostafanezhad *et al.*, 2010). The advances in hardware and signal processing have enabled the measurement of various physiological parameter in addition to respiration and heart rate such as respiratory tidal volume, Heart rate variability (HRV) and respiratory sinus arrhythmia (RSA) (Massagram *et al.*, 2009), (Massagram, Lubecke and Boric-Lubecke, 2009). Initial investigations have also shown promise of tracking changes in pulse pressure using a Doppler radar (Singh, Lubecke and Boric-Lubecke 2011).

Although the studies discussed above improve our understanding of Doppler radar systems and solve a lot of problems associated with it, there are still some important challenges that need to be solved to make a robust radar system that could be used in the applications discussed above.

1.3 Challenges in Doppler radar system

Many of the limitations arise in a CW Doppler radar system due to the fact that it is not selective and would detect any motion that is in its field of view. This lack of selectivity leads to other problems such as inability to track multiple motion, effect of torso motion on vital sign monitoring and interference by moving objects or people that are not the subject of interest. The problem of interference by clutter motion is depicted in Fig. 1.3. Depending on the application, these problems may or may not affect the results too much. For example, effect of torso motion on long term monitoring and sleep measurement might be little as the duration of torso movement is insignificant with respect to the total duration of measurement.

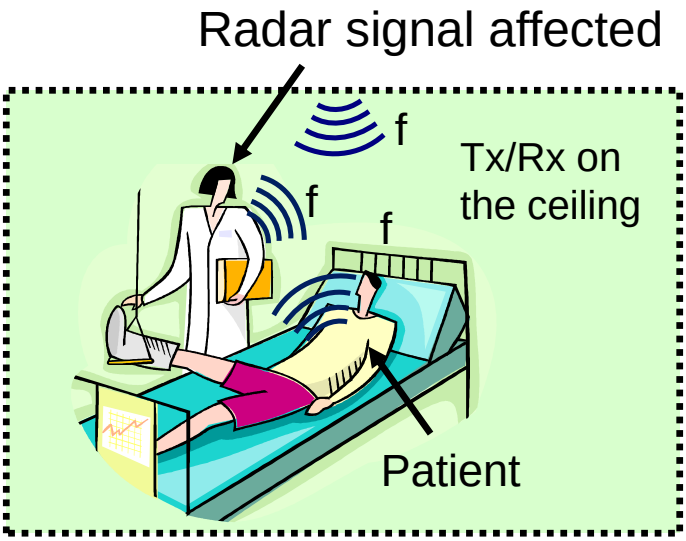

Fig. 1.3 Sources of undesired motion. Anybody who enters the room would affect the radar signal and may cause false alarms or loss of data. The radar cannot distinguish between the subject and the people moving around him.

Most of the advances discussed in section 1.2 do not address the selectivity of the system and assume the presence of single or multiple subjects and absence of clutter motion. Even though MIMO techniques can identify two respiratory signals, they cannot identify the source of the motion. This problem is illustrated in Fig. 1.4. The lack of selectivity limits the use of radars for application discussed above. The aim of this dissertation is to incorporate selectivity to the radar through modifications in hardware, communication techniques or advanced signal processing that would make the radar more robust and the applications more diverse.

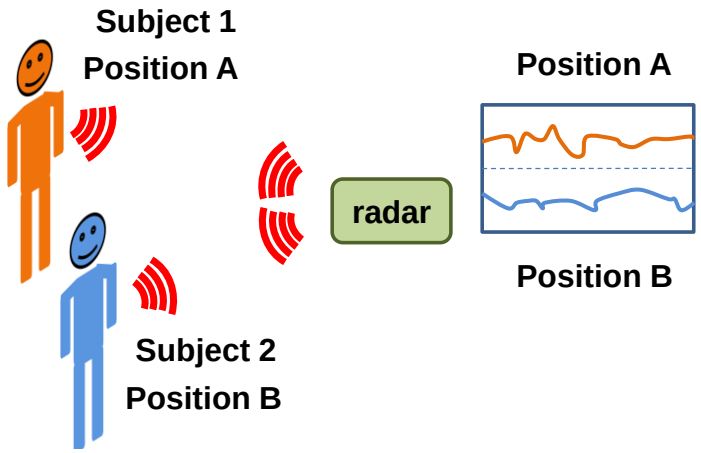

(a)

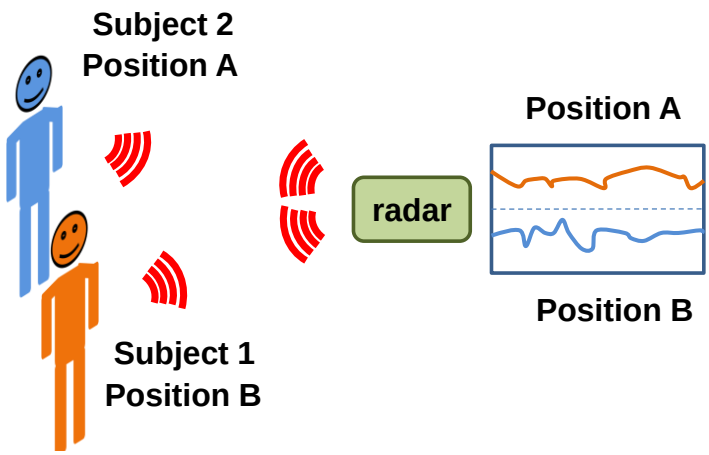

(b)

Fig. 1.4 Schematic illustrating the inability of MIMO radar to identify the sources of motion. The radar can detect two rates corresponding to position A and position B (a). However, when the subjects change place with each other in (b), the radar is unable to provide any information on the reason for the change in rate and will continue to associate the rate at position A to subject 1 and rate at position B to subject 2 which is wrong.

1.4 Scope of this dissertation

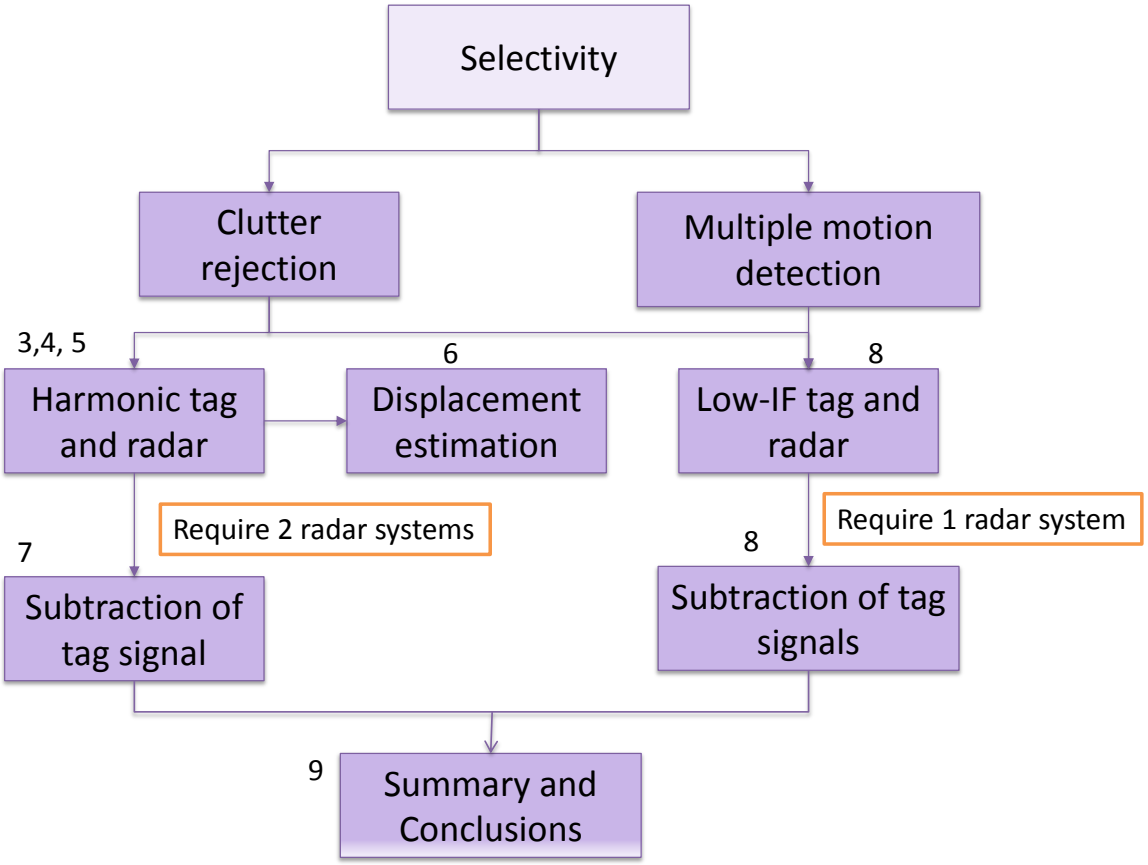

Fig. 1.5. Scope of the dissertation. The numbers outside the box represent the chapter numbers.

This dissertation consists of nine chapters (Fig. 1.5). Chapter 1 presents an introduction to Doppler radar and its applications. It also highlights some of the recent advancements made in the area of Doppler radar physiological monitoring, existing challenges and the research goals. Chapter 2 will provide an overall background to Doppler radar systems. It would include the theory of operation, residual phase noise, receiver topologies, choice of frequency and demodulation techniques. Chapter 2 will also discuss possible solutions that could solve the problems discussed in chapter 1. Chapter 3 will present the simulation, design, fabrication and testing of passive harmonic tags. The application of passive harmonic tags with CW Doppler radar will be discussed

in chapter 4. A homodyne receiver would be successfully used to track the motion of the tag while sufficiently rejecting motion that is non-tagged. Chapter 5 will discuss the problem of phase noise and present an analysis of different receiver topologies that could be used to obtain information from the harmonic tag and the tradeoffs between them. Chapter 6 will introduce a new data-based measurement technique for computing imbalance in a quadrature receiver and implement this technique to highlight the advantages of harmonic tags with respect to displacement measurement. In chapter 7, adaptive filtering techniques will be used with two frequency radars to detect tag motion and non-tagged motion simultaneously. Chapter 8 will introduce another radio frequency tag architecture that could be used to detect and monitor multiple objects simultaneously. The theory behind these tags (termed as low-IF tags) will be illustrated and extensive measurement results will be presented. A summary of the work done in this dissertation will be provided in chapter 9 with methods to optimize both of the tag systems. In the following chapters, CW Doppler radar for activity or physiological monitoring may be referred to as Doppler radar for physiological monitoring or Doppler radar.

Chapter 2. Doppler Radar for Physiological Sensing

CW Doppler radar topology was chose for physiological monitoring due to its simplicity, simple filter requirements owing to narrow signal bandwidth and unambiguous velocity detection at any range and in heavy stationary clutter (Skolnik, 2001). Extensive research has been performed in the area of Doppler radar for physiological monitoring (Droitcour, 2006), (Park, 2007), (Massagram, 2008). Before finding solutions to the challenges discussed in chapter 1, a thorough understanding of Doppler radar system is required. The following sections will give a brief description on the theory of operation of Doppler radar, its design features and analysis of acquired data. It is important to find solutions that provide clutter rejection and selectivity to the system operate within the same realm or, in other words be compatible with the existing system. That would allow us to keep the benefits gained through prior research and give the researchers a familiar but more robust system to test their ideas. This chapter will also discuss the different solutions possible for making a Doppler radar system selective.

2.1 Theory of Doppler radar physiological sensing

Doppler theory states that a constant frequency signal reflected off an object with a zero net velocity and periodically varying displacement $x(t)$ results in a reflected signal at the same frequency but with a time varying phase $\phi(t)$ that is directly proportional to the displacement as shown in (2.1). (Droitcour *et al.*, 2001).

$$\phi(t) = \frac{4\pi}{\lambda} x(t) \tag{2.1}$$

If the object's displacement is very small compared to the wavelength of the carrier signal, the reflected signal is similar to a phase modulated signal and can be demodulated by mixing with the transmitted signal. The basic theory and operation of a Doppler radar system with a human target is shown in Fig. 2.1.

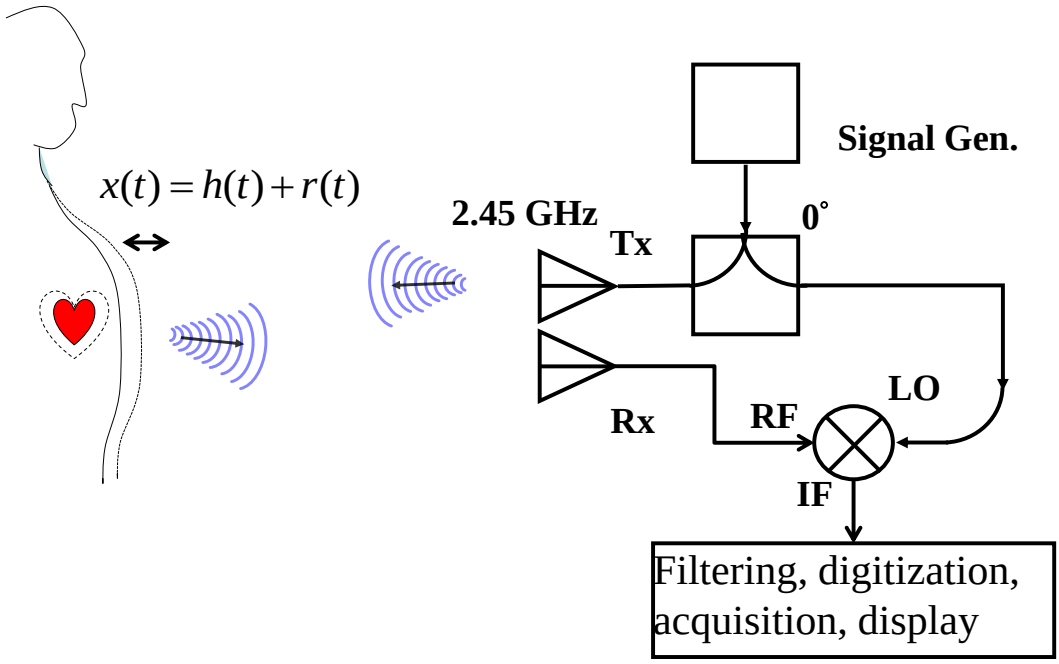

Fig. 2.1 A single channel Doppler radar transceiver.

For physiological measurements, the radar is usually aimed towards the subject's chest. The motion arising on the surface of human body is a complex motion occurring due to different physiological events such as breathing, heartbeat, arterial and venous pulsations. Most of the motion is visible on the thoracic area, where the lungs and heart are situated, and arterial pulsations can be physically felt at several locations on the body. Each physiological motion causes a series of motion. The breathing cycle includes inspiration and expiration and causes the movement of not only the chest wall but the abdomen as well. The functioning of heart is also explained through a series of

movements each of which result in some motion on the skin (Braunwald and Perlkoff, 2001). However, it is the left ventricular motion that is most pronounced on the skin. Heart beats faster than a typical respiration cycle and has a smaller motion at the surface of the skin that causes sophisticated interaction in the radar return signals.

2.1.1 Receiver architecture

Several receiver topologies have been suggested for use with a microwave Doppler radar. Direct conversion receivers (zero-IF receivers) mix the received signal with the local oscillator at carrier frequency to directly yield baseband signals. When the local oscillator signal is derived from the transmitter (synchronized in phase with the received signal), the receivers are known as homodyne receivers. Homodyne receivers are the natural choice for detecting phase changes in the received RF signal. Homodyne receivers do not suffer from the conventional image problems as the heterodyne systems and do not require the bulky, off chip, image reject filters (Svitek and Raman, 2005), (Razavi, 1997). By eliminating the use of off chip filters, the circuits for inter stage matching are simplified and the RF integration becomes easier with lower costs.

Some of the disadvantages of direct conversion receivers include dynamic range limitations due to flicker (1/f) noise, I/Q mismatch and dc-offsets, and have been discussed in literature (Abidi, 1995), (Madsen and Skou, 1990), (Razavi, 1997). The dc offset primarily results from self-mixing of any leakage LO signal in the mixer and from reflected signal from stationary objects in the field of view of radar.

The received signal in homodyne receiver can be multiplied with the local oscillator signal to obtain information about the target motion. The local oscillator signal is represented by

$$A_L \cos\left(2\pi ft + \phi(t)\right) , \tag{2.2}$$

where A_L and f are the amplitude and frequency of the transmitted signal respectively and $\phi(t)$ is the phase noise of the local oscillator. The reflected signal by the target and can be represented as

$$A_R \cos\left(2\pi ft + \theta + \frac{4\pi x(t)}{\lambda} + \phi\left(t - \frac{2R}{c}\right)\right) , \tag{2.3}$$

where θ is the constant phase shift, $x(t)$ is the movement of the target, R is the range of the target and c is the speed of light. The baseband signal obtained after mixing and passing the signal through a low pass filter is

$$A_B \cos\left(\theta + \frac{4\pi x(t)}{\lambda} + \Delta\phi(t)\right) , \tag{2.4}$$

where A_B is the baseband amplitude, $\Delta\phi(t)$ is the residual phase noise and $x(t) = h(t) + r(t)$ is the chest motion mainly composed of heart motion $h(t)$ and respiration $r(t)$.

2.1.2 Residual phase noise and range correlation

The presence of residual phase noise can be explained by range correlation theory (Budge and Burt, 1993a), (Budge and Burt, 1993b). Phase noise is a term used to describe the short term random fluctuations in the frequency or phase of an oscillator

signal. These random fluctuations, that are caused by various noise sources appear as a broad continuous distribution localized about the output signal as shown in Fig. 2.2.

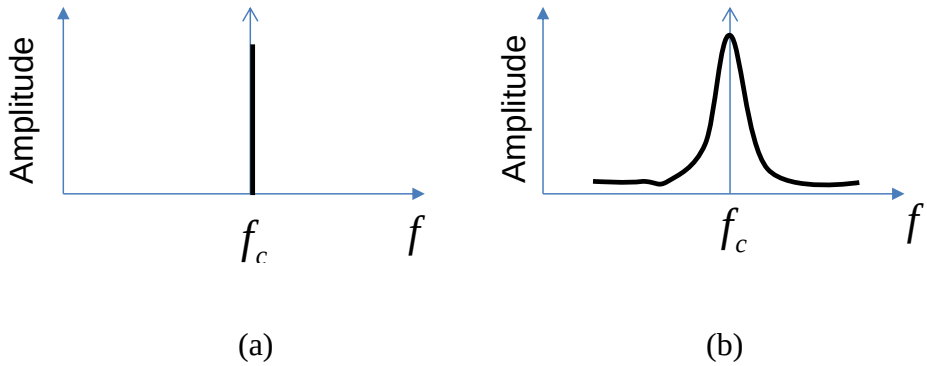

Fig. 2.2 Signal spread in frequency domain due to phase noise. The ideal oscillator signal is shown in (a) and the true signal that is generated by the oscillator (b).

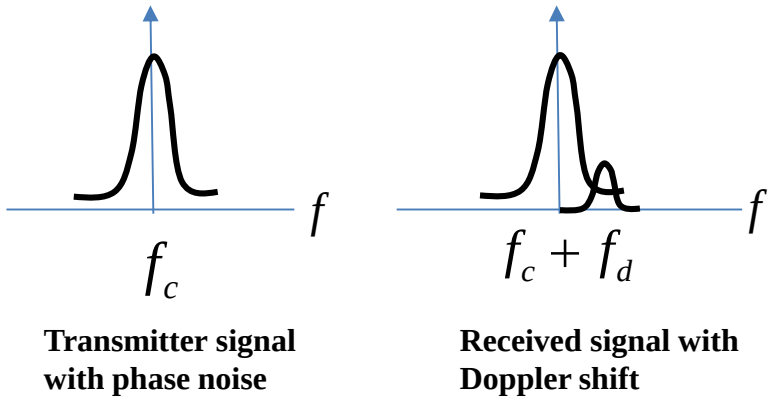

Fig. 2.3 Expected received signal with Doppler shift when the transmitted signal has phase noise. However, the SNR does not degrade as shown due to range correlation. f_d denotes Doppler shift.

This phase noise should in principle make the detection of the slow phase variations very difficult by reducing the SNR as they both lie in the same region (Fig. 2.3). However, this is not the case. The transmitted signal and the local oscillator signal

come from the same source. Hence, the received signal is just a time delayed version of the transmitted signal as shown in 2.3. When these signals are mixed together to obtain baseband signal, the correlated part of phase noise is cancelled out as well, leaving the residual phase noise (Budge and Burt, 1993b). The amount of correlation is determined by the time delay between the local oscillator signal and the received signal which in turn is determined by the distance or range of the target (Droitcour *et al.*, 2004).

2.1.3 Single channel and quadrature system

Single channel receivers are very simple but demodulation sensitivity is determined by the targets position relative to radar. Position related sensitivity is a function of wavelength and hence the choice of frequency used. This phenomenon that results in 'null' and 'optimum' points for demodulation has been discussed in (Park *et al.*, 2006). The null points occur at every integral multiple of quarter wavelength ($\frac{n\lambda}{4}$) and the optimum points occur at $\frac{2n+1}{8}\lambda$. At null points, the received baseband signal is not sensitive to physiological motion whereas at optimum points, the signal would have a linear relationship to physiological motion. The other limitations of single channel receiver include its inability to give any information about the direction of motion. This results from the fact that both negative and positive sidebands are converted to the same baseband spectrum. The limitations of a single channel receiver can be alleviated by the use of well known quadrature receivers that are widely used in communication systems. A Doppler radar system with quadrature receiver is shown in Fig. 2.4.

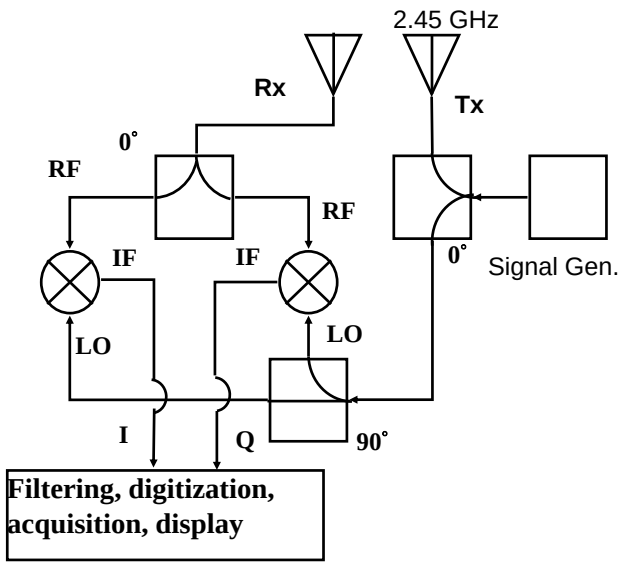

Fig. 2.4 A quadrature Doppler radar transceiver.

With a quadrature receiver, we obtain an in-phase signal (I) and a quadrature signal (Q). The quadrature signal is obtained by mixing the received signal with a 90^0 phase shifted LO signal. The corresponding baseband signals obtained are

$$\begin{aligned} B_I &= A_B \cos(\theta + x(t) + \Delta\phi(t)) \\ B_Q &= A_B \sin(\theta + x(t) + \Delta\phi(t)) \end{aligned} \tag{2.5}$$

When channel I is at null point, channel Q will be at optimum and vice versa. With quadrature channels, we can also detect the direction of phase changes. The quadrature baseband signals can be represented as a complex signal ($B_I + jB_Q$) and form an arc of a circle in the complex plane as shown in Fig. 2.5.

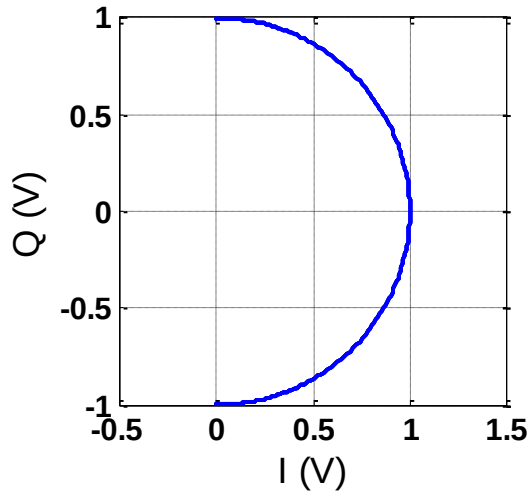

Fig. 2.5 Arc formed with (0,0) as center due to I and Q channels.

While quadrature receiver improves the detection sensitivity of the radar receiver, it introduces problems of its own. Signal processing techniques now need to account for two signals and find ways to efficiently combine information from both baseband signals. Amplitude and phase imbalances will also be introduced in the system and have to be accounted for correct processing of data (Churchill *et al.*, 1981), (Park, Yamada, and Lubecke, 2007), (Yan *et al.*, 2010).

2.1.4 Baseband conditioning and data acquisition

Baseband noise is a significant factor in determining the sensitivity of a microwave Doppler radar. Low noise amplifiers and filters are used to condition the baseband signal before it can be acquired digitally. Along with phase noise, flicker noise and thermal noise also contribute to noise in baseband. Flicker noise that results from dc offset due to LO self-mixing has been characterized as the dominant noise source at baseband in a system with a stable local oscillator. The baseband signal contains a large dc offset due LO self-mixing problem inherent in homodyne receivers. This large dc

offset may cause saturation in the low noise amplifier, limiting the dynamic range. Dc offset can be removed in hardware by using ac-coupling or by dc offset compensating (Park, Boric-Lubecke, Lubecke, 2007). Ac coupling is simpler but along with baseband filtering could introduce distortion in the signal whereas dc offset compensation requires careful tuning if done manually. Since, there might be a dc drift with time in the system, it could be better to have a system adjust the dc offset as needed (Vergara and Lubecke, 2007). Ac coupling, which is basically a high pass filter, also results in large time constants due to low corner frequency (for example 0.01 Hz) and results in slower time response for the system.

The conditioned signal is acquired through a data acquisition system (DAQ). The requirements on sampling rate are not high since the information content from human respiratory data usually lies between 0.2 Hz-0.8 Hz while that from cardiac data lies between 0.6 Hz-2 Hz. In general, physiological signals have a band width of 0-8 Hz. The highest amount of motion of human chest wall due to respiratory activity can be put in the range of centimeters and that due to cardiac activity can be put in the range of millimeters. The length of arc transcribed in I/Q plane is a function of the amount of motion being measured and the frequency used for measurement. If f_1 and f_2 ($f_2 > f_1$) are two radar frequencies used to measure the same motion, the arc transcribed in I/Q plane will be longer for f_2. If f_1 is used to measure two motions m_1 and m_2 ($m_2 > m_1$), then the arc transcribed in I/Q plane will be longer for m_2. This is shown in Fig. 2.6.

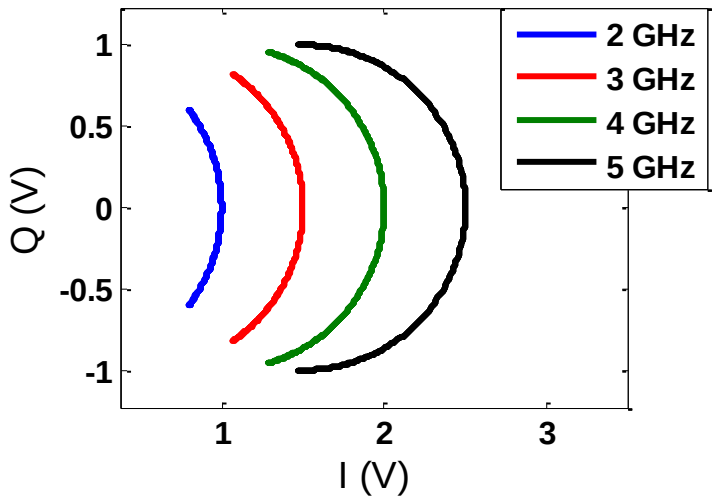

Fig. 2.6 Effect of increasing frequency on the perceived arc length for same motion. As the operating frequency is increased, the same motion results in a longer arc.

2.1.5 Demodulation and signal processing

The obtained baseband signal can be processed to give information about respiration rate, heart rate and other physiological parameters. As these parameters change with time, it is important to track them. As discussed in the previous section, the baseband signals could be processed individually or can be combined. The various methods that have been proposed for combination of I and Q channels include linear demodulation (also referred to as Eigen demodulation) (Massagram, 2008), non linear demodulation or arctangent demodulation (Park, Boric-Lubecke, and Lubecke, 2007) and complex demodulation (Li and Lin, 2008b).

Linear demodulation is a simple procedure of projecting the two dimensional baseband data to a single dimension through linear combination, maximizing variance in the data and suppressing redundant information. It can be applied to multidimensional dataset as well. To perform linear demodulation, any dc offset is first removed from the

data. The covariance matrix between I and Q channels and the eigenvectors and eigenvalues of the covariance matrix are then calculated. After multiplying the eigenvectors matrix with the data, we can pick the data with the maximum variance. Since we are essentially approximating a line for an arc, this method would give accurate only for small arcs. This is represented in Fig. 2.7. Linear demodulation is useful because of its simplicity and robustness to noise.

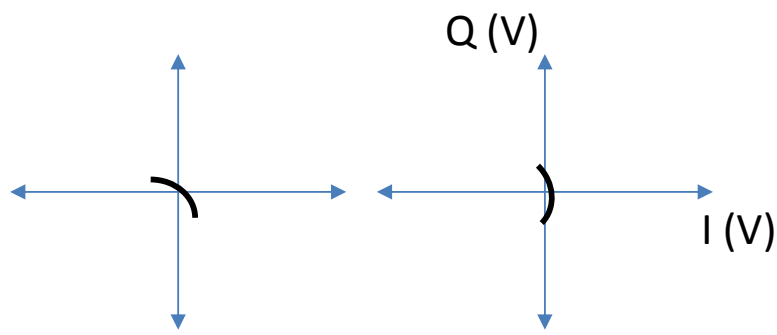

Fig. 2.7 Graphical representation of linear demodulation.

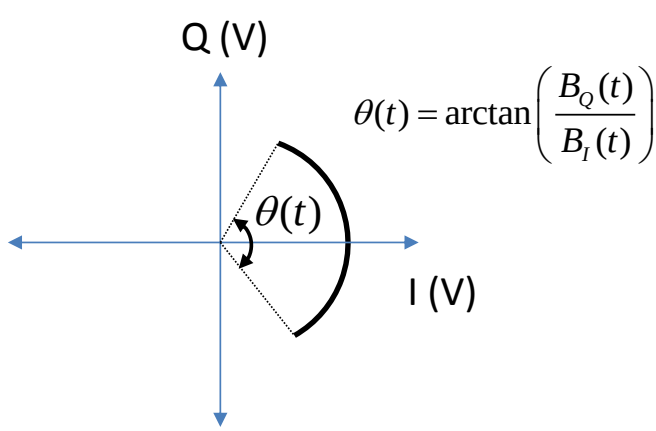

Fig. 2.8. Simple representation of arctangent demodulation.

Non linear demodulation (arctangent demodulation) makes use of the fact that I and Q channels form a circular arc in the complex plane. The phase of the signal can then be simply calculated as

$$\theta(t) = \arctan\left(\frac{B_Q(t)}{B_I(t)}\right) \tag{2.6}$$

In 2.5, we did not consider the presence of any dc offset. By adding dc offsets to the signal, the phase of the signal can be represented as:

$$\theta(t) = \arctan\left(\frac{V_Q + A_B \sin(\theta + \frac{4\pi x(t)}{\lambda} + \Delta\phi(t))}{V_I + A_B \cos(\theta + \frac{4\pi x(t)}{\lambda} + \Delta\phi(t))}\right) \tag{2.7}$$

If V_Q and V_I are negligible,

$$\begin{aligned} \theta(t) &\cong \frac{4\pi x(t)}{\lambda}; \\ x(t) &\cong \frac{\theta(t) \times \lambda}{4\pi} \end{aligned} \tag{2.8}$$

Arctangent demodulation gives the displacement of the detected motion which is its biggest advantage. Equation 2.7 assumes balanced I and Q data (same amplitude and perfect quadrature phase) which is rarely the case for practical receivers. As can be seen, for application of arctangent demodulation, the baseband signals have to be first corrected for any amplitude or phase imbalance (Park, Boric-Lubecke, and Lubecke, 2007). Methods for center estimation and clutter dc cancellation are also required and critical for correct calculation of phase. The use of circle fitting techniques implies that the demodulation technique is very sensitive to noise.

Another demodulation technique could be to represent I and Q data as complex signals and perform signal processing on the complex signal itself. The advantage of using complex signals is that many signal processing algorithms can directly be applied to complex signals and they can easily be represented in exponential form.

Various signal processing techniques could be used for rate estimation. Some of the estimation techniques include peak detection, auto correlation, Fast Fourier Transform (FFT), Short time Fourier transform (STFT) and wavelet analysis. The techniques have been described in detail in signal processing texts (Proakis and Manolakis, 1996). Advances in signal processing have led to development of many more techniques such as Hilbert Huang transform and empirical mode decomposition that overcome the limitations of existing techniques (Oppenheim and Schafer, 2009). Most of the work done in this dissertation will rely on FFT and STFT for rate estimation.

2.2 Clutter rejection and subject identification

With an understanding of Doppler radar, we can now attempt to look at the problem that needs to be solved. Bringing selectivity to the radar implies introducing ways to ensure that the obtained motion signals correspond to the desired source. By rejecting clutter motion and detecting one subject from the clutter, we are implementing the first stage of selectivity. The second stage of selectivity would be to detect and identify multiple sources of motion while ignoring clutter and noise. The way to achieve selectivity is to have some form of modulated backscatter from the subject while no modulated backscatter from other objects. There are two approaches to introduce modulation:

1) Introduce modulation at the transmitter.
2) Introduce modulation at the source of motion.

The only ways to resolve targets without placing any circuit on them is by spatial resolution and range. Spatial resolution can be brought to the radar through coherent detection using pulse Doppler radar. This principle is used in synthetic aperture radars (SAR) and Inverse synthetic aperture radars (ISAR) (Skolnik, 2001). In order to achieve good resolution, we would have to use millimeter wave signals and associated circuitry, and would still have ambiguities in the range as discussed previously. Spatial resolution can also be obtained through MIMO systems the limitations of which have been discussed in chapter 1. Range can also be calculated using frequency modulated continuous wave (FMCW) radars but then Doppler processing would become more challenging. The resolution provided by FMCW radar is also limited by the bandwidth of frequencies used. Introducing modulation at the source of motion may allow more flexible solutions compatible with the current Doppler radar system. The need for identification relates to the existing technology in use termed as radio frequency identification (RFID).

2.2.1 Radio frequency identification (RFID)

RFID enables the detection of an object without visual contact or line of sight (Dobkin, 2008). A radiofrequency circuit is placed on the object to uniquely identify it. That circuit is most commonly referred to as an RFID tag or an RFID transponder. RFID systems are very commonplace today being used for various applications such as toll collection, vehicle identification and theft protection in stores. A typical RFID system

consists of an interrogator, also known as a reader, and a transponder. Both the reader and transponder contain antennas to communicate. In addition to the antenna, a transponder also contains an integrated circuit (IC) containing the ID and communication protocol. The components of a typical RFID system are shown in Fig. 2.9.

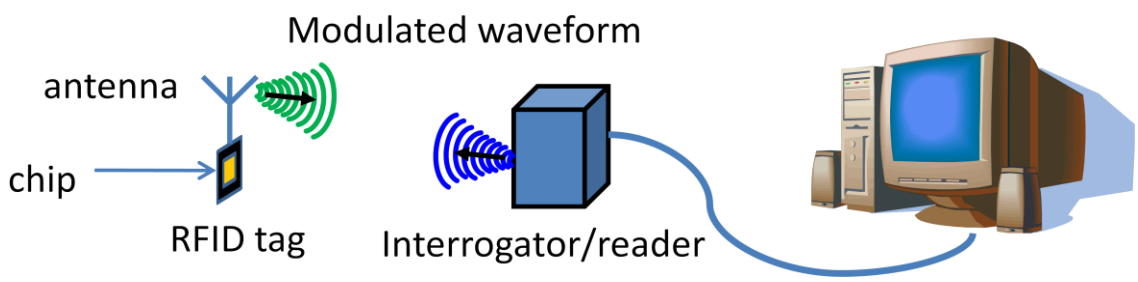

Fig. 2.9 A typical RFID system consisting of an interrogator, an RFID tag, and a computer.

RFID systems can be passive, semi-passive or active based on the power requirements of the tag used. Passive RFID systems employ tags that use the incoming signal to power themselves and backscatter the information. Semi-passive tags use a battery to power the tag circuit but they still use backscattering for tag to reader communication. Active RFID tags contain a radio along with a circuit and require a battery to operate both. RFID systems span a wide range of frequencies, from kHz to GHz, which indicates their feasibility to be operated around Doppler radar frequencies. Typical frequency bands of operation are 125 kHz-134.2 kHz, 13.56 MHz, 433 MHz 840-960 MHz, 2.45 GHz. RFID systems functioning at lower frequencies use inductive coupling to power the tags and use radiative coupling to power the tags at higher frequencies (Want, 2006). Standard communication protocols have been defined for

RFID systems. Some RFID air interface protocols for 860-960 MHz and 2.45 GHz are shown in table 2.1 (Dobkin, 2008).

Table 2.1. RFID air protocols

Tag Type	Frequency	
	860-960 MHz	**2.45 GHz**
Passive	ISO18000-6A,B,C EPC class 0 EPC class 1 Intellitag Title 21 AAR S918 Ucode	ISO18000-4 Intellitag μ-chip
Semi-Passive	AAR S918 Title 21 EZPass Intelleflex Maxim	ISO18000-4 Alien BAP
Active		ISO18000-4 ANSI 371.1

Although RFID technology is mature and easily available, it is difficult to apply for motion sensing applications. The primary reason is that RFID systems are made to ignore motion and detect the ID from the tag. For example, in tolling booths, the RFID systems are designed to detect the ID and payment from a car irrespective of its speed and they do not detect the speed of a car. Proprietary hardware of most RFID systems prevents us from modifying the system without incurring huge costs. Yet another reason why current RFID systems are inappropriate for our application is that most tags at higher

frequencies (2.45 GHz and above) are active. Considering all the factors, alternative backscattering schemes need to be studied.

2.2.2 Non-standardized backscatter schemes

A convenient way to identify a subject from the clutter could be to change the reflected frequency from that subject. In such a case, by detecting the backscattered modified frequency and rejecting any unmodified backscatter, we can achieve the first stage of selectivity. The most convenient method for modifying the incident frequency is by generating harmonics that can be done using passive non linear devices such as diodes. This technique in fact has been used for monitoring insects and bees (Mascanzoni and Wallin, 1986), (Riley *et al.*, 1996), (Colpitts *et al.*, 1999), (Brazee *et al.*, 2005). The passive radio frequency tags that generate harmonics are called as harmonic tags. Although, we can make sophisticated circuits for the same purpose, the objective is to first assess the feasibility of using passive harmonic tags with Doppler radar for physiological monitoring, which has not been done before and carries its own set of challenges, as will be discussed in the following chapter.

Chapter 3. Harmonic Tag Design

The simplest way to study the behavior of a CW Doppler radar system with RF tags could be with harmonic or frequency doubling tags. Though employing non-planar antennas and higher levels of radiating power, harmonic tags have been successfully used for separating a target from the environment uniquely (Mascanzoni and Wallin, 1986), (Colpitts and Boiteau, 2004), (Riley and Smith, 2002), (Kiriazi *et al.*, 2007). A harmonic tag consists of a tag antenna with a non linear element at its port. In most cases, the non linear element is a Schottky diode. The biggest advantage of such tags is that they are completely passive. The incoming signal is converted into harmonics by the diode and the tag is designed to also transmit the second harmonic back to the receiver. The receiver is designed to detect the second harmonic content while ignoring the backscattering of transmitted signal. This concept is illustrated is Fig. 3.1. The most popular application of harmonic tags has been for identification and tracking of animals and insects. By sensing their motion, the advantages of harmonic tags could be applied to applications such as cardiopulmonary monitoring and motion assessment.

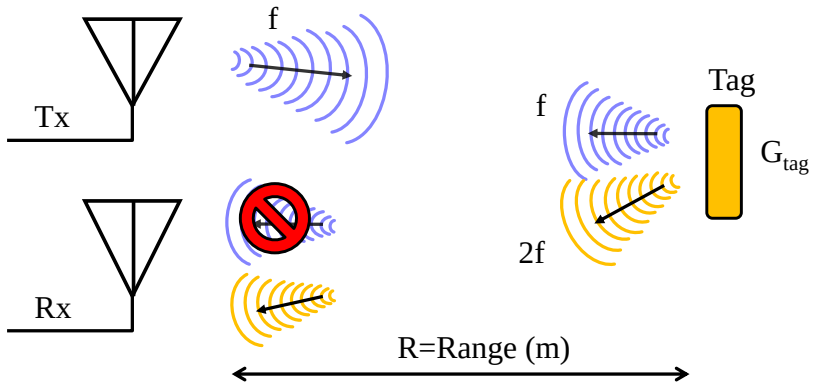

Fig. 3.1 Schematic illustrating the concept of use of harmonic tags.

3.1 Background

The design of earlier tags was very simplistic with a Schottky diode across a wire dipole with an inductive element. The dipole was treated as a resistor, inductor and capacitor (RLC) circuit in the simulation with carefully selected RLC parameters to represent its performance at fundamental and harmonic frequencies (Colpitts *et al.*, 1999). One of the major disadvantages of wire dipole tags used for animal/insect monitoring was that it would restrict the motion of the subject by getting snagged in leaves or foliage (Kiriazi *et al.*, 2007). Other physical limitations included the achievable loop diameter that was a function of the wire gauge and also affected the precision of fabrication. Yet another limitation was the placement of diode across the loop. Some of the tags for insect monitoring have been shown in Fig. 3.2 (Colpitts and Boiteau, 2004), (Brazee *et al.*, 2005). In the past, the use of harmonic tag was also associated with transmission of high power levels (~4W) owing to its outdoor use for animal tracking. The current design aim would be to use harmonic tag with lower transmitting power levels and closer distances for health monitoring applications.

The design process described for wire dipole tags cannot be used to design complex tag shapes. This chapter highlights a design methodology used to design a low power passive planar harmonic tag to be used with a Doppler radar to monitor respiratory and cardiac motion. The design objectives for our application would be a planar configuration, ability to function while placed on human body and low power operation with reasonable distance for health monitoring. The design methodology described in this paper is such that it enables the design of unconventional tag shapes that could not be represented purely by series RLC circuits, as was the case for wire dipoles. The idea is to

design a tag and evaluate its performance as a radiating element and as a circuit element in order to improve the efficiency of the design process. The fabricated tag is used to measure and isolate human respiration at distances greater than a meter.

Fig. 3.2 A wire dipole harmonic tag (Colpitts and Boiteau, 2004).

3.2 Harmonic radar theory

Harmonic tag theory has been well described by Colpitts and Boiteau (Colpitts and Boiteau, 2004). The three important functions of a tag are to effectively capture the incident radiation at the fundamental frequency, to generate harmonic signals from the received fundamental and to effectively transmit the second harmonic signal back to the reader. The three functions also highlight the differences and challenges faced in designing a harmonic tag as opposed to conventional RFID tags (Rao, Nikitin and Lam, 2005), (Dobkin, 2008). Although the design principles are the same, RFID tags most often operate at a single frequency and matching has to be obtained for one frequency of operation that is more straightforward than matching harmonic tags, where matching needs to be performed at fundamental and second harmonic frequencies. For the harmonic tag to effectively capture the incident radiation, the tag antenna should be

matched with the diode at the incident frequency (2.45 GHz in our case). Generation of harmonic signals is a function of Schottky diode and will depend on the type of diode used. Hence, the selection of diode is important. For the generated harmonics to be transmitted, the tag antenna should be matched with the diode at second harmonic of the incident frequency (4.9 GHz in our case). Matching circuits could be used to improve the performance but will also result in extra losses in the circuit itself. Hence, efforts will be focused towards designing an antenna that would work with the diode without requiring any matching circuitry.

Combined with the complexity of application (body-worn) and limitation of space, some tradeoffs in design will have to be made. The design methodology used in this paper is different from previous approaches and gives a better approximation. The parameters of tag antenna were obtained by simulation using a method of moments (MoM) simulator Advanced Design Systems (ADS) 2006 (Agilent, 2012). The power received by the tag could be calculated by Friis power transmission equation,

$$\mathrm{P_r} = P_t \frac{G_t G_r \lambda^2}{\left(4\pi r\right)^2} \quad , \tag{3.1}$$

where P_t is the transmitted power, G_t and G_r are gain of the transmitting and receiving antenna respectively, λ is the wavelength and r is the distance between the transmitting and receiving antenna.

Using the received power at fundamental frequency, the power given across the diode and the generated harmonic power was calculated using a circuit simulator. By exporting the S parameters of the tag antenna, a large signal S parameter simulation was

performed on antenna with diode that yielded the return loss of the whole tag. A harmonic simulation was also performed to observe the amount of generated harmonics. An assumption was made that half of the generated harmonic power was transmitted by the tag. By combining the above results, the transmitted harmonic power from the tag could be calculated. The power received at the reader was again given by the Friis transmission equation. Any change in tag antenna can be readily incorporated into the schematics and system simulations performed again to yield the results. This system can also be used for evaluating the performance two separate antennas for transmitting and receiving. For most optimum design, the passive body-worn tag has to be matched to the diode impedance at both fundamental and harmonic frequencies.

3.3 Tag design

3.3.1 Diode selection

Zero-bias beam lead Schottky diodes have been widely used for harmonic tags due to efficient conversion at lower powers. Since most of the applications have been in the area of insect monitoring, the small size and mass of the package has helped keep the mass of the tag within specified limits. However, the small size of beam lead diodes can make it very difficult to work with in a regular laboratory environment. Low barrier Schottky diodes can also be used to generate harmonics and are available in surface mount packages such as SOD 523 that are small and lightweight but can still be easily worked with using a regular solder station. The diode used in our harmonic tag was Avago's HSMS-286Y low barrier Schottky diode (Avago, 2012). A model for the diode was created in Agilent ADS with parasitic components as shown in Fig. 3.3 and a large

signal S parameter analysis was performed. Since the impedance of the diode is a function of drive level, simulations were performed at 2.45 GHz and 4.9 GHz for different power levels the results of which are presented in table 3.1. From those simulations, it could be seen that for an input power of -12 dBm, the diode impedance at 2.45 GHz and 4.9 GHz was 6.01 – j 218 and 5.64 - j62.79 respectively. From table 3.1, it can also be observed that as the input power to diode increases, the reactive impedance decreases whereas the resistive impedance increases.

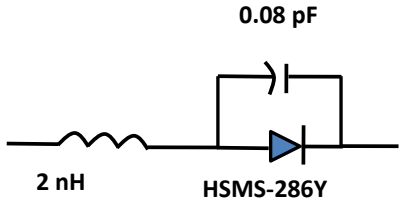

Fig. 3.3 Model of the Schottky diode HSMS-286Y.

Table 3.1. Diode impedance at 2.45 GHz and 4.9 GHz for various input power

Input Power	Impedance	
	F=2.45 GHz	F=4.9 GHz
-30	3 – j219	2.91 – j63.37
-15	3.78 – j218	3.45 – j63.06
-12	6.01 – j218	5.64 – j62.79
-9	19.14 – j217	14.52 – j60.49
-6	62.89 – j204	26.85 – j51.89
-3	117 – j155	37.28 – j39.46
0	138 – j89.91	44.42 – j26.44

3.3.2 Antenna design

The antenna element for the tag was designed as shown in Fig. 3.4 and the simulation results are shown in Fig. 3.5. The idea was to create a double dipole structure with each dipole inductively loading the other in order to match with the diode. The inductive element across the diode at the ports will further help in matching. Another consideration for tag design is the surface on which it is going to be placed, in this case being the human body (above the clothing). In a wearable tag, the human body presents a large conducting mass in close proximity, and is thus an integral part of the antenna design. The effect is detrimental, in that the body blocks and absorbs RF energy, and complicates impedance matching in a variable manner that is difficult to quantify (Sanad, 1994), (Kamarudin *et al.*, 2005), (Rajagopalan and Samii, 2010), (Occhiuzzi *et al.*, 2010). In order to lessen the affects of human body on the radiation pattern of the tag antenna, the tag antenna was placed on styrofoam substrate. The fundamental frequency being 2.45 GHz, the tag was designed for optimum performance at 2.45 and 4.9 GHz. The designed tag was approximately 16 cm long and the total width was around 1.5 cm.

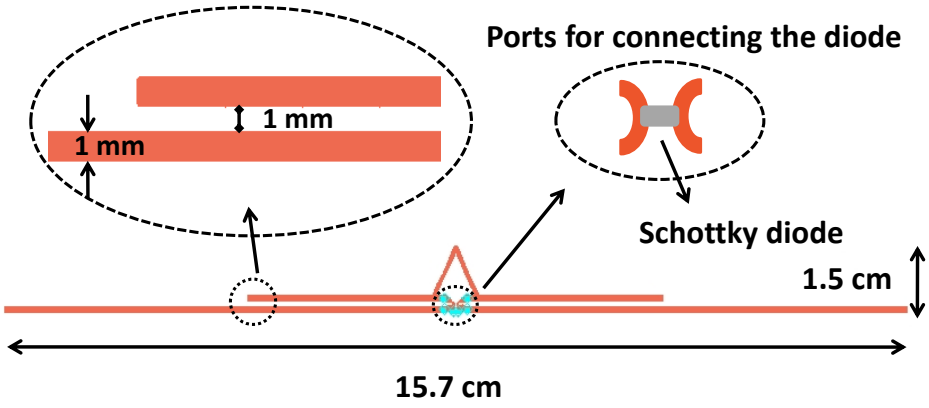

Fig. 3.4 Designed planar body-worn tag (not to scale).

Fig. 3.5(a) shows the return loss of the tag antenna for a port impedance of 50 ohms. Fig. 3.5(b) and Fig. 3.5(c) show the E-plane and the H-plane radiation pattern at 2.45 GHz respectively. Fig. 3.6 shows the E-plane radiation pattern and the H-plane radiation pattern for 4.9 GHz. The pattern is very similar to a dipole but with extra lobes. Other parameters of the tag antenna such as gain were also noted down. The gain of the tag antenna at 2.45 GHz was 5 dB and at 4.9 GHz was 5.2 dB. The antenna impedance at fundamental and second harmonic frequency was 190.622 + j399.321 and 205.291 + j191.250 respectively.

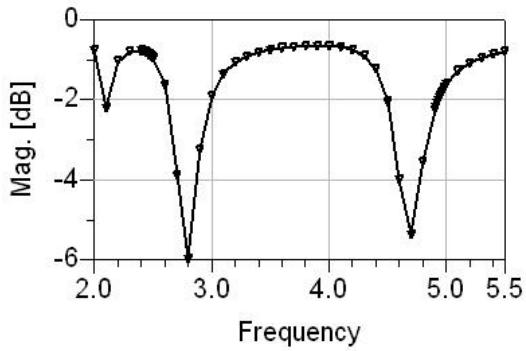

(a)

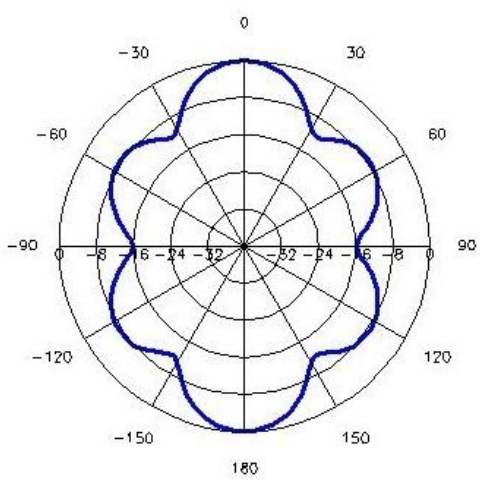

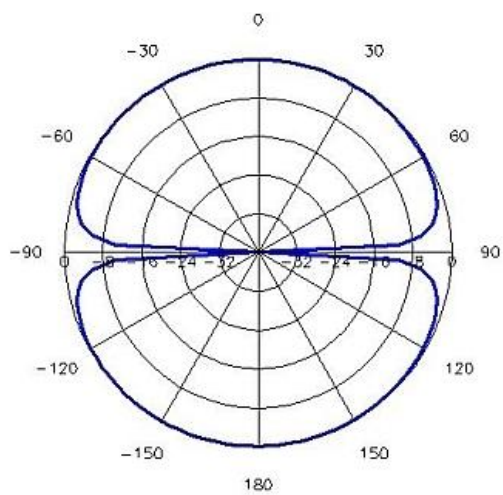

(b) (c)

Fig. 3.5 Simulated return loss of the tag antenna (a), radiation pattern in E-plane of the tag antenna at 2.45 GHz (b), and H-plane radiation pattern at 2.45 GHz (c).

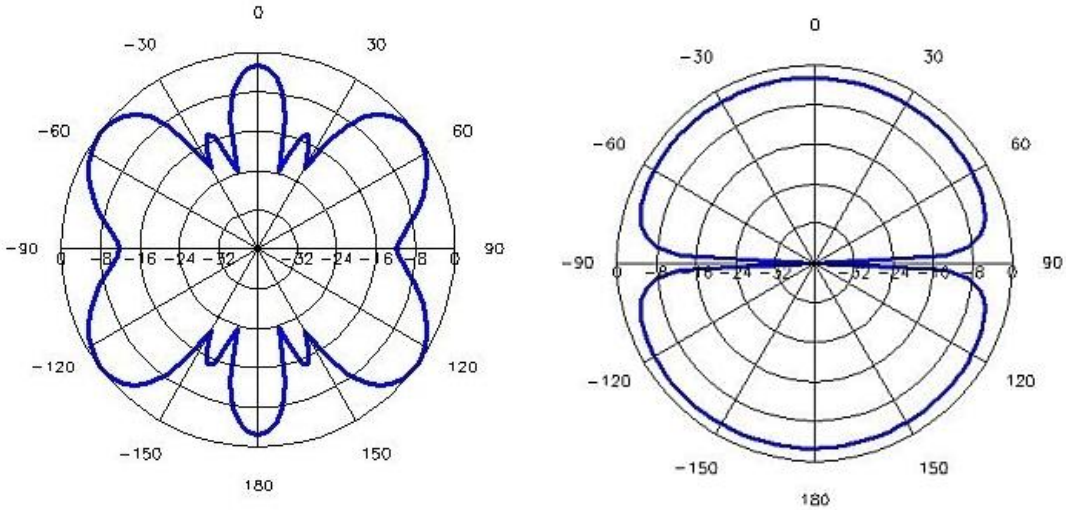

(a) (b)

Fig. 3.6 Radiation pattern for tag antenna at 4.9 GHz. E-plane radiation pattern (a), and H-plane radiation pattern (b).

It is important to note that for RFID tag design or harmonic tag design, the resonance frequencies for the antenna element with the diode is the most important factor and may be different than the resonant frequency of the antenna element itself.

3.3.3 System simulations

The antenna parameters were exported into 1 port S parameter block in ADS and simulations were performed with antenna and diode at its ports. LSSP simulations were performed in order to evaluate the matching. The schematic to evaluate the return loss of the tag with diode is shown in Fig. 3.7(a) and the results are shown in Fig .3.7(b). Note that Fig .3.7(a) simulates a case in which the tag is being fed by a 50 ohm cable and hence is not an accurate representation for calculating the return losses of tag as a backscatter element. The return loss at second harmonic is more critical than the return loss at fundamental frequency.

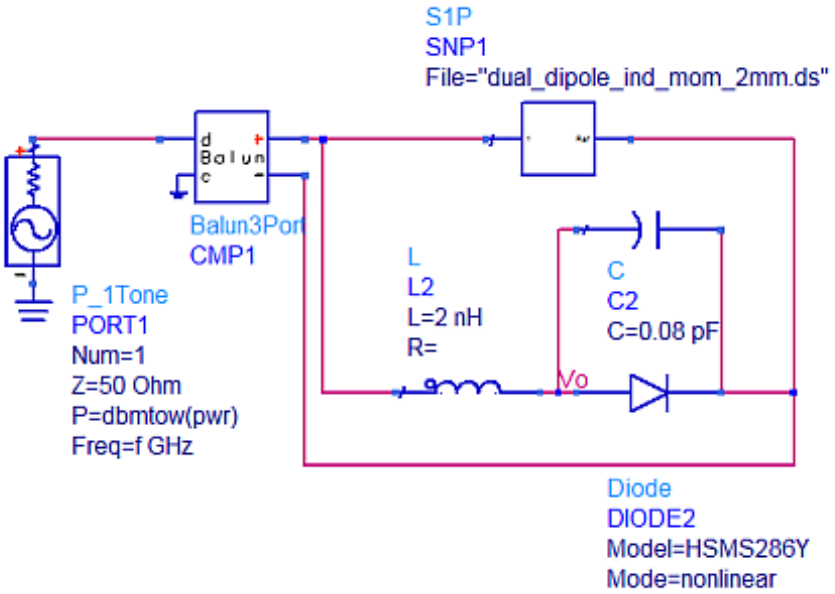

(a)

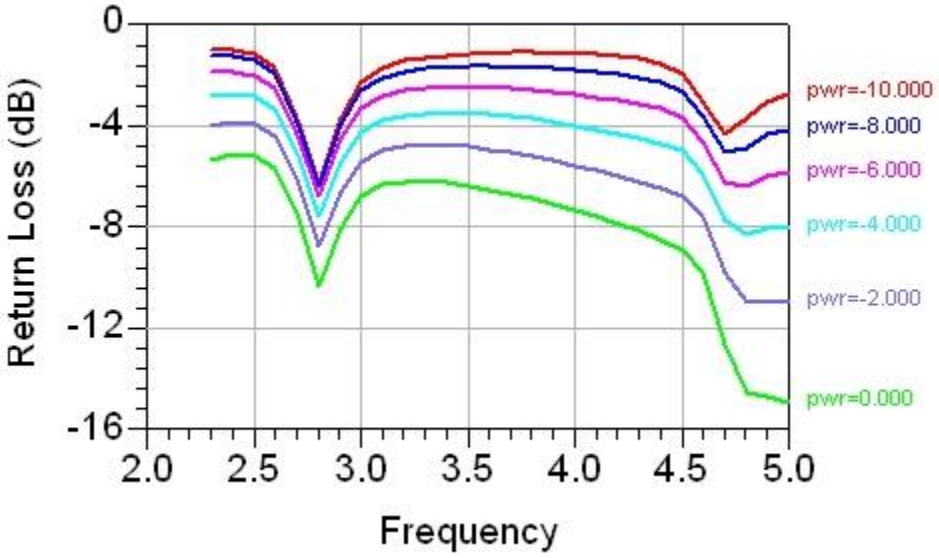

(b)

Fig. 3.7 Schematic for calculating S parameters of the tag with diode (a), and return loss of tag at different power levels (b).

From fig. 3.7(b), it can be seen that the tag is better matched to diode at higher drive levels. The simulation setup to calculate the generated harmonic power is shown in the Fig.3.8.

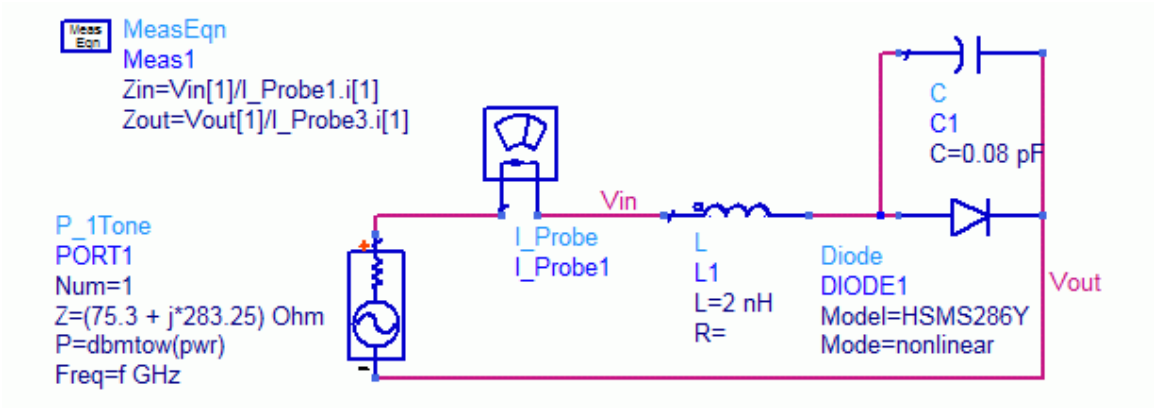

Fig. 3.8 ADS schematic to calculate the generated second harmonic across the diode.

Tag antenna impedance and received power calculated using Friis equation are entered as a source parameter and the generated harmonic powers are given by a harmonic balance simulation. Note that since ADS calculates 'dBm' values using an impedance of 50 ohms, input impedance (Z_{in}) was also calculated and power was calculated with reference to Z_{in}. Knowing the generated harmonic power, we can then again calculate the power received by the receiving antenna assuming half of generated harmonic power is transmitted back. For any change in tag antenna design, the MOM simulations would have to be performed again and the S-parameters exported to the circuit. Thus the tag characterization as an antenna and as a circuit element can be obtained using one software environment. More recent versions of Agilent ADS provide even more functionality and flexibility in terms of combining Momentum results with circuit schematics.

3.4 Testing

The tag was fabricated using copper sheets and placed on a Styrofoam substrate to closely emulate the dielectric properties of air. The fabricated tags are shown in Fig. 3.9. Fig. 3.9(a) would be referred to as 'htag1' in this dissertation and Fig. 3.9(b) would be referred to as 'htag2'. For receiving the tag signal at 4.9 GHz, a single patch and an array of patches were simulated, designed and fabricated in house to function as the receiving antenna.

(a)

(b)

Fig. 3.9 Fabricated harmonic tags. (a) 'htag1' placed on flexible Styrofoam substrate and (b) 'htag2' placed on a rigid Styrofoam substrate

3.4.1 Receiving antennas

Patch antennas as receivers were chosen owing to its design simplicity, planar configuration, narrow bandwidth and simple fabrication techniques. A patch antenna was

designed with an inset feed using simple design steps (Balanis, 1997). The layout of the designed patch antenna is shown in Fig. 3.10(a) with its simulated return loss shown in Fig. 3.10(b). Simulations were performed in Agilent ADS 2006. Inset feed was chosen to simplify the fabrication of the antenna, which was done in-house. The patch antenna was designed on Rogers substrate RT duroid 6002 having a dielectric constant of 3.1. The far field radiation pattern of the simulated patch antenna is shown in Fig. 3.11(a) along with its E-plane and H-plane radiation in Fig. 3.11(b). Simulation results show that the antenna has a return loss of more than 20 dB. The gain of the antenna as determined by simulation was 5.82 dBi at 4.9 GHz.

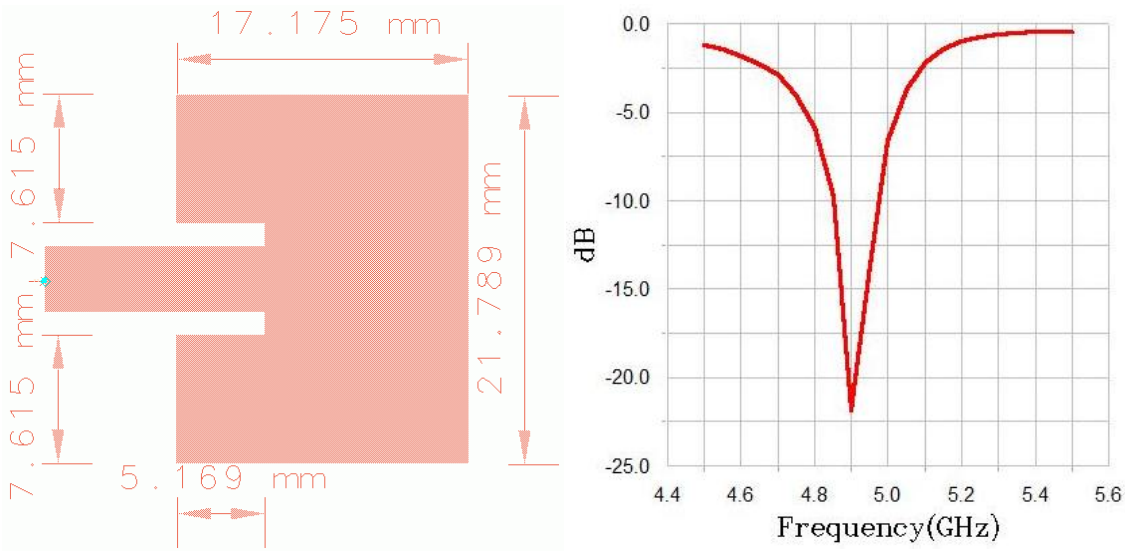

(a) (b)

Fig. 3.10 Designed patch antenna at 4.9 GHz (a), and its simulated return loss (b).

The designed antenna was then fabricated in-house without the use of any electronic fabrication equipment. As a result, some performance deviation was expected of the fabricated antenna. The fabricated antenna is shown in Fig. 3.12(a). Area of the

ground plane was approximately 5 by 5 cm^2. The return loss of fabricated antenna was measured using a vector network analyzer to be 12.36 dB as shown in Fig. 3.12 (b).

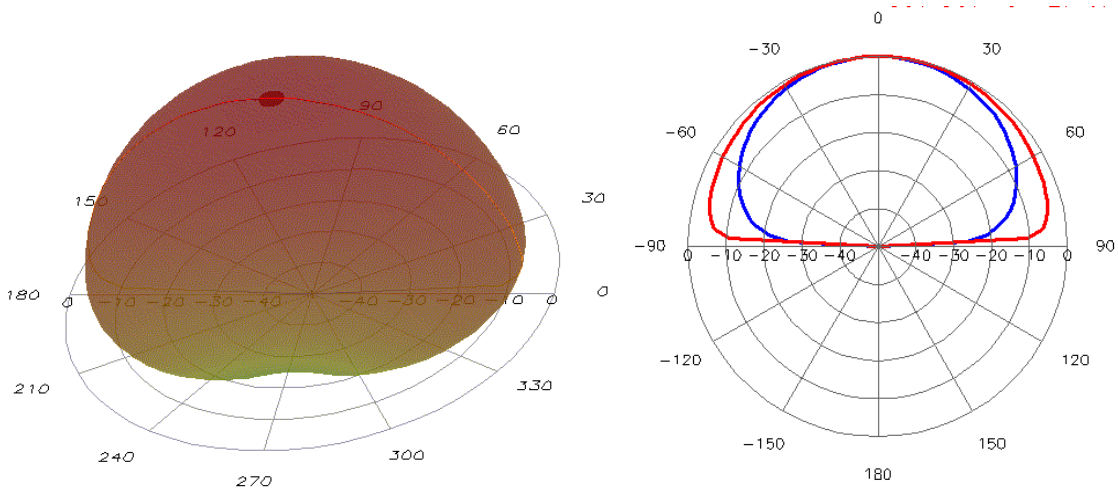

(a) (b)

Fig. 3.11 Far field 3D radiation pattern of the single patch antenna (a), and polar plot of radiation in E-plane (red) and H-plane (blue) of the antenna normalized to 50 dB (b).

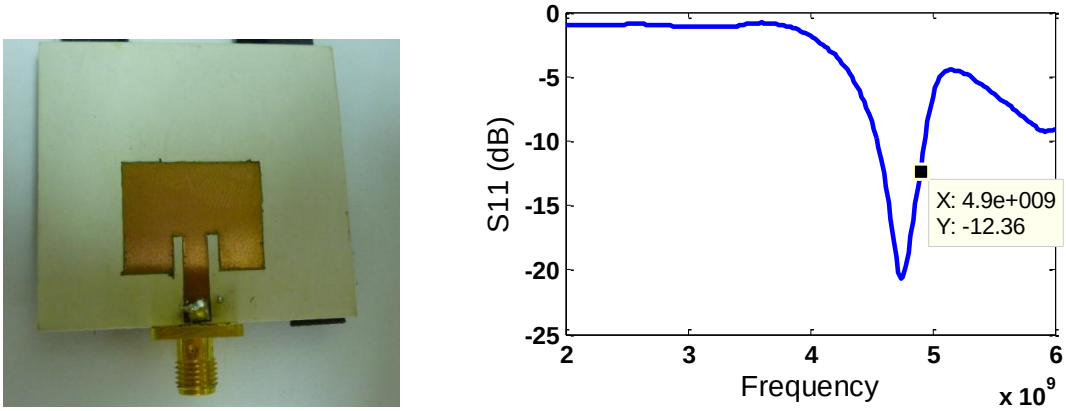

(a) (b)

Fig. 3.12 Fabricated patch antenna (a), and measured return loss (b).

It is an established fact that a well designed array of patch antennas can provide a higher directivity and gain than a single patch antenna. Since the returned tag signal is expected to be at very low levels, it would be beneficial to design an array of patch

antennas having a higher gain to better detect the tag signal at 4.9 GHz. A linear array of patch antennas was designed with a corporate feed network as shown in Fig. 3.13 (Garg *et al.*, 2001). The spacing between the individual patch antennas was a little more than $\lambda_{4.9}/8$ to keep the overall size of antenna small. The feed network was designed with same impedance value owing to fabrication complexity associated with etching thin lines without the use of electronic etching instrument. The simulated return loss of the patch array is shown in Fig. 3.14(a). The radiation pattern in E-plane and H-plane is shown in Fig. 3.15(b) indicating that the antenna is directive in E-plane. From simulation, the gain of antenna was determined to be 11 dBi.

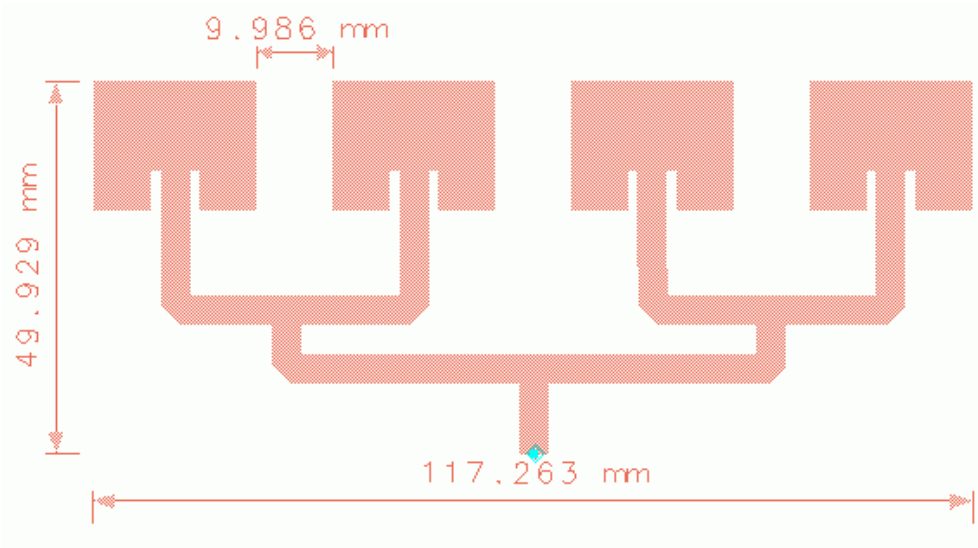

Fig. 3.13 Layout of patch antenna array.

The fabricated antenna array is shown in Fig. 3.15(a) with its measured return loss shown in Fig. 3.15(b). The return loss at 4.9 GHz is 11.99 dB indicating that most of the power is transmitted/ received at 4.9 GHz. There would be some loss of power due to mismatch in the corporate feed network but it would not severely impair our receiver's ability to detect the tag signal.

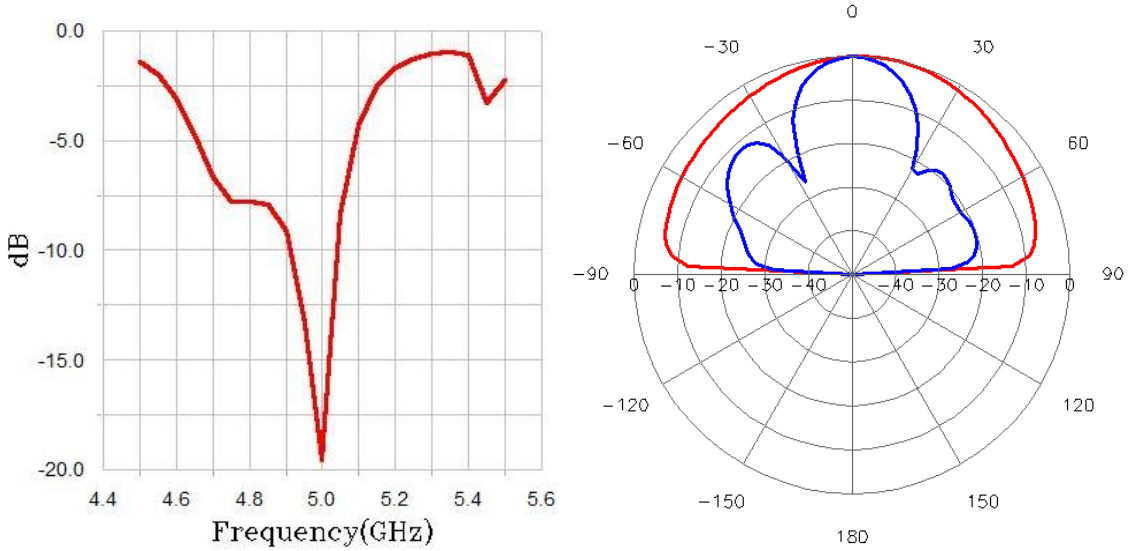

(a) (b)

Fig. 3.14 Simulated return loss for patch antenna array (a) and polar plot of radiation in E-plane (red) and H-plane (blue) of the antenna normalized to 50 dB (b).

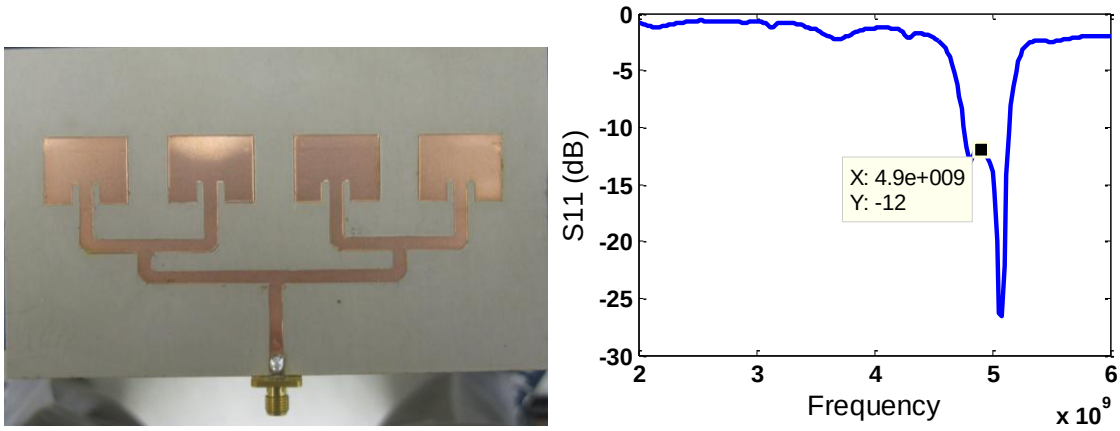

(a) (b)

Fig. 3.15 Fabricated patch antenna array (a), and measured return loss (b). To fabricate the antenna, the substrate was covered with painter's tape and a paper cutter was used to cut the desired shape. The tape outside the shape was removed and etching chemical was used to remove the copper.

3.4.2 Tag power budget

The performance of fabricated harmonic tag (htag 2) was tested at a distance of 1 meter from the transmitting and receiving antenna. The receiving antenna was connected to a spectrum analyzer (SA) to measure the detected signal at 4.9 GHz. The transmitted power at 2.45 GHz from the antenna was approximately 10 dBm. ASPPT 2998 from Antenna Specialist was used as transmitting antenna. The gain of the antenna was 8 dBi and the E- plane beam width was 60^0. The received power as shown in Fig. 3.16 was compared to the simulated received power shown in table 3.2. From table 3.2, it can be seen that the experimental results exceed the simulation that could be explained by minor deviations caused during fabrication.

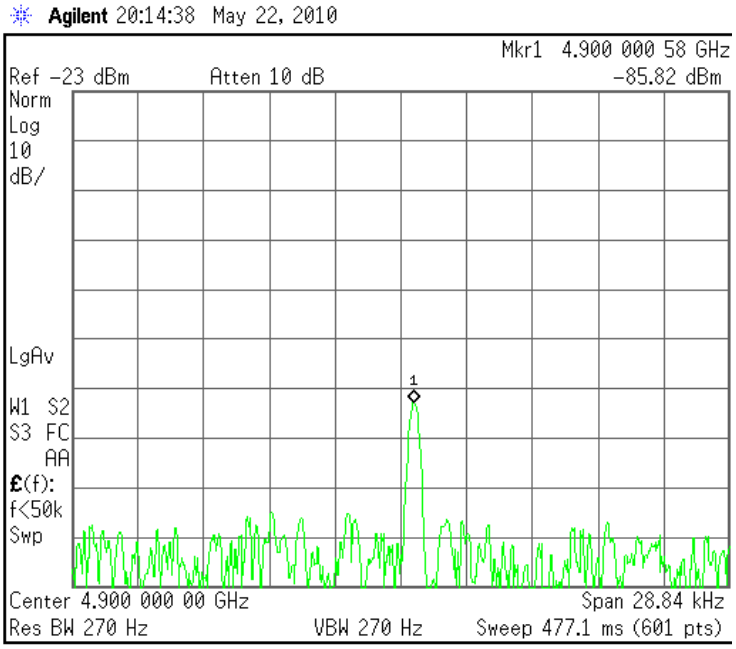

Fig. 3.16 Measured received power from harmonic tag at the spectrum analyzer with 10 dBm transmitted power and range of 1 meter.

Table 3.2. Simulated and experimental results for harmonic tag (htag 2) performance at a distance of 1 m.

$Z_{2.45}$ (Ω)	Transmit Power (dBm)	Received Power at the tag (dBm)	Generated harmonic (simulation) (dBm)	Assumed retransmitted harmonic (-3dB)	Simulated received power (dBm)	Actual received power at SA (dBm)
104.45 + j319	10	-17.231	-60.285	-63.285	**-93.34**	**-85.82**

3.5 Discussion

A passive harmonic tag was designed using one electronic and design automation tool. A simple tag structure was chosen for easy prototyping and quick testing of the concept. By placing the tag on a Styrofoam substrate, enough separation was created between the tag and human body to reduce its detrimental effects. Even though the tag was fabricated without the use of sophisticated tools, the measurement results indicate that the tag performance is comparable to the existing harmonic tags described in literature. The results were similar for htag1 and htag 2. By having a systematic design procedure, the problems of tag efficiency and its size can always be revisited. However, the interesting aspect now would be to study the use of the designed tags with Doppler radar systems.

Chapter 4. Homodyne System

When a harmonic tag is placed on human body; in the simplest case, ignoring the phase noise of the oscillator and the phase shift due to the distance of the target, the signal at the receiving antenna will consist of mainly two components: RF backscatter at 2.45 GHz and an RF signal at 4.9 GHz. These signals could be represented as

$$\begin{aligned} &A_{rf}\cos\left[\omega t-\frac{2\omega d}{c}-\frac{2\omega x(t)}{c}\right] \\ &+A_{rh}\cos\left[2\omega t-\frac{4\omega d}{c}-\frac{4\omega x(t)}{c}\right], \end{aligned} \tag{4.1}$$

where the term ωt represents the fundamental frequency of 2.45 GHz, d represents the nominal distance between the transmitting antenna and the subject, $x(t)$ is the periodic motion of the target. The terms A_{rf} and A_{rh} represent the amplitude variations corresponding to the received fundamental and harmonic components of signal respectively. The LO signal without the phase noise can be represented as

$$A_L\cos(2\omega t) \tag{4.2}$$

After mixing, the required baseband signal,

$$A_L A_{rf}\cos\left[\frac{4\omega d}{c}+\frac{4\omega x(t)}{c}\right] \tag{4.3}$$

is filtered out and decoded to yield the respiration rate. A quadrature receiver is used to alleviate measurement issues with null points existing at every λ/4 distance (Droitcour *et al.*, 2004), (Park *et al.*, 2006). On the complex I-Q plot, these equations form an arc that belongs to a circle centered at the origin.

A Doppler radar transceiver operating at 2.45 GHz needs to be modified in order to receive 4.9 GHz. The transmitted frequency remains the same at 2.45 GHz but the local oscillator frequency needs to be 4.9 GHz for obtaining the baseband signal. In order to generate 4.9 GHz from the same source to maintain the range correlation benefit, a frequency multiplier would be needed in the LO side of the receiver. The output power of the multiplier also needs to be amplified in order to have an optimum LO power for mixer. Since the received RF power is low, we would also need some amplification in the receive chain before we would send it to the mixers. Another criterion for 'f-2f' or harmonic radar system is to not receive any scattering from fundamental frequency (in this case, 2.45 GHz); for which appropriate high-pass and band-pass filters would be needed. The block diagram of a quadrature homodyne system for 'f-2f' system is shown in Fig. 4.1.

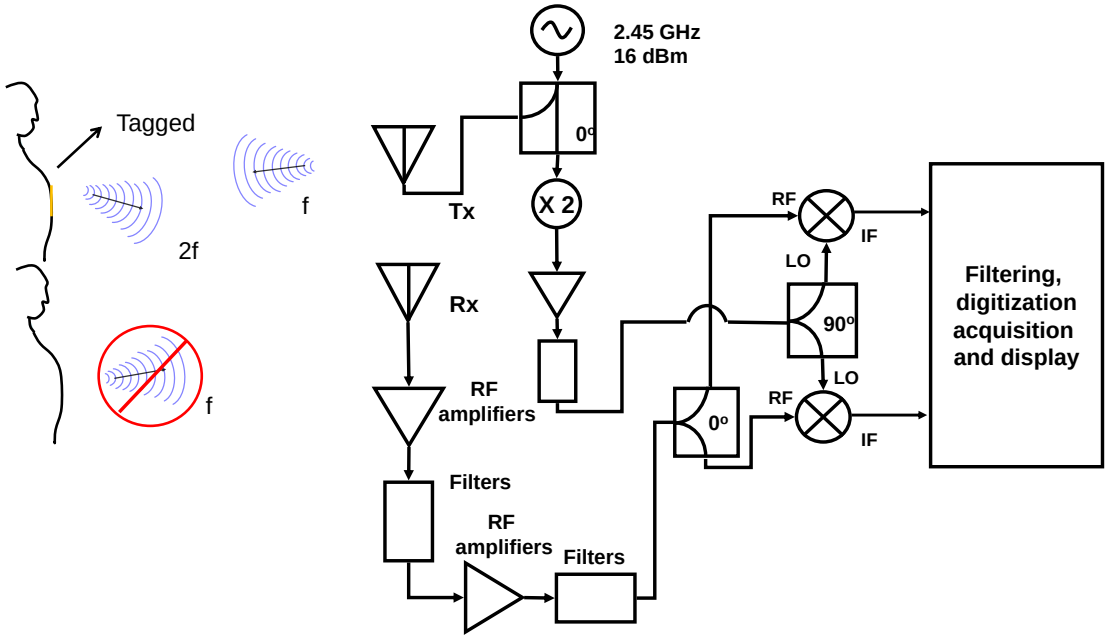

Fig. 4.1 A quadrature Doppler radar in 'f-2f' configuration.

This chapter presents the results from various experiments performed to make qualitative and quantitative performance assessment of harmonic Doppler radar systems with homodyne architecture.

4.1 Experiment I

Doppler radar was setup using connectorized components mostly from Mini-circuits. Two targets were moved at two different frequencies to distinguish the data from each other. The two targets consisted of the tag and a styrofoam ball having a diameter of an inch. The Styrofoam ball was wrapped in aluminum foil to increase the scattering. The motion of the tag was very close to 0.3 Hz while the motion of the styrofoam ball was at 1.3 Hz. The distance between the targets and the antennas was approximately 30 centimeters. The transmitted power to the antenna was 10 dBm. Five high pass filters (Mini-circuits VHF-3300 & VHF-3500) and two RF amplifiers (Mini-circuits ZX60-6013E-S) were used in the receiving circuit to condition the signals. The LO for the mixers was generated by a splitter (Mini-circuits ZFSC-2-2500) splitting the transmitted signal from the signal generator (HP E3344B) and running it through a commercial frequency doubler (Mini-circuits ZX-90-2-36). Two high pass filters and an RF amplifier (Mini-circuits ZX60-6013) were used to generate the LO input. Measurements were taken for three scenarios.

a) Tag in motion/ball stationary (I(a))

b) Tag stationary/ball in motion (I(b))

c) Tag in motion/ball in motion (I(c))

The three scenarios have been considered to evaluate three aspects of performance of the radar. First, how well can the radar detect the motion of the tag. Secondly, how well can the radar reject the motion due to fundamental backscatter signal and thirdly, how well can the radar isolate the motion of the tag from the motion of other non-harmonic scattering objects. The Styrofoam ball was controlled by a rotational servo with a plexiglass arm attached to it (Hafner and Lubecke, 2009). The plexiglass arm had slots to hold the Styrofoam ball in place. The servo was controlled by a controller board (arduino duemilanove) that could be programmed using a PC. The movement of the Styrofoam ball was set to be around 1 cm. The tag was placed in between the line of sight of transmitting and receiving antenna while the ball was in front of the receiving antenna (Fig. 4.2).

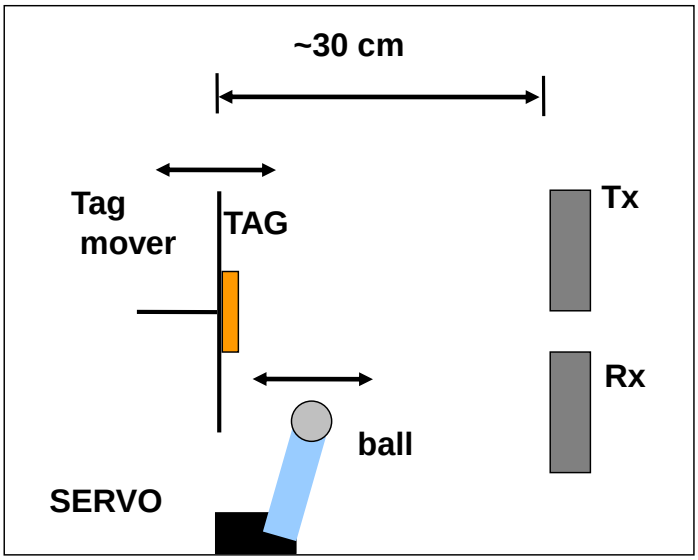

Fig. 4.2 Orientation of mechanical targets for measurements.

The data obtained from I and Q channel were combined using linear demodulation technique and then FFT was performed on the data using MATLAB®. Fig.

4.3 is a combined plot of data gathered from moving tag and moving target in a separate instance (I(a) and I(b)). Fig. 4.3(a) shows the raw data after it has been combined using linear demodulation from which very low level of detected untagged motion can be observed. The IQ plot in Fig. 4.3(b) complements Fig. 4.3(b). FFT data in Fig. 4.3(c) shows that the received signal from the tag is ~25 dB more than that of the non-tagged target. This test is measure of the effectiveness of the radar in rejecting the reflected fundamental frequency. This test could also be used as a calibration procedure before conducting measurements on human subjects.

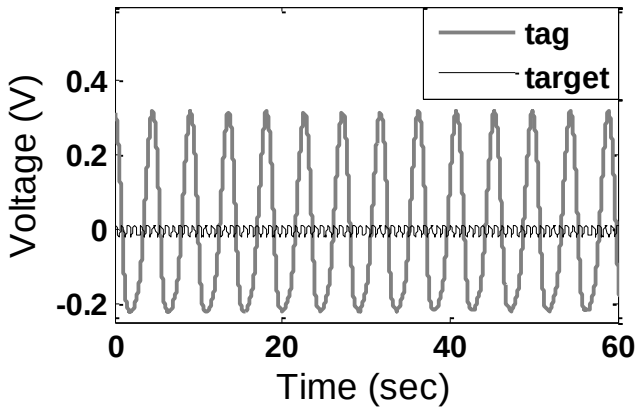

(a)

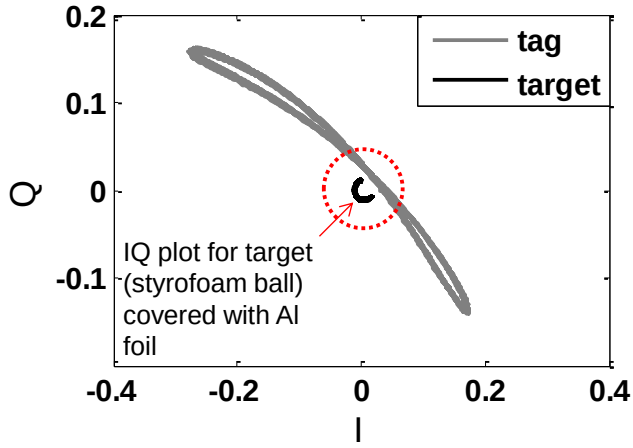

(b)

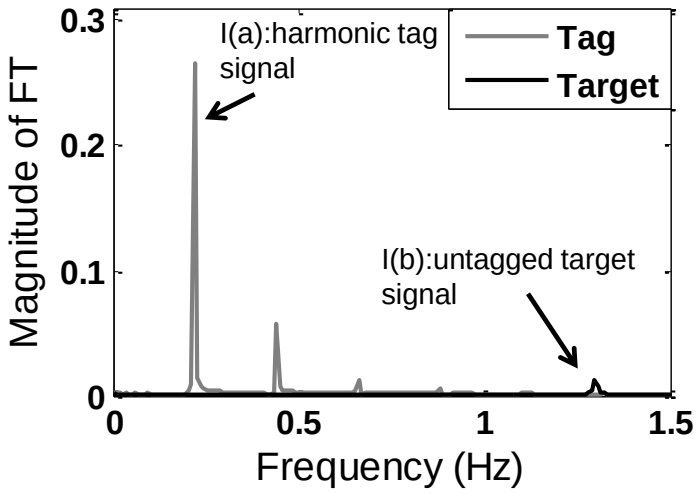

(c)

Fig. 4.3 Measurement results from experiment I. Linear demodulated data from I(a) and I(b) (a), I/Q plots from experiments I(a) and I(b) showing the relative amplitudes of the motion (b), and FFT of data from experiments I (a) and I (b) (c).

The interaction between two moving objects and radar is a little more complicated than when only a single moving object is present in front of the radar. Fig. 4.4 presents the results obtained from I(c) where the tag and target are moving simultaneously at frequencies of 0.2 Hz and 1.3 Hz respectively. We can notice the effect of untagged motion on the baseband signals in Fig. 4.4(a). The I/Q plot shows that the detected signals have different initial phase and results in a two arcs being continuously superimposed on each other, making it more difficult to extract direct phase information from the I/Q plot. Fig. 4.4 (c) shows the frequency spectrum of the combined baseband data. The untagged motion now appears to have a larger magnitude even though the motion is the same as in I(b). This suggests that the relative motion of the sources present in front of the radar also affect the backscattering from each source. For example,

experiment I(c) suggests that some signal from untagged object is being scattered towards the tag mover and the tag and is being reflected towards the receiving antenna.

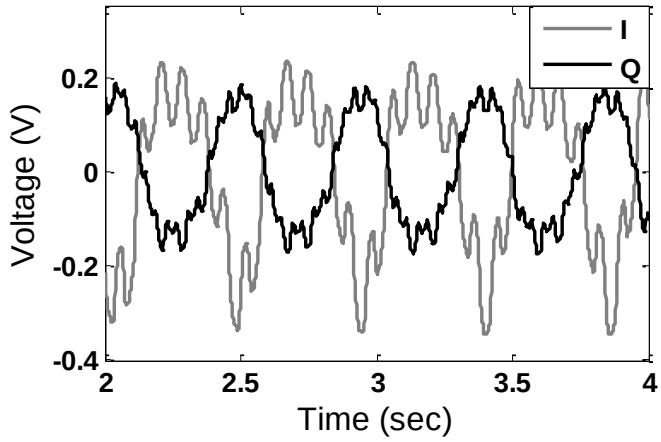

(a)

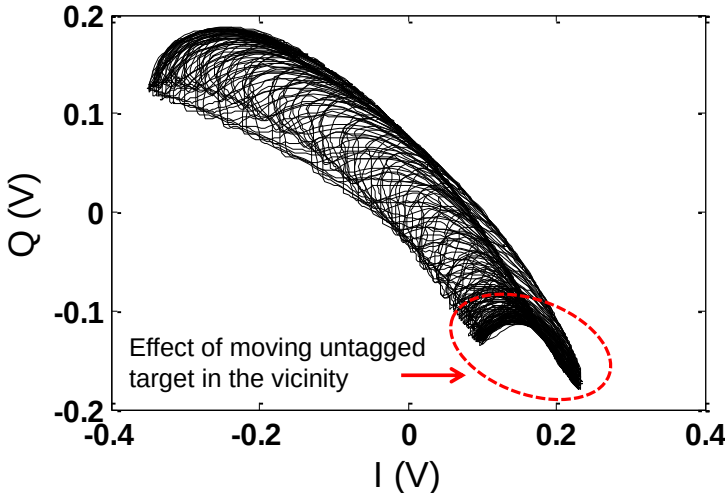

(b)

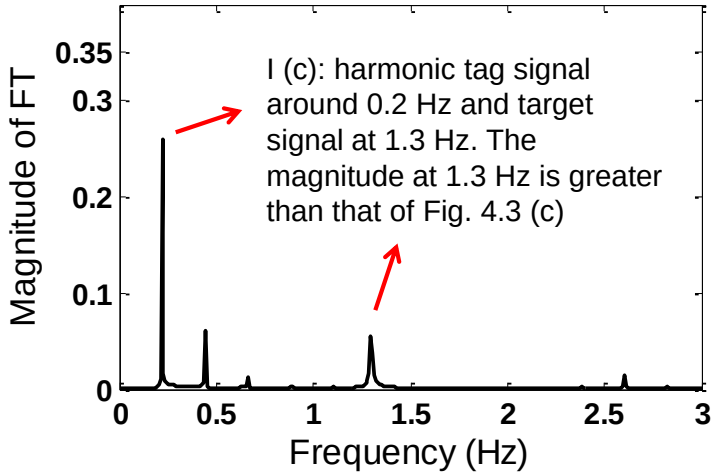

(c)

Fig. 4.4 Measurement results from I(c). Raw data showing the baseband signals (a), I/Q plot showing the presence of two frequency components and the phase relation between the two (b), and FFT data for experiment I (c) (tag and mechanical target moving together) showing an increase in detected target motion compared to case I (c).

4.2 Experiment II

After testing the concept on mechanical targets, the setup was then modified to measure the respiratory motion of human subjects using the tag. The results of this experiment were important to find out the tag performance when placed on human body and the radar response to a tagged and non-tagged human. The modified setup is shown in Fig. 4.5. The tag was placed on the left side of the human chest. The distance between the tag and the antennas was increased to 60 cm. A high pass filter and an RF amplifier were added in the receiving chain. The data was recorded using an analog to digital (A/D) converter and MATLAB®. The baseband signal was passed through an SR560 Low Noise Amplifier (LNA) before sending to the A/D converter. Ac coupling was used to couple the data to LNA and a gain setting of 500 was used. The sampling rate was

selected to be 100 Hz. A respiratory belt (Pneumotrace II) from UFI was used as a reference for measurements on human subject. All the measurements on human subjects were done in accordance with University of Hawaiʻi at Mānoa institutional review board (IRB) under protocol CHS 14884. Measurements were taken considering two scenarios as shown in Fig. 4.6. The experiments will be referred to in the text as follows.

Experiment II:

a) Human subject with harmonic tag in front of radar

b) Human subject with a metal foil

The tag was attached to the subject's chest above loose clothing. In the case where the reference belt had to be wrapped around the subject's chest, the harmonic tag was attached to the reference belt.

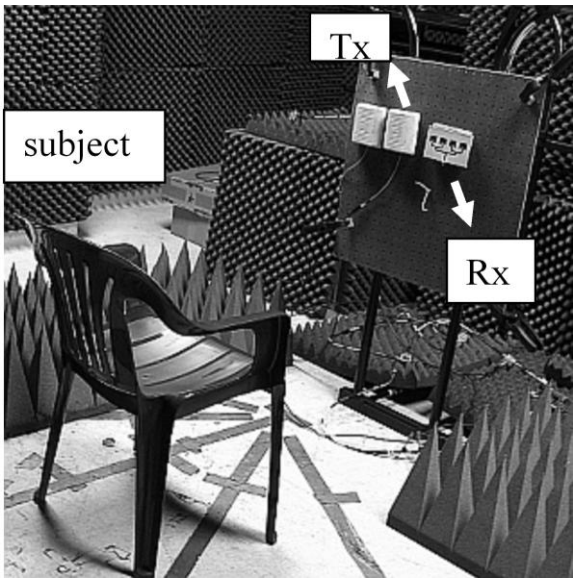

Fig. 4.5 Photograph of the modified setup to carry out measurements on human subjects.

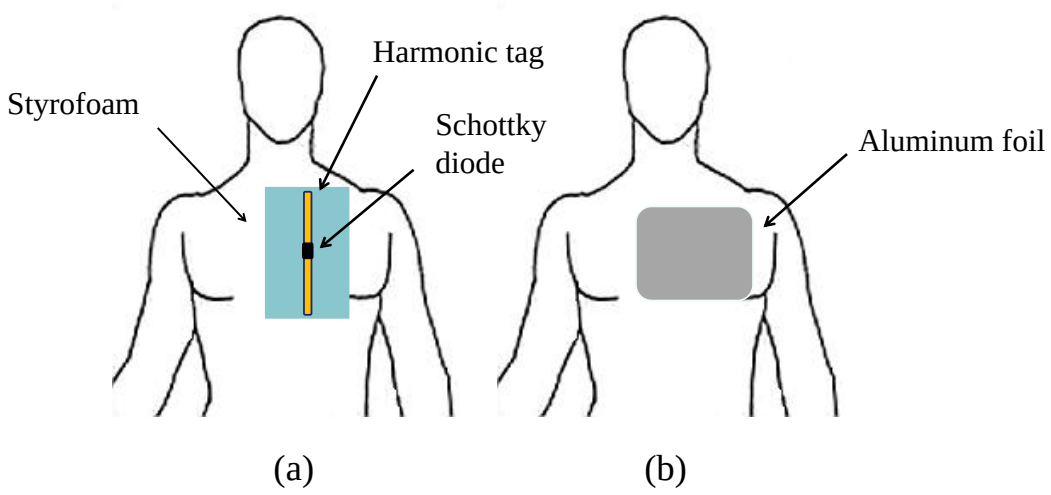

Fig. 4.6 Two experimental conditions for measurements on a human subject. Measurements were performed with the harmonic tag (a), and with an Aluminum foil (b). Note that the cross sectional area of the foil is more than the tag used. The subject was wearing a T-shirt at all times during the measurements and the tag and the foil were placed on the shirt.

The measured baseband signals were combined using linear demodulation. The measurement results showed in Fig. 4.7 compare the radar data with the reference chest belt for a human subject (Experiment II (a)). The rate was calculated using FFT on windowed data (12-18 s) with an overlap of 6 seconds and picking out the maximum values in each window. Based on our rate calculation, the maximum difference between the radar data and the reference does not exceed 0.5 beats per minute (bpm).

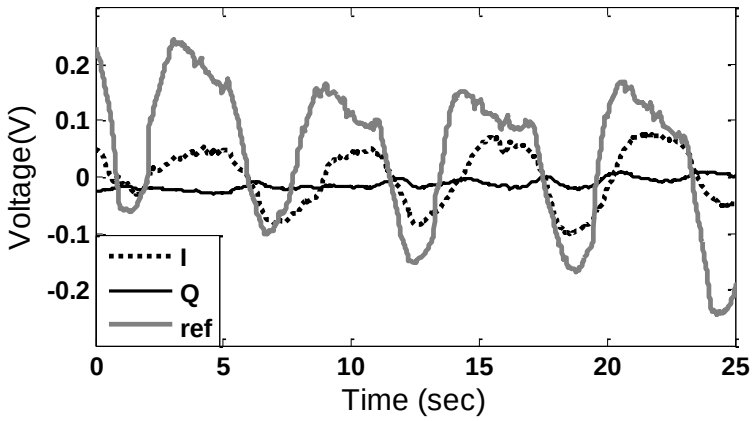

(a)

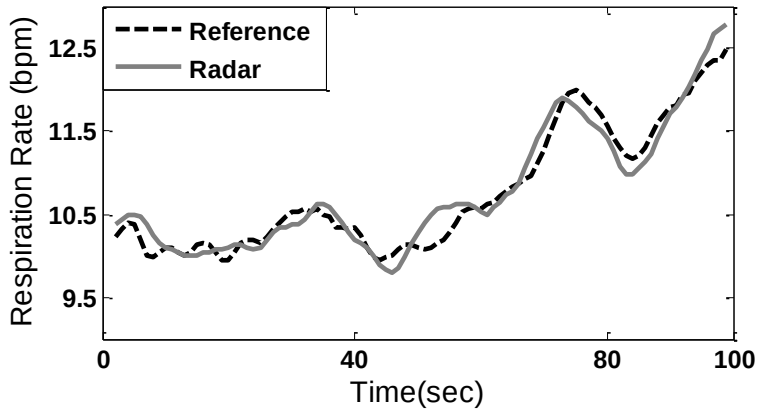

(b)

Fig. 4.7 Segment of raw data showing the agreement in I, Q, and reference data (a), and respiration rate showing that harmonic radar can track the motion of the tag on a human body very well (b).

Fig. 4.8 compares the strength of received respiratory data from the tag and the metal foil placed on a human subject's chest. The FFT data shows that the harmonic radar can still detect the backscattered 2.45 GHz signal. If 2.45 GHz data is considered as noise for harmonic radar, then the signal to noise ratio is around 10 dB for the above mentioned system. However, it should be noted that the cross-sectional area of the sheet attached is more than the tag physically. It was also shown in a separate experiment (Singh and

Lubecke, 2009) that there was a very low detection rate of fundamental reflected component when nothing was attached to the human chest. The data from Fig. 4.8 shows the feasibility of detecting human respiratory activity at a distance of ~60 cm.

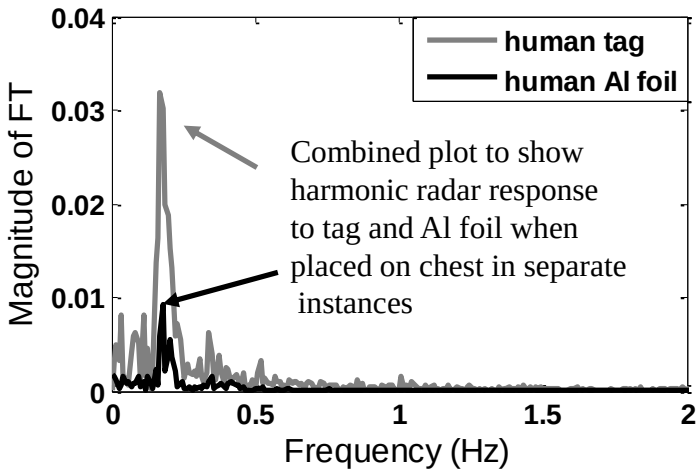

Fig. 4.8 Comparison of FFT data for a human subject with a tag and a metal foil placed on the chest.

4.3 Experiment III

After the initial testing and calibration with mechanical targets, a system was set-up to measure the respiration of a human subject in presence of a large moving object that would scatter back 2.45 GHz. The object was again a Styrofoam hemisphere with a radius of 10 cm covered with aluminum foil. The target motion was set to 0.2 Hz with a linear displacement of about a centimeter in order to observe radar response to interference near respiratory frequencies. The distance between the subject and the antenna was approximately 1m. The received antenna was connected to two chains of two high pass filters (Mini-circuits VHF-3500, VHF-3100) and an RF amplifier (Mini-circuits ZX60-542LN-S+). The amplified and filtered signal was split and then fed to

mixers (Mini-circuits ZX05-14-S+). The signal from signal generator was filtered through a band-pass filter and split and fed to the commercial frequency doubler (Mini-circuits ZX-90-2-36-S+) through a variable attenuator (0-30dB). The output from the doubler was amplified using an RF amplifier (Mini-circuits ZX60-6013) and passed through three high pass filters. This signal was then split using commercial hybrid (Pasternack PE 2058) and fed as the LO to the two mixers. The IF signals were fed to LNA's using ac coupling and gain setting of 200 was used. NI- DAQ 6289 was used to acquire the data at a sampling rate of 100 Hz. The same experiment set-up was then used to evaluate the response of a 2.45 GHz quadrature Doppler radar system shown in Fig 4.9. The 2.45 GHz radar system consisted of single antenna (Antenna Specialists, ASPPT 2998) with a gain of 8 dBi connected to a splitter that was used as a circulator. The signal from the signal generator was split using a two-way splitter (Mini-circuits ZFSC-2-2500).

Experiment III:

a) 2.45 GHz Doppler radar human testing with noise source
b) Harmonic Doppler radar human testing with noise source

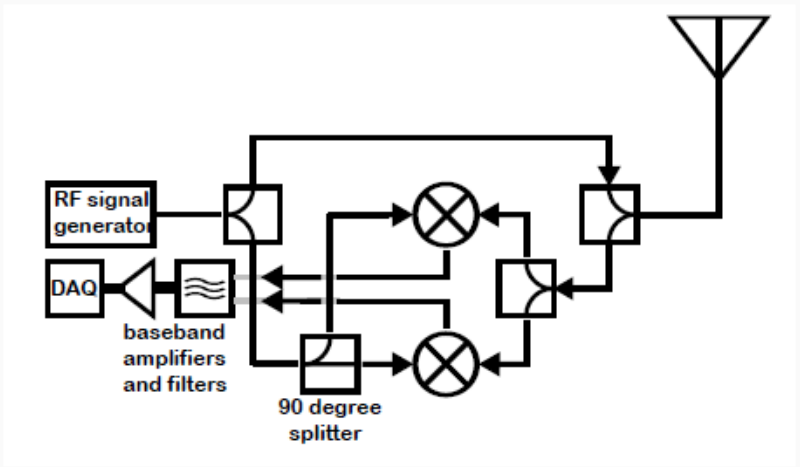

Fig. 4.9 Schematic of the dual channel 2.45 GHz Doppler radar used for experiment III.

Doppler radar is very sensitive to motion which enables us to detect even heart-rate. Hence, it is logical to assume that any other motion in the vicinity of the subject should affect the measurements in an adverse way. Fig. 4.10 displays the response of 2.45 GHz radar when two objects are simultaneously moving in front of it. One is a human subject while the other is linear target with 0.2 Hz of motion. The raw data and the beat rate obtained of the radar data from 2.45 GHz quadrature Doppler radar shown in Fig. 4.10 show that radar is not able to track the motion of any one of the objects. The radar data in Fig. 4.10(b) shows the same trend as the reference (rise and fall) but it is centered at 12 bpm which is the rate at which the Styrofoam target is moving. The results obtained from harmonic Doppler radar for the same experiment scenario (two simultaneous moving objects with one being tagged) are shown in Fig. 4.11. The harmonic radar clearly tracks the respiration rate as accurately as the reference.

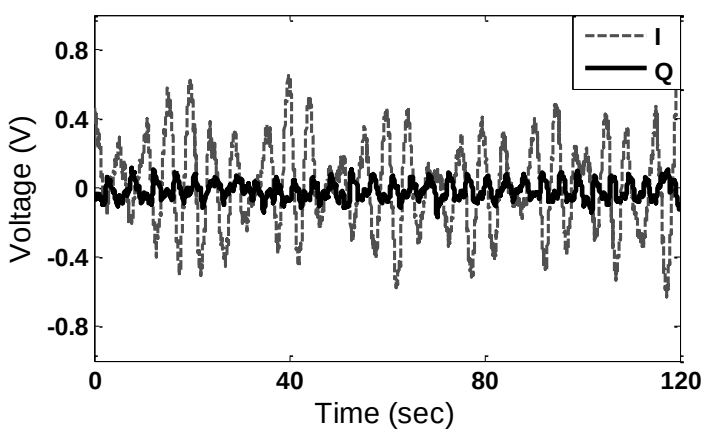

(a)

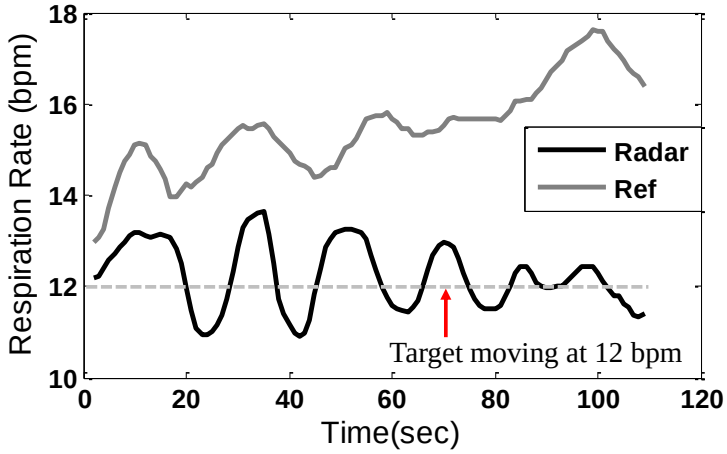

(b)

Fig. 4.10 Response of 2.45 GHz CW Doppler Radar to two simultaneous moving objects in its view, experiment III(a). Raw data showing the amplitude changes due to EM interaction between the two targets (a), and the rate indicating the inability of the radar to clearly isolate the motion of any of the two moving objects (b).

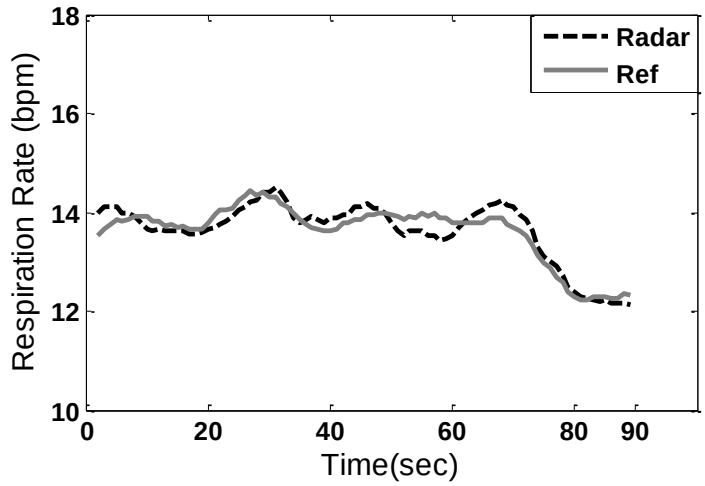

Fig. 4.11 Respiration rate of a human subject with an untagged moving scattering object in front of ‘f-2f’ radar (experiment III(b)).

4.4 Experiment IV

After evaluating the response of two radar systems separately, the experiment was performed with both the radar systems connected simultaneously to see the time response of the radars together. The measurements were first made for a tagged human subject breathing normally in front of radar with the untagged target present but motionless. Then, the target was moved at 0.2 Hz and data was recorded. The experiments are labeled as follows:

Experiment IV:

a) Both radars, human testing without noise source

b) Both radars, human testing with noise source moving 1cm (amplitude)

c) Both radars, human testing with noise source moving 2cm (amplitude)

Fig. 4.12 shows the time synchronous response of both the radars to a tagged person and a stationary/non-stationary object in front of it (Experiment IV (a)). From Fig. 4.12(a), we can see that the radars track the respiration rate of the human subject very well when the target is stationary. When the target starts moving at 0.2 Hz (Experiment IV (b)), the 2.45 GHz radar is unable to track the respiratory motion while 4.9 GHz radar tracks it with sufficient accuracy (Fig. 4.12(b)). The error rates for both radars have been shown in Fig. 4.12(c). The maximum error rate for 4.9 GHz radar is around 0.5 bpm. It is interesting to note the relatively low error rate for 2.45 GHz radar between 40-50 seconds. This might result due to EM interaction between the two targets and also depends on their relative motion signature. However, this result serves to show that even a small scattering target can affect the performance of a Doppler radar. With multiple

moving objects in front, it would be difficult to distinguish the source of motion using a conventional medical Doppler radar. A moving person would present an even bigger radar cross section. Another factor to consider is that error resulting from above mentioned sources is not a constant and hence cannot be treated as apriori information.

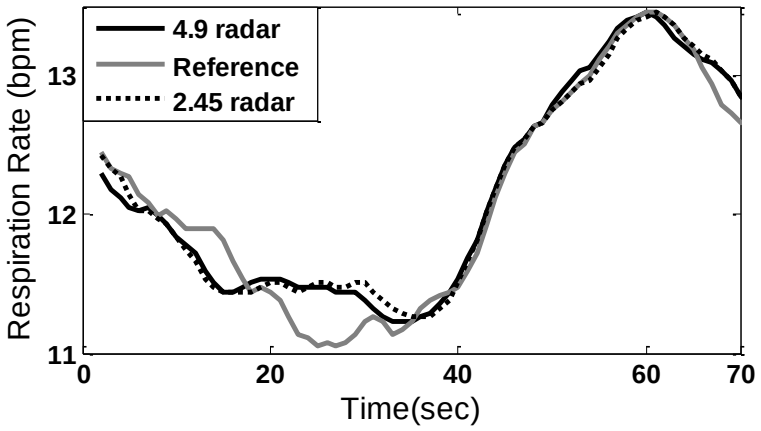

(a)

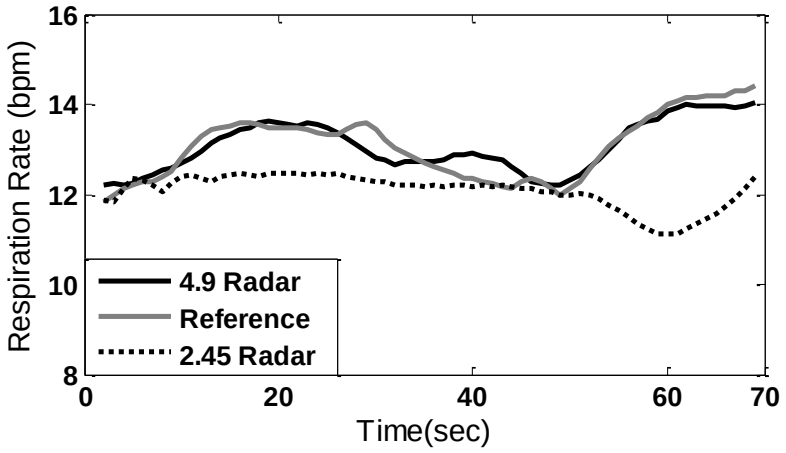

(b)

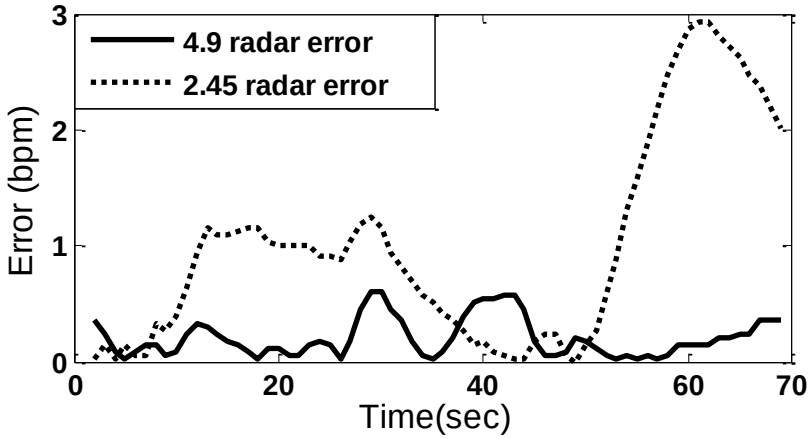

(c)

Fig. 4.12 The response of 2.45 GHz and 4.9 GHz radar to experiment IV. A tagged human subject in front of radar when the target is not moving (a) (Experiment IV (a)), tagged human with the target moving at 0.2 Hz (b) (Experiment IV (b)), and the error rate in the detected respiration rate for the two radars (c). As expected, both the radar can track respiration accurately when mechanical target is stationary (12 (a)) but 2.45 GHz radar cannot track the respiration accurately in (12 (b)) when the mechanical target starts moving.

Fig. 4.13 shows the worst case scenario for a 2.45 GHz Doppler radar where it tracks the mechanical target instead of tracking the respiration rate (Experiment IV (c)). The measurement was performed for 5 minutes. The results indicate the possibility of erroneous detection and triggering of false alarms when two moving objects are present in front of 2.45 GHz radar. The radar might be detecting motion but it is difficult to interpret the source of the detected motion. However, harmonic radar still tracks the tag and thus respiration of the human subject.

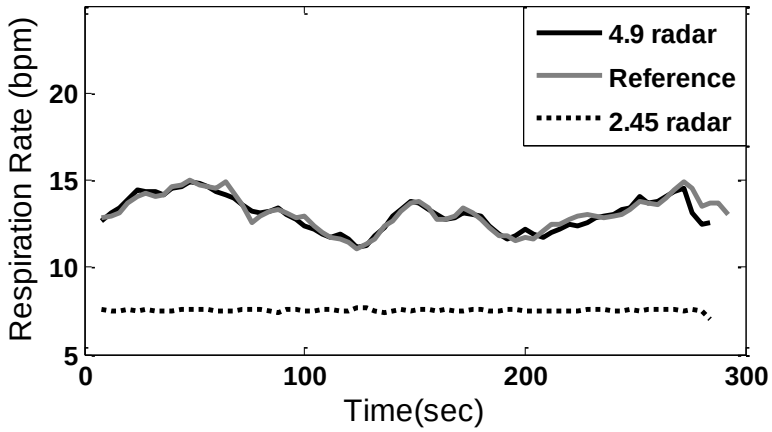

Fig. 4.13 Response of 2.45 GHz and 4.9 GHz radar to a tagged human and a mechanical untagged object. The mechanical target is moving 2 cm at a frequency of approximately 0.15 Hz. This condition represents the worst case scenario where 2.45 GHz radar would completely detect the undesired motion.

4.5 Discussion

The harmonic radar was tested at different ranges for the same amount of transmitted power (10 mW). The range of such radar primarily depends upon the ability of the tag to generate and reflect back harmonics, which is influenced by tag-diode matching at lower incident powers and the incident power. The current system has been tested at 1m for 10dBm (10 mW) antenna transmitting power. The system should function at several meters with transmitted power (antenna) still below 100 mW. The novelty of the tag lies in its design, planar structure and the fact that it can be used on the body. The tag can successfully reject any clutter motion in the vicinity and also any other body motion that does not affect the respiratory motion. For respiration activity estimation, the tag could be placed anywhere on the chest as long as it is facing the receiving antenna or in the field of view of receiving antenna. The tag could effectively

be placed anywhere on the body where motion is caused due to respiration such as on abdomen or shoulders. The radar response and SNR depends on the magnitude of the motion of the tag and its orientation with the receiving antenna.

The measurement results presented in this chapter show the feasibility of using Doppler radar with passive backscatter tags to detect physiological motion with non stationary clutter being present around the subject. Similar measurements with 2.45 GHz system resulted in failure to accurately track the desired motion. An ideal harmonic radar should reject any amount of fundamental backscatter that is being directed towards the receiving antenna. However, the measurement results indicate that the signal (tag) to noise (untagged) ration for harmonic radar system is a function of the separation between the tag and the untagged object, the relative motion between them and the size of the untagged object. Although, it is very difficult to obtain ideal behavior from a physical system, it is worth investigating the causes of deviation from the ideal behavior in order to make improvements in the system. Chapter 5 will present results from such an analysis.

Chapter 5. Analysis of Receiver Architectures for Harmonic Doppler Radar

In the previous chapter, a continuous wave Doppler radar with body-worn harmonic tag has been used to extract the respiratory information in presence of an untagged moving object (Singh and Lubecke, 2012c) showing a clear advantage over conventional Doppler radar in certain environments. The most conventional receiver architecture for Doppler radar physiological monitoring is the direct conversion homodyne architecture as it offers advantages of simplicity, low power and more integration capability (Razavi, 1998). Although filter and amplifier chains were used in the receiver to condition the signals, complete suppression of non-tagged motion was not achieved.

Implementation of homodyne harmonic radar receiver requires the use of a frequency doubler and an RF amplifier on the LO side. The presence of such non-linear components may affect and increase the phase noise of the system that could decrease the SNR of the receiver (Gillespie *et al.*, 1961). The range and sensitivity of a Doppler radar system have a strong dependence on the phase noise of the system since we are demodulating the phase to obtain relevant information. One way to circumvent the use of the multiplier and amplifier is through the use of sub-harmonic mixers, but commercial sub harmonic mixer use is generally restricted to higher frequencies (>10 GHz) as it reduces the cost associated with the design of high frequency signal sources. In a system to extract baseband information contained within the second harmonic of the transmitted signal, another way could be the use of heterodyne/dual-conversion receiver architecture.

The use of 2.45 GHz transmitting source as LO in both stages would remove the use of frequency multiplier and amplifier in the local oscillator chain while maintaining range correlation benefits without adding complexity to the system (Fig. 5.1). We can also use intermediate frequency (IF) filters to remove the unwanted signals and increase the sensitivity of the receiver. Such receiver architecture is similar to a wide-IF architecture with quadrature mixing being utilized only in the second stage of mixing (Behbahani *et al.*, 2000), (Rudell *et al.*, 1997).

This chapter will analyze the sources of noise in the homodyne harmonic radar system, propose a zero-IF heterodyne architecture for the harmonic radar receiver and investigate the phase noise and noise floor in the system to verify if there are certain advantages to using a heterodyne receiver over homodyne receiver.

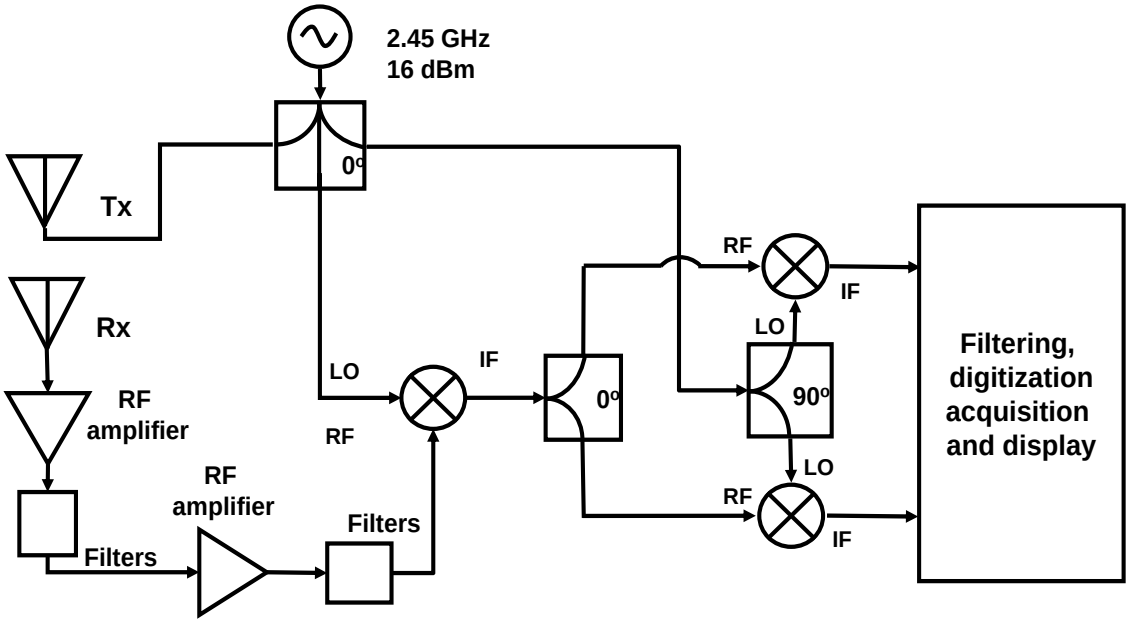

Fig. 5.1 Proposed heterodyne architecture for harmonic radar system.

5.1 Sources of noise in harmonic radar system

The two primary sources of leakage that could result in untagged motion (that is noise to the system) being detected are detected 2.45 GHz in the receiver and transmitted 4.9 GHz. Harmonics can be generated by the signal generator and can propagate in the system to yield undesirable results. A band-pass filter (Mini-circuits VBFZ-2340+) was added before the antenna in order to further suppress any amount of transmitted 4.9 GHz. An attempt to minimize the detected 2.45 GHz is made by adding of two low noise amplifiers (Mini-circuits ZX60-542LN-S+) and four high pass filters (Mini-circuits VHF-3300 and VHF-3100) to the receiver chain before mixing. Although precautions were taken, having a quantitative assessment of each of the sources of leakage would provide a better understanding of the radar system.

As discussed, the primary source of leakage at 4.9 GHz is the signal generator/oscillator itself. The two signal generators in the lab that are frequently used are Agilent E4433B ESG-D series signal generator and HP 83640B series swept signal generator. The output of these signal generators was connected to spectrum analyzer to assess the level of harmonics present. Measurements were made without and with a band pass filter (Mini-circuits VBFZ-2340+) connected at the output of the signal generators to suppress harmonics. The output power from E4433B was set to 15 dBm and for 86340B was set to 12 dBm due to the fact that for 2.45 GHz, power above 13 dBm was unleveled. Fig. 5.2 and Fig. 5.3 show the observed signal levels at 4.9 GHz with and without the connected filter. It can be concluded that most signal sources generate significant amount of harmonics but can be suppressed with the use of one or more filters.

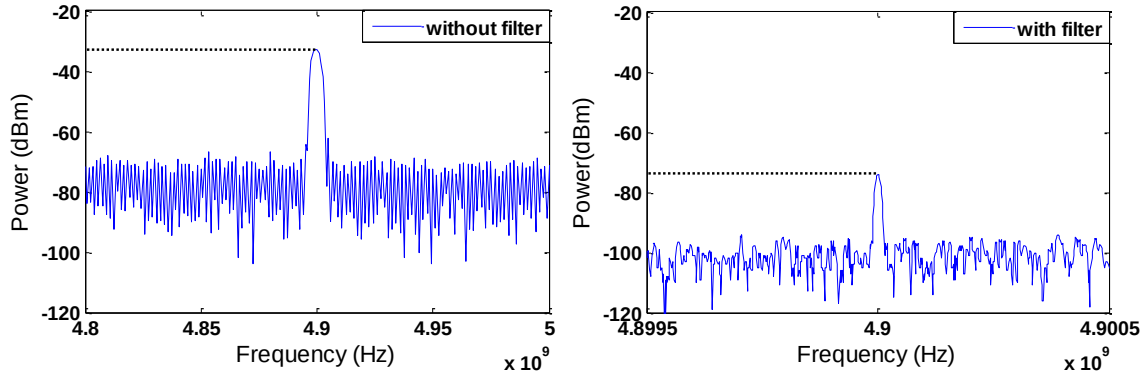

(a) (b)

Fig. 5.2 Output of signal generator E4433B without band pass filter (a) and with band pass filter (b). Note that the in (a), the frequency span is over 500 MHz whereas in (b), the span is 1 MHz.

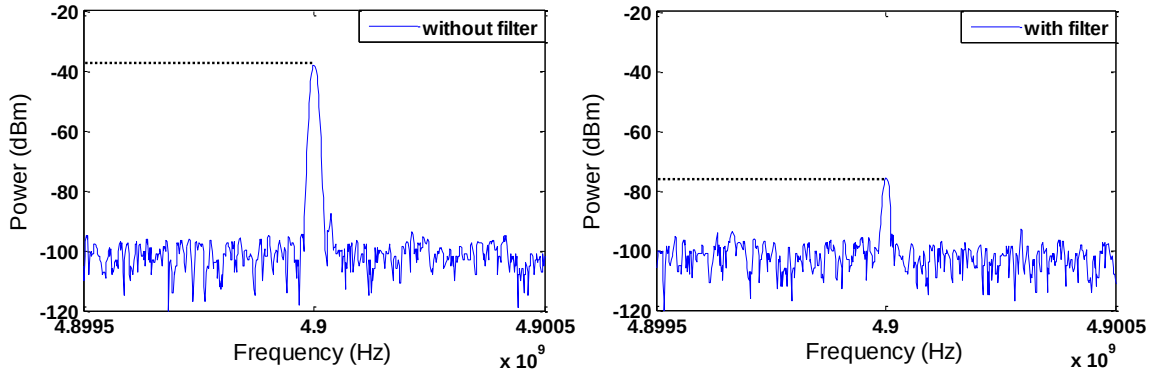

(a) (b)

Fig. 5.3 Output of signal generator HP83640B without filter (a) and with filter (b). A frequency span of 1 MHz was used for both measurements.

In order to assess the presence of any leakage 4.9 GHz signal in the receiver, the output of the receiving antenna was connected to a spectrum analyzer (Part) with transmitting antenna radiating. The signal generator used for most of the measurements is E4433B unless otherwise specified. The power sent to the transmitting antenna was approximately 10 dBm. A band pass filter was connected at the output of the signal generator to suppress the harmonics. First, the signal output at the receiving antenna was

observed (Fig. 5.4(a)). The received signal was measured for 4 cases. The measurements were repeated to observe the signal levels after amplification and filtering (Fig. 5.4(b)). For measurements at 4.9 GHz and 2.45 GHz, the spectrum was centered around 4.9 GHz and 2.45 GHz respectively with a span of 29 kHz. The tests were repeated to observe the effect of amplifiers and filters by observing the signal at the output of receiver signal conditioning chain in the spectrum analyzer. The plots for the two tests and different cases are shown together for comparison.

Case I: No target in front of antennas.

Case II: 20 cm hemisphere (Styrofoam covered with aluminum foil) in front of antennas.

Case III: Harmonic Tag in front of antennas.

Case IV: Analysis at 2.45 GHz with no target in front of antennas.

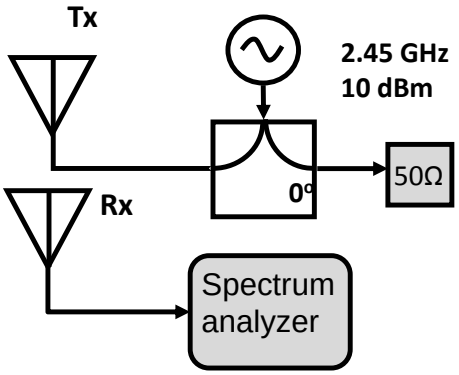

(a)

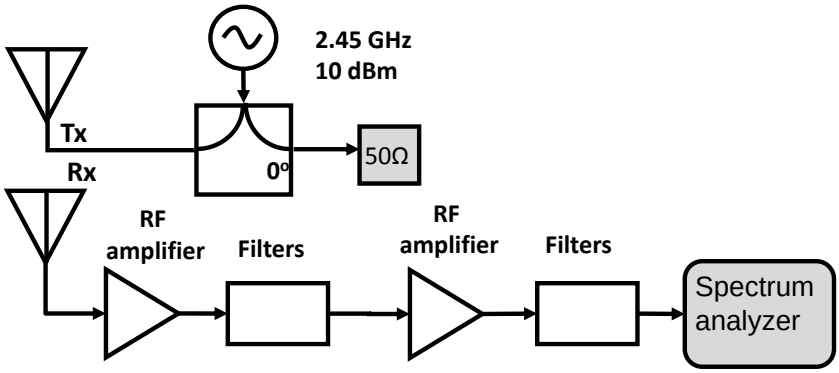

(b)

Fig. 5.4 Test setup for measurement of different signals received by the radar receiver at the receiving antenna (a), and at the output of the receiver signal chain consisting of filters and amplifiers (b).

The results from both test conditions for case I are shown in Fig. 5.5. Without any harmonic tag being present, the system can detect ~-99 dBm of 4.9 GHz signal. This signal gets amplified to -52 dBm after passive through amplifiers. Although, the transmitting antenna is designed for 2.45 GHz, some 4.9 GHz signal will be radiating and thus getting detected by the receiving antenna. We would ideally want such spurious 4.9 GHz transmission to be lower around -130 dBm.

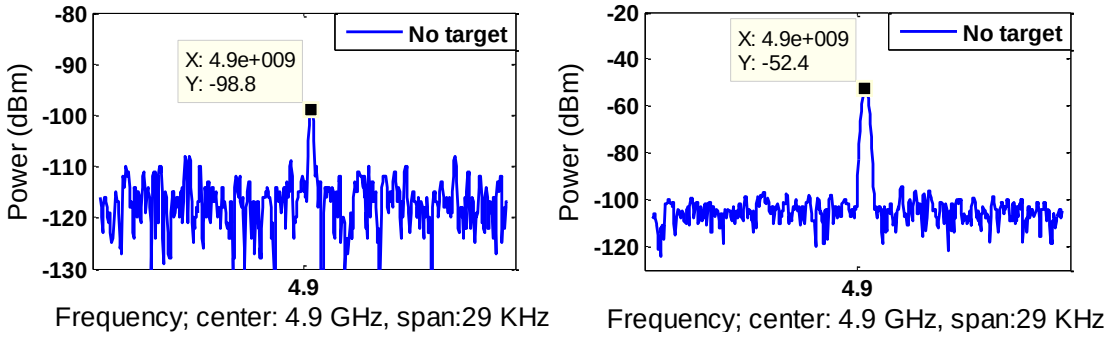

(a) (b)

Fig. 5.5 Spectrum analyzer output for case I with no target present in front of the antennas. Antenna output is shown in (a), and output of the receiver chain connected to antenna output is shown in (b).

From Fig. 5.5, the presence of 4.9 GHz EM field is confirmed. An important test now would be to test the effects of a moving untagged object on this field which could result as noise in the system. A Styrofoam hemisphere having a diameter of 20 cm and covered with aluminum foil was placed at a distance of 1 m from the antennas. Its effect on the power level of detected 4.9 GHz signal is shown in Fig. 5.6. An increase of

approximately 2 dB in the signal is observed. This signal would increase with the physical size of the scatterer.

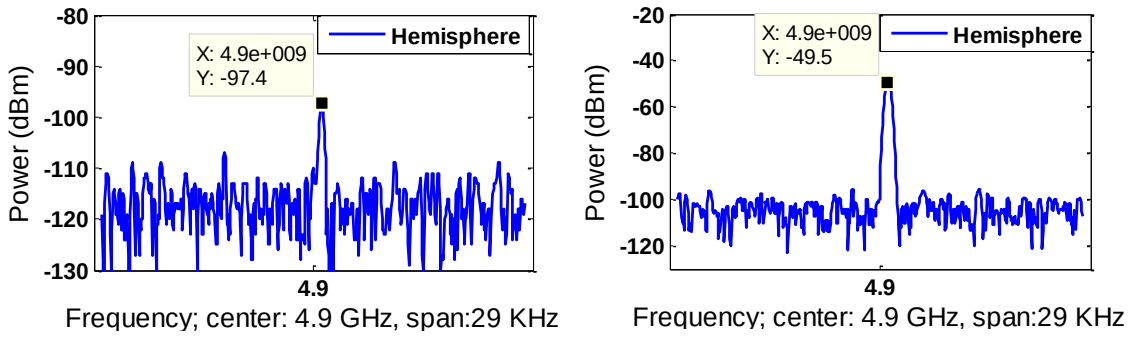

(a) (b)

Fig. 5.6 Spectrum analyzer output for case II with untagged target present in front of the antennas. Antenna output is shown in (a), and output of the receiver chain connected to antenna output is shown in (b).

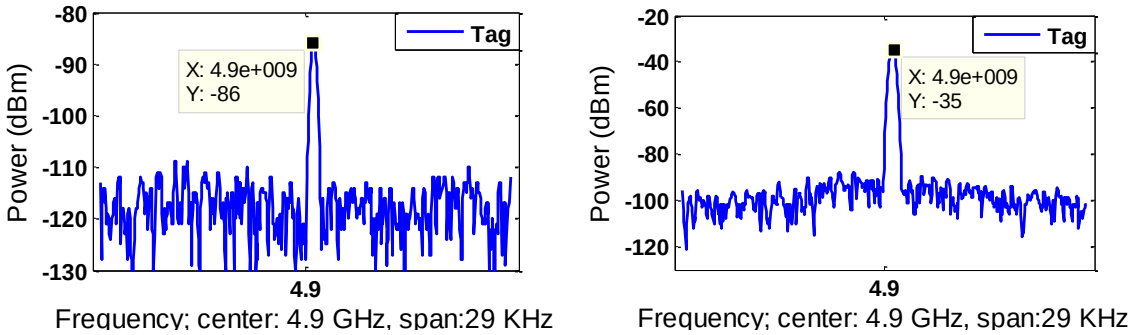

(a) (b)

Fig. 5.7 Spectrum analyzer output for case III with harmonnic tag present in front of the antennas. Antenna output is shown in (a), and output of the receiver chain connected to antenna output is shown in (b).

For harmonic tag to be detectable, the generated signal power at the receiving antenna has to be more than -97 dBm. Fig. 5.7 shows the detected power level when harmonic tag is placed at a distance of 1m from the antennas. After amplification, the

received power is approximately 12-15 dB higher than the detected untagged motion. This corresponds to the results obtained in chapter 4.The other possible cause for detection of untagged signal was attributed to the presence of 2.45 GHz signal in the received signal that could reach the mixing stage. To test the presence of 2.45 GHz signal, the spectrum was centered around 2.45 GHz. The results shown in Fig. 5.8 are very interesting. Fig. 5.8(a) shows the significant level of 2.45 GHz being detected without a target being present at the receiving antenna. However, after signal conditioning by hardware, the level is brought down to noise floor as shown in Fig. 5.8(b).

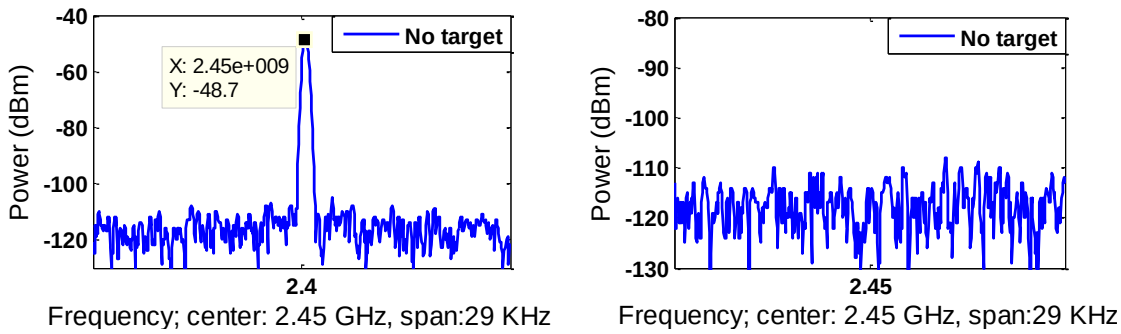

(a) (b)

Fig. 5.8 Spectrum analyzer output at 2.45 GHz for case IV with untagged target present in front of the antennas. Antenna output is shown in (a), and output of the receiver chain connected to antenna output is shown in (b).

To further test the presence of any unintended radiation from the local oscillator chain, the transmitting antenna was disconnected and terminated with 50Ω. By disconnecting the transmitting antenna, the intention was to remove any source of 4.9 GHz radiation. The signal from signal generator was passed through the multiplier and amplifier. The amplifier was also terminated with 50Ω. The measurement set up is shown

in Fig. 5.9(a). For the measurement setup of Fig. 5.9(a), there should not exist any 4.9 GHz in the received signal spectrum. However, even with RF amplifier off, signal strength of approximately -67 dBm was detected. This signal strength was reduced after multiplier was disconnected and the 0^0 splitter was terminated with 50Ω. This radiation from frequency multiplier was verified by eliminating cables and directly connecting the multiplier to the signal generator as shown in Fig. 5.10(a). The resulting detected radiation can be seen in Fig. 5.10(b).

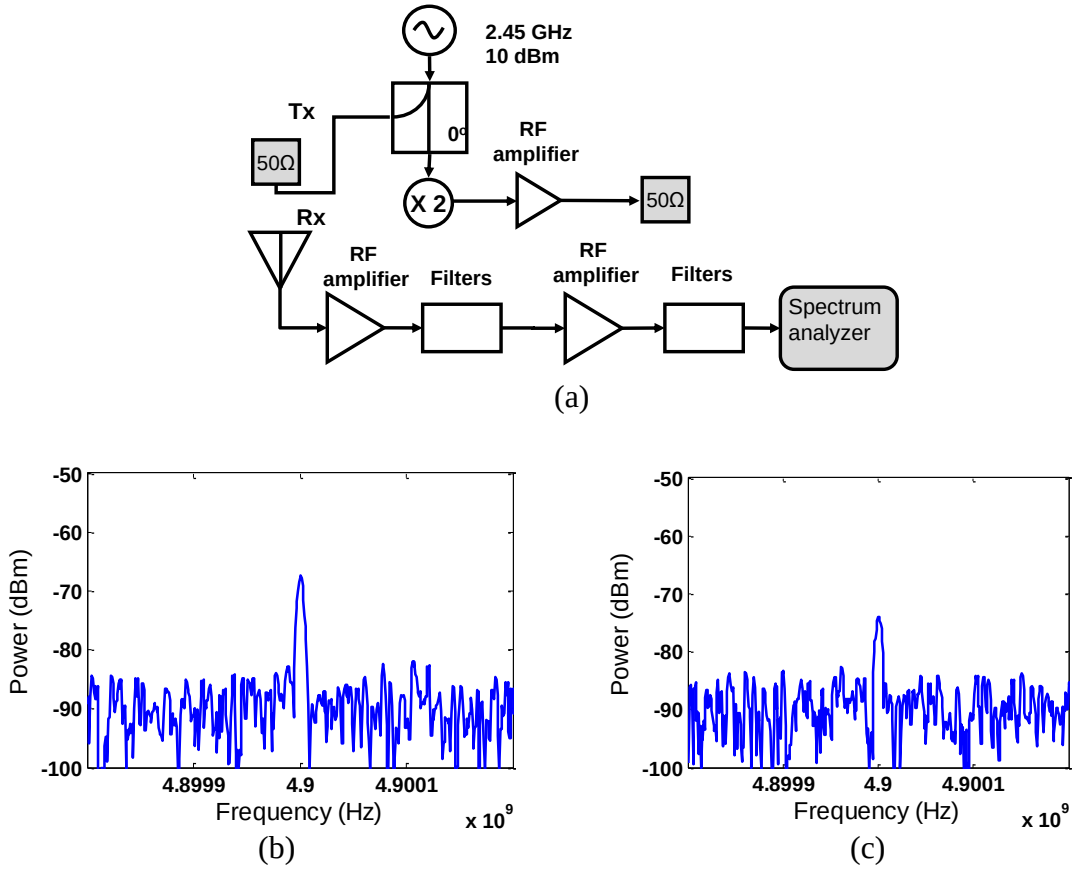

Fig. 5.9 System block diagram for locating the source of transmitted 4.9 signal with the transmitting antenna being replaced by 50 Ω (a), spectrum analyzer output with RF amplifier off (b), and spectrum analyzer output after the multiplier and RF amplifier were disconnected and the splitter was terminated with 50 Ω(c).

(a)

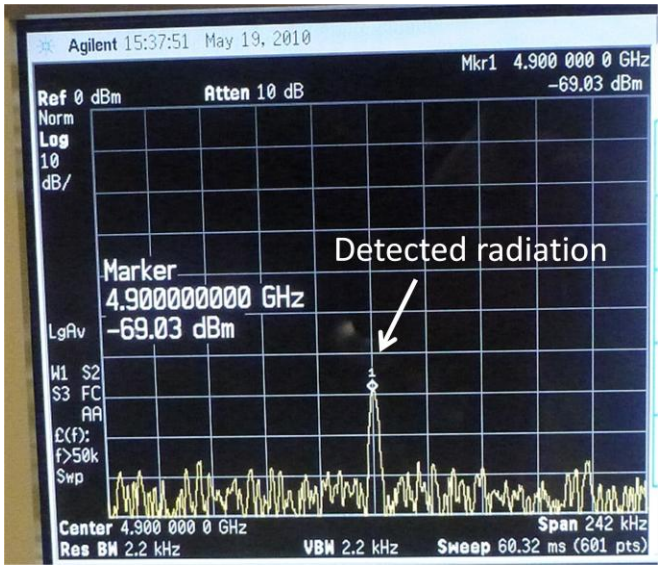

(b)

Fig. 5.10 Verification of radiation from coaxial components, in particular, the frequency multiplier by connecting the components without any cables to the signal generator (a), and the detected signal spectrum (b).

The level of detected 4.9 GHz signal is related to the level of transmitted harmonics from the signal generator and the antenna. The harmonics can be attenuated to a certain level by the use of appropriate filters. As we increase the distance of the tag, the generated harmonic signal from the tag will decrease but the noise floor remains the same. Hence, a reduction in SNR can be expected that limits the range of operation of the tags. However, an increase in range could be compensated by increase in transmitted power but may increase the noise floor. To prevent the noise floor from increasing, more filters could be used before antenna or at the output of the signal generator.

5.2 Heterodyne receiver architecture

For a harmonic Doppler radar under ideal conditions, the received signal would primarily consist of all the reflected signals at transmitted frequency 'f' and the reflected signal by the tag at '2f'. This received signal could be represented as:

$$\begin{aligned} R(t) = {} & A_{rf} \cos\left[\omega t - \frac{2\omega d}{c} - \frac{2\omega x(t)}{c} + \varphi + \theta\right] \\ & + A_{rh} \cos\left[2\omega t - \frac{4\omega d}{c} - \frac{4\omega x(t)}{c} + \varphi + \theta\right] \end{aligned} , \tag{5.1}$$

where the term ωt represents the fundamental frequency of 2.45 GHz, d represents the nominal distance between the transmitting antenna and $x(t)$ is the periodic motion of the target. The terms A_{rf} and A_{rh} represent the amplitude variations corresponding to the received fundamental and harmonic components of signal respectively. The LO signal without the phase noise can be represented as

$$A_L \cos(\omega t) \ . \tag{5.2}$$

After the first stage of mixing, the signal components that would be obtained are:

$$0.5A_{rf}A_L\left[\cos\left(-\frac{2\omega d}{c}-\frac{2\omega x(t)}{c}+\varphi+\theta\right)+\cos\left(2\omega t-\frac{2\omega d}{c}-\frac{2\omega x(t)}{c}+\varphi+\theta\right)\right]$$
$$+0.5A_{rh}A_L\left[\cos\left(\omega t-\frac{4\omega d}{c}-\frac{4\omega x(t)}{c}+\varphi+\theta\right)+\cos\left(3\omega t-\frac{4\omega d}{c}-\frac{4\omega x(t)}{c}+\varphi+\theta\right)\right] \quad (5.3)$$

The component that we are interested in is:

$$0.5A_{rh}A_L\left[\cos\left(\omega t-\frac{4\omega d}{c}-\frac{4\omega x(t)}{c}+\varphi+\theta\right)\right] \quad (5.4)$$

This component can be filtered out using a band pass filter, mixed again with $A_L\cos(\omega t)$ and $A_L\sin(\omega t)$ and low pass filtered to obtain quadrature baseband signals as:

$$B_I = A_B\left[\cos\left(\frac{4\omega d}{c}+\frac{4\omega x(t)}{c}-\varphi-\theta\right)\right]$$
$$B_Q = A_B\left[\sin\left(\frac{4\omega d}{c}+\frac{4\omega x(t)}{c}-\varphi-\theta\right)\right] \quad (5.5)$$

An important possible benefit of the use of heterodyne system over homodyne system is the use of 2.45 GHz as the LO signal throughout the system. As such, the need for a multiplier and RF amplifier is eliminated and the components are instead replaced by a splitter and a mixer. The next section will investigate the phase noise in the receiver and will attempt to find if the phase noise in homodyne system is more than the heterodyne system.

5.3 Phase noise

Phase noise is a term used to describe the short term random fluctuation in the frequency or phase of an oscillator signal. These random fluctuations, that are caused by various noise sources appear as a broad continuous distribution localized about the output

signal as shown in Fig. 5.11. Being close to the oscillation frequency, it cannot be removed with filtering without affecting the oscillation frequency.

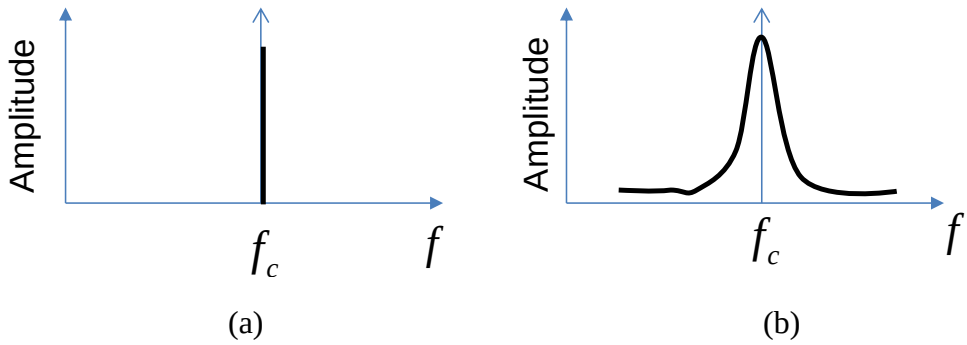

(a) (b)

Fig. 5.11 Ideal transmitter signal (a), and transmitter signal with phase noise (b).

Phase noise is defined as the ratio of power in one phase modulation sideband to the total signal power per unit band width (1 Hz) at a particular offset, f_m, from the signal frequency (Pozar, 2005). It is denoted by $\mathcal{L}(f_m)$ and is typically expressed in decibels relative to the carrier power per Hertz of bandwidth (dBc/Hz). A detailed analysis of phase noise has been presented in (Pozar, 2005). A simplified analysis is presented here for brevity. For an oscillator, the general output voltage is given by

$$v_0(t) = V_0\left[1 + A(t)\right]\cos\left[\omega_0 t + \theta(t)\right] \tag{5.6}$$

By representing small changes in the oscillator frequency as frequency modulation of the carrier where f_m is the modulating frequency,

$$\theta(t) = \frac{\Delta f}{f_m}\sin\left(\omega_m t\right);\ f_m = \frac{\omega_m}{2\pi},$$

phase noise is given by :

$$\mathcal{L}(f) = \frac{\theta_{rms}^2}{2}; \theta_{rms} = \frac{\theta_p}{\sqrt{2}} \ , \tag{5.7}$$

where θ_{rms} is the rms value of the phase deviation.

The process of frequency multiplication causes phase multiplication as well and the noise levels are increased by the multiplication factor for a frequency multiplier (Pozar, 2005). From 5.7, the increase in noise level is given by 20 log n, where n is the multiplication factor. Based on the above equation, it can be calculated that the output of a frequency doubler will be at least 6 dB more than the phase noise of the fundamental oscillator. The presence of amplifier in the system would also affect phase noise although not as much as the multiplier. For a Doppler radar system measuring phase perturbation, phase noise in the system restricts the range and sensitivity of the radar.

A spectrum analyzer was used to observe phase noise of the homodyne and heterodyne system on the LO side at the output of 90^0 hybrid. A phase noise spectrum was obtained beginning at 10 Hz (the lowest permitted by the analyzer) and see if there is a noticeable change in the phase noises of the two systems. Although, the 90^0 splitter for homodyne system (Pasternack PE 2058) is different than heterodyne system (Narda 4033c), it has been assumed that their effect on phase noise is negligible. The transmitted power was 13 dBm from the signal generator (HP83640B). The 0^0 output of the hybrid in homodyne and heterodyne system is shown in Fig. 5.12(a) and the 90^0 output for homodyne and heterodyne system has been shown in Fig. 5.12(b). Note that while phase noise for homodyne system has been measured at a carrier frequency of 4.9 GHz, phase noise for heterodyne system has been measured for 2.45 GHz. The measurements were repeated with Agilent E4433B signal generator to check for consistency. The output

signal was set to 13 dBm. The 0^0 output of the hybrid in homodyne and heterodyne system is shown in Fig. 5.13(a) and the 90^0 output for homodyne and heterodyne system has been shown in Fig. 5.13(b). The plots in general indicate the lower level of phase noise for heterodyne system.

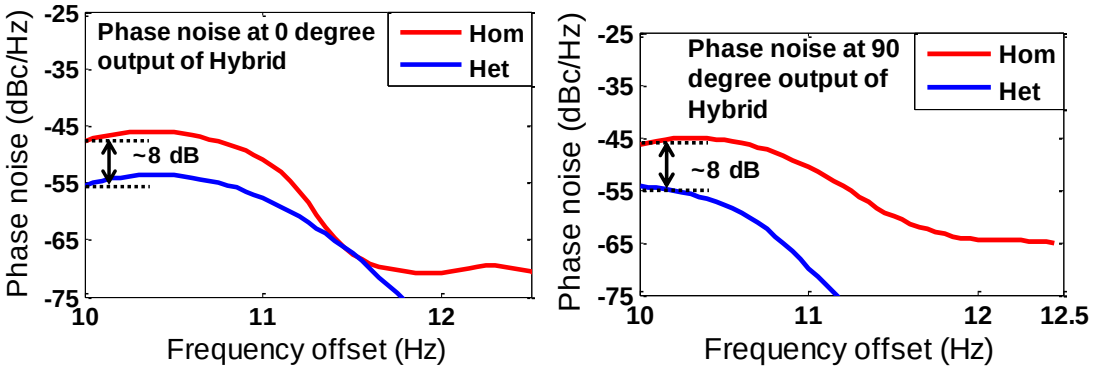

(a) (b)

Fig. 5.12 Measured phase noise for homodyne and heterodyne system using HP83640B at the 0^0output of the hybrid (a), and at 90^0 output of the hybrid (b).

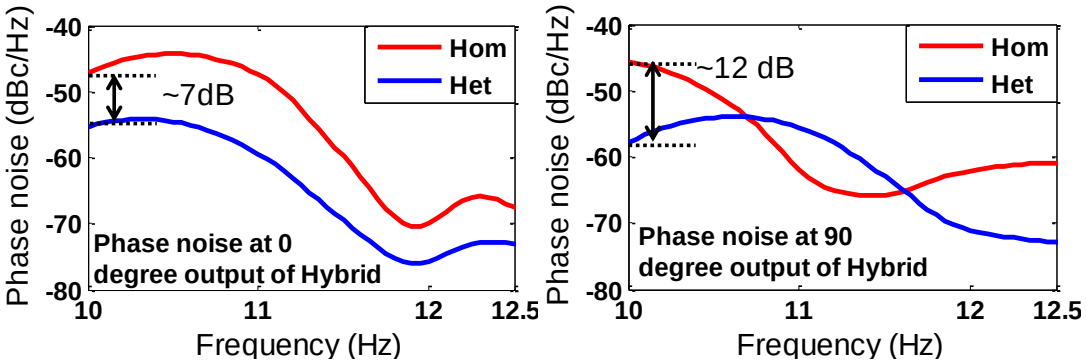

(a) (b)

Fig. 5.13 Measured phase noise for homodyne and heterodyne system using Agilent E4433B at the 0^0output of the hybrid (a), and at 90^0 output of the hybrid (b).

5.4 Measurement results

Measurements need to be made in order to verify the theory and performance of the two receiver systems. For a fair comparison, measurements should be made for both receiver systems together. However, this is rather tricky because the spurious radiations from the multiplier in the homodyne receiver could affect the measurement results for heterodyne receiver. This was observed in the measurement results that were taken with simultaneous operation of both receivers. To circumvent this problem, measurements were taken independently with the two receivers. First, a mechanical target was moved in front of homodyne radar at a distance of approximately 1m. The target was moved at a frequency of 0.5 Hz. After a measurement was taken, the target was replaced with harmonic tag and a measurement was made. The heterodyne receiver was then connected and measurements were repeated with the tag and the target. FFT was performed on the acquired data that was combined using complex demodulation. The results are shown in Fig. 5.14. With the target signal considered as noise, the SNR in the system was calculated and shown below.

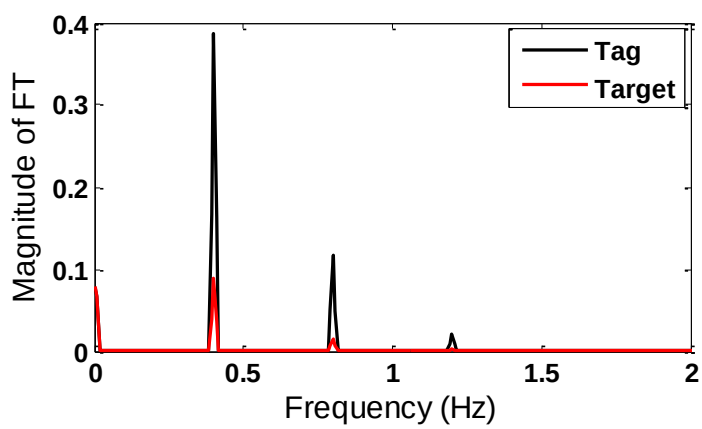

(a)

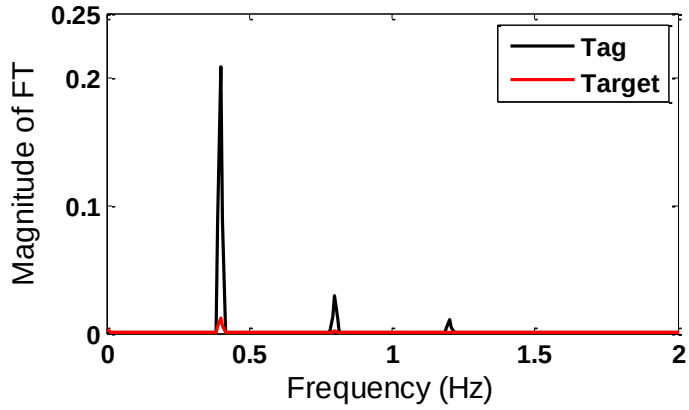

(b)

Fig. 5.14 FFT results comparing the SNR (tag/target) for baseband data acquired from homodyne system (a), and heterodyne system (b).

Table 5.1. Calculation of SNR from FFT analysis of data acquired from homodyne and heterodyne receivers

Receiver	**Distance (cm)**	**Tag (Magnitude)**	**Target (Magnitude)**	**SNR (dB)**
Homodyne	100	0.3875	0.08892	12.78
Heterodyne	100	0.2084	0.01245	24.47

The measurement results indicate that the heterodyne system does provide better rejection of non-tagged objects. The comparison was made using connectorized components for this study that resulted in unintended radiation from some components. These problems may not exist if the design is translated to a printed circuit board or a chip. In such a case, the performance of homodyne and heterodyne receiver may not differ by a large value. However, heterodyne system would still be suitable for board level design as it would replace the use of multiplier, amplifier and filters by a passive mixer, thereby avoiding the use of power lines near the RF transmission lines on the board.

Chapter 6. Displacement Estimation With Tags

Measurements of absolute displacement of thoracic wall using Doppler radar could enable tidal volume and pulse pressure measurements. Pulse pressure, as an independent predictor for myocardial infarction, congestive heart failure, cardiovascular death (Safar, 2000), (Safar, 2001), is of great interest for study of long-term monitoring on hypertensive patients. It is possible to correlate chest cardiac motion displacement with changes in stroke volume and pulse pressure (Singh *et al.*, 2011).

The motion originating from respiration and heart beat results in displacements of chest wall on the order of millimeters to few centimeters depending on the subject. Because the amplitude of the motion is so small, the presence of any other motion in the vicinity can severely distort the signals. The interfering motion can come from either the subject's body parts or from other people moving close by. Another problem is the accuracy of displacement estimation. For example, for the chest motion range of 4-12 mm reported in (Zakrzewski *et al.*, 2012), the quadrature output of the radar receiver at 2.45GHz forms a circular arc of approximately 16% of the corresponding circle. The available arc length brings issue in estimating the arc radius in the process of center estimation (Zakrzewski *et al.*, 2012).

One way to obtain greater resolution is to increase the operating frequency of the radar. As the wavelength decreases, the same amount of motion would result in a larger arc. However, that would still not solve the problem of removing the effects of interfering motion from other sources. Doppler radar with frequency doubling tags (harmonic Doppler radar) has been proven to effectively reject any motion arising from non-tagged

motion (Singh and Lubecke, 2012c). In such radar, a passive tag is put on the subject whose physiological parameters are measured by designing the receiver to receive only the second harmonic generated from the tag. Since the operating frequency of the receiver is doubled, the arc length formed by in-phase and quadrature baseband signals for the same amount of motion is doubled. The increased arc length should result in increased accuracy for center estimation and consequently displacement estimation.

Displacement measurement can be made by the use of arctangent demodulation or non linear phase demodulation with dc coupled data. However, the quadrature data needs to be corrected for any amplitude or phase imbalance before demodulation for accurate displacement estimation. Methods for measurement of amplitude imbalance and phase imbalance for Doppler radar system exist. This chapter will discuss the limitations of the existing methods and propose an efficient and accurate data based quadrature imbalance correction method. We then use this correction technique to investigate the accuracy of displacement estimation through the use of passive harmonic RF tags with Doppler radar systems.

6.1 Data-based quadrature imbalance compensation

Quadrature radio transceivers are subject to amplitude and phase imbalance problems due to hardware imperfections (Abidi, 1995), (Chang *et al.*, 2009), (Rykaczewski *et al.*, 2005). For a communication system transmitter, the primary source of distortion in RF modulators is the presence of in-phase/quadrature (I/Q) imbalance (Cao *et al.*, 2009). These imbalances are known to corrupt signal quality (Fatadin *et al.*, 2008), and thus must be corrected for proper signal extraction. The effects of I/Q

mismatch in a quadrature microwave Doppler radar have been previously documented (Yan *et al.*, 2010).

Coherent optical communication systems use Gram Schmidt (GS) or ellipse correction (EC) methods to compensate and correct for imbalances. The EC method employs a least square fit to match data to an ellipse which is then used for correcting the orthogonality of the IQ signals by a known transformation (Chang *et al.*, 2009). The GS ortho-normalization method uses a set of equations to transform the data into an orthonormal set of vectors (Rykaczewski *et al.*, 2005). Digital communication receivers' use advanced digital signal processing techniques (DSP) to automatically correct for the imbalances that cannot be applied to Doppler radar for physiological sensing (Park, Yamada, and Lubecke, 2007). Application of the GS method for Doppler radar data requires *a priori* information about the amplitude and phase imbalance (Cao *et al.*, 2009). These factors are used to correct the received data.

Unlike optical communication systems data that result in a complete ellipse or circle, data obtained from CW Doppler may not always produce a complete ellipse. For a communication system employing QPSK, baseband data is always a complete circle and emphasis is laid on correcting the phase between data circles. For a Doppler radar system, the arc produced by baseband signals can provide information about the rate of the motion, the size of the target and the absolute displacement of the target. As such, accuracy is dependent on correction of imbalances and the emphasis is on correcting the shape of the arc. The percentage of ellipse obtained in a Doppler radar system is a function of motion amplitude and frequency. At 2.45 GHz, respiratory motion (1 cm-2 cm) will constitute 15-30 percent of a closed 360° loop which makes ellipse correction a

challenging proposition. To extract correction coefficients for GS method, a more complete data sample is required. A method for measurement of amplitude imbalance and phase imbalance for a single antenna quadrature Doppler radar system using the GS method has been described (Park, Yamada, and Lubecke, 2007). This method requires adding phase shifters to simulate a moving target in front of the radar and produce a more complete phase cycle. However, it may not always be practical or desirable to make a modification to an existing radar system for such measurements. Another method of imbalance measurement involves using two synchronized oscillators to feed in RF and LO signals at slightly different frequencies and use time domain analysis to measure the imbalance factors. However, this method is not suitable for single antenna systems involving a circulator. The imbalance measurement method should be such that it could be used without any modification with different Doppler radar system architectures, at the user's convenience.

In this chapter, an efficient and accurate data-based quadrature imbalance correction method that does not involve any hardware modification will be proposed and studied. A mechanical target is used that provides a sufficient arc length to perform the best fit ellipse method for calibration. The imbalance coefficients determined from the best fit ellipse method are used to perform Gram-Schmidt correction. Simulations were carried out to examine the effectiveness of this method as a function of ellipse segment in the presence of noise. Experimental results, consistent with simulations, indicate that phase and amplitude imbalances measured with this method are obtained with high accuracy.

6.1.1 Effect of imbalances on radar data

In radio and optical communications systems, channel imbalance factors causes insufficient image rejection, increases bit error rates, deteriorate achievable SNR, and have evident impact on the baseband spectrum (Chang *et al.*, 2009), (Yan *et al.*, 2010), (Umstattd, 1993), (Valkama *et al.*, 2001). Fig. 6.1(a) and Fig. 6.1(b) depict the effects of phase imbalance (in degrees) and amplitude imbalance, respectively, on Doppler radar displacement measurements simulated for sinusoidal motion with 4cm of displacement. The simulated IQ data with imbalances was demodulated using an arctangent demodulation technique (Park, Boric-Lubecke, and Lubecke, 2007) to yield the displacement. The simulation was performed for typical values of imbalance observed in quadrature systems. Fig. 6.1(c) shows the effects of amplitude imbalance and phase imbalance on displacement when the phase imbalance is fixed at 20 degrees and amplitude imbalance is varied. Channel imbalance in Doppler radar physiological monitoring systems may introduce errors in rate estimation, radar cross section (RCS) and volumetric measurements due to distortion in demodulated data as shown in Fig. 6.1 (Singh *et al.*, 2012e). For example, it can be observed from Fig. 6.1(b) that an amplitude imbalance of 3dB would result in a displacement estimation of 3.43 cm, which corresponds to an error of 14%. From Fig. 6.1(a), it can be observed that the effect of phase imbalance is not symmetric for the maximum and minimum but the effects of amplitude imbalance are symmetric for Fig. 6.1(b). Demodulation of data from systems containing both imbalances would further deteriorate the estimation of physiological parameters as shown in Fig. 6.1(c).

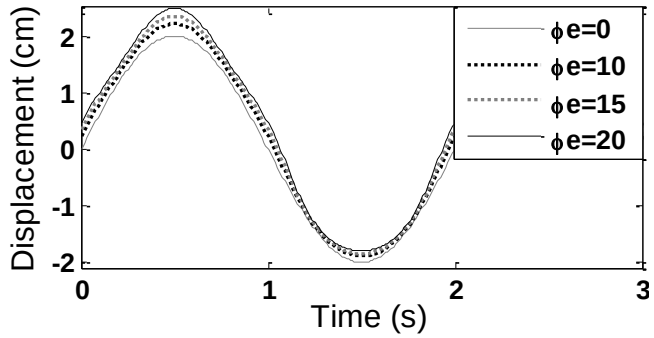

(a)

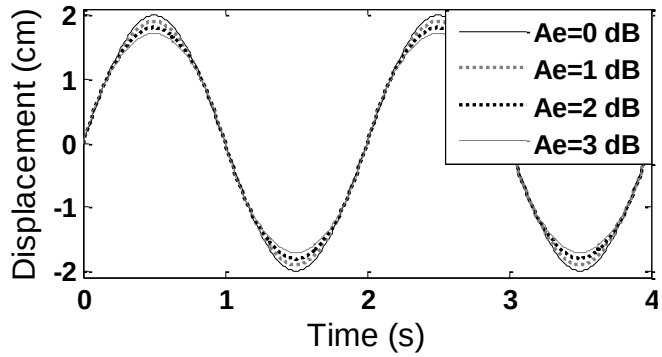

(b)

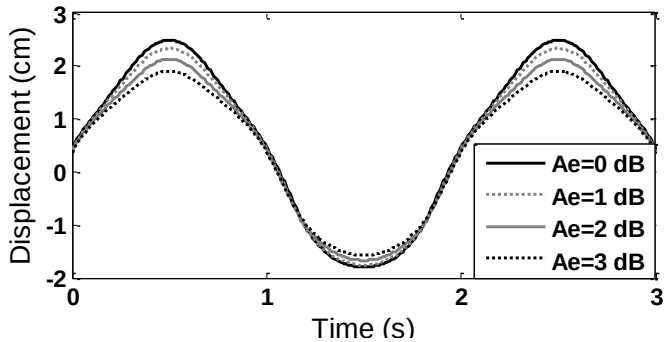

(c)

Fig. 6.1 Effect of imbalances on Doppler radar system. Effect of phase imbalance on displacement when there is no amplitude imbalance present in the system (a), effect of amplitude imbalance on displacement when there is no phase imbalance present in the system (b), and effect of amplitude imbalance on displacement when a phase imbalance of 20 degrees is present in the system (c).

6.1.2 Imbalances and ellipse equation

In a quadrature Doppler radar system, the signals in I and Q channel can be represented by:

$$I = A_I \cos(\frac{4\pi x(t)}{\lambda} + \phi_I) + B_I \tag{6.1}$$

$$Q = A_Q \sin(\frac{4\pi x(t)}{\lambda} + \phi_Q) + B_Q \tag{6.2}$$

where B_I and B_Q represent dc offsets, *x(t)* is the time varying displacement of the target, λ is the radar wavelength, the amplitude imbalance is $A_e = \frac{A_Q}{A_I}$, and the phase imbalance is $\phi_e = \phi_Q - \phi_I$. By expanding (6.2) and combining with (6.1) we have

$$\left(\frac{Q}{A_Q} - \frac{B_Q}{A_Q}\right)^2 + \left(\frac{I}{A_I} - \frac{B_I}{A_I}\right)^2 - 2\left(\frac{Q}{A_Q} - \frac{B_Q}{A_Q}\right)\left(\frac{I}{A_I} - \frac{B_I}{A_I}\right)\sin\left(\phi_e\right) - \cos^2(\phi_e) = 0 \ . \tag{6.3}$$

Here, the coefficients of the Q^2, I^2 and IQ terms are of interest. After expanding (6.3), we get

$$\frac{A_I^2}{A_Q^2} Q^2 + I^2 + 2\frac{A_I}{A_Q}\sin(\phi_e) QI .... = 0 \ . \tag{6.4}$$

Knowing that

$$A_e = \frac{A_Q}{A_I} \quad , \tag{6.5}$$

equation (6.4) can be written as

$$\frac{Q^2}{A_e^2} + I^2 + \frac{2\sin(\phi_e)}{A_e} QI \ldots = 0 \quad . \tag{6.6}$$

The normalized standard equation of an ellipse (I is the horizontal axis, and Q is the vertical axis) could be written as

$$I^2 + A \times Q^2 + B \times IQ + C \times I + D \times Q + E = 0 \ . \tag{6.7}$$

Comparing the coefficients of (6.6) and (6.7), amplitude imbalance and phase imbalance can be determined as

$$A_e = \sqrt{\frac{1}{A}} \text{ and } \phi_e = \sin^{-1}\left(\frac{B}{2\sqrt{A}}\right) \ . \tag{6.8}$$

Assuming we have measured N (N>>5) samples of data (I_1, Q_1), (I_2, Q_2)…..(I_N, Q_N), in an ideal situation, all of these N points would satisfy the ellipse equation, as following:

$$A \times Q_N{}^2 + B \times I_N Q_N + C \times I_N + D \times Q_N + E = -I_N{}^2 \ . \tag{6.9}$$

Let the coefficient matrix of the above linear system be an N by 5 matrix.

$$M = \begin{bmatrix} Q_1^2 & I_1 Q_1 & I_1 & Q_1 & 1 \\ \vdots & \vdots & \vdots & \ddots & \vdots \\ Q_N^2 & I_N Q_N & I_N & \cdots & 1 \end{bmatrix}, \tag{6.10}$$

and let the right hand side of the linear system be

$$b = \begin{bmatrix} -I_1^2 \\ \vdots \\ -I_N^2 \end{bmatrix} \quad . \tag{6.11}$$

The best solution for A, B, C, D, E can be found as (Strang, 2003)

$$\begin{bmatrix} A' \\ B' \\ C' \\ D' \\ E' \end{bmatrix} = \left(M^T M\right)^{-1} M^T b \quad . \tag{6.12}$$

Once the coefficients have been estimated, the imbalance factors can be computed using (6.8) and GS method can be applied to correct the data.

6.1.3 Simulation Results

6.1.3.1 Basic simulation

Simulations were performed in MATLAB® to test and validate the theory. Baseband signals corresponding to respiratory data were generated using equations (6.1) and (6.2) and imbalances were introduced in Q channel. For a quadrature Doppler radar, the arc transcribed in the IQ plane is a function of the transmitted frequency (wavelength) and displacement of the target. At 2.45 GHz, a target displacement of approximately 6.1 cm (half-wavelength) would result in a complete circle. The best fit ellipse method was then used to extract the values of amplitude and phase imbalance. Simulations were performed for different values of imbalance as shown in Fig. 6.2 (Singh *et al.*, 2012e). For these proof-of-concept tests, we generated noise free data that would generate a full

ellipse in the I/Q plot. It was found that for all cases, the error of calculated imbalance factors was less than 10^{-13} units/degrees.

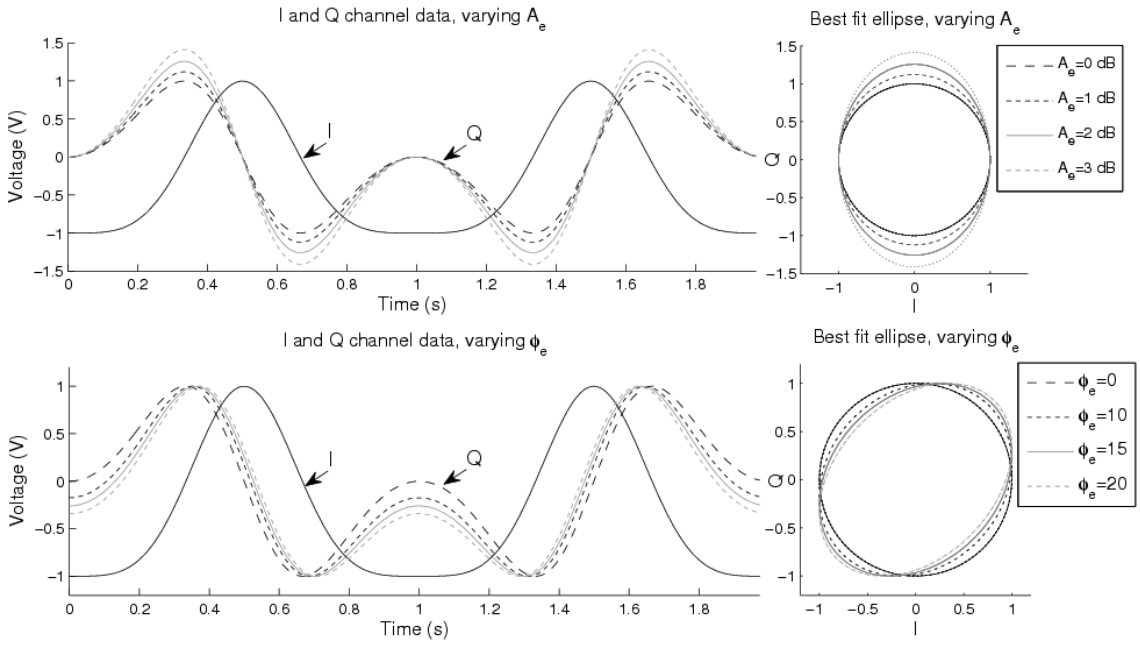

Fig. 6.2 Time domain and I/Q plots for simulated baseband data with varying amplitude imbalance A_e values, while phase imbalance φ_e was zero (a), and varying phase imbalance φ_e, while amplitude imbalance A_e was one (b). The imbalance values were accurately calculated by the best fit ellipse method.

6.1.3.2 Parametric analysis

Simulations were performed in MATLAB® to analyze the accuracy of this method for different percentages of ellipse available and for varying noise to signal ratio (NSR). In this analysis, the noise to signal ratio (NSR) is a parameter that controls the magnitude of uniform noise applied to the baseband I and Q signal. With the noise, the original I signal becomes:

$$I = A_I \cos(\frac{4\pi x(t)}{\lambda} + \phi_I) + B_I + N_I(t) \quad , \tag{6.11}$$

where $N_I(t)$ is a uniform random signal with amplitude within the interval (-NSR × A_I; NSR × A_I), varying with time. The original Q signal becomes:

$$Q = A_Q \sin(\frac{4\pi x(t)}{\lambda} + \phi_Q) + B_Q + \frac{A_Q}{A_I} N_Q(t) \quad , \tag{6.12}$$

where $N_Q(t)$ is a uniform random signal with amplitude within the interval (-NSR × A_Q; NSR × A_Q) , varying with time. The effect of varying level of noise on simulated baseband data is shown in Fig. 6.3.

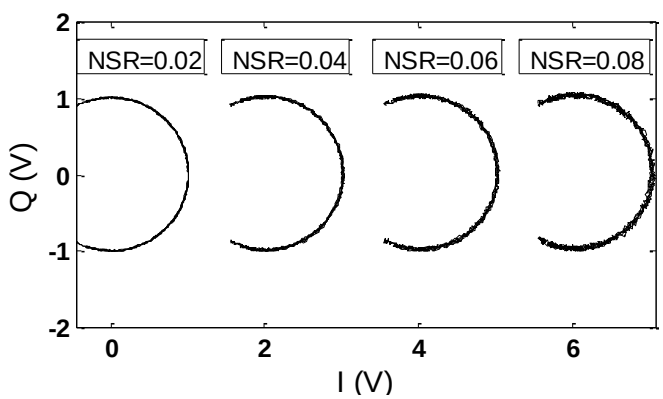

Fig. 6.3 Effect of uniform noise on simulated baseband data for 65% circle (4 cm motion at 2.45 GHz).

The amplitude imbalance and phase imbalance of I and Q signal were pre-set (A_e=2, ϕ_e=20) for simulation, and the percentage of ellipse was varied. At the same time, noise was added to the signals. The computed amplitude and phase imbalance values were compared to the pre-set values. Each simulation was performed 100 times and the average values for amplitude and phase imbalance were stored. Fig. 6.4 shows the

average percent error of amplitude and phase correction obtained using the best ellipse fit method in presence of specified noise levels. It is evident that with higher noise level, a greater percentage of ellipse data (longer motion) is required in order to correctly estimate the imbalance factors. It is interesting to note that phase imbalance can be obtained more accurately than amplitude imbalance for the same NSR. It can be concluded that amplitude and phase imbalances can be calculated with sufficient accuracy for any data transcribing more than 70% of the arc in the I-Q plane.

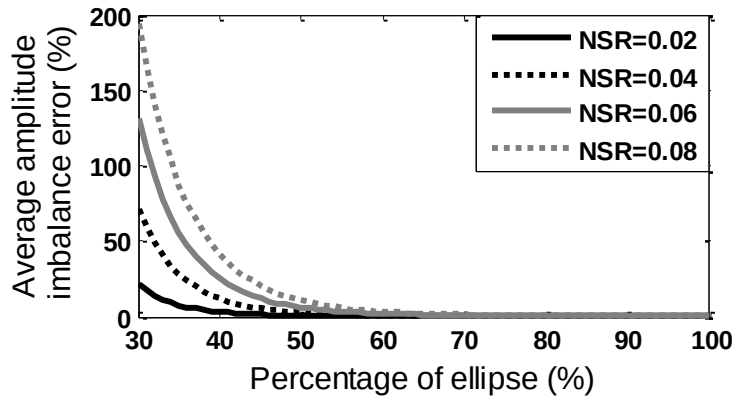

(a)

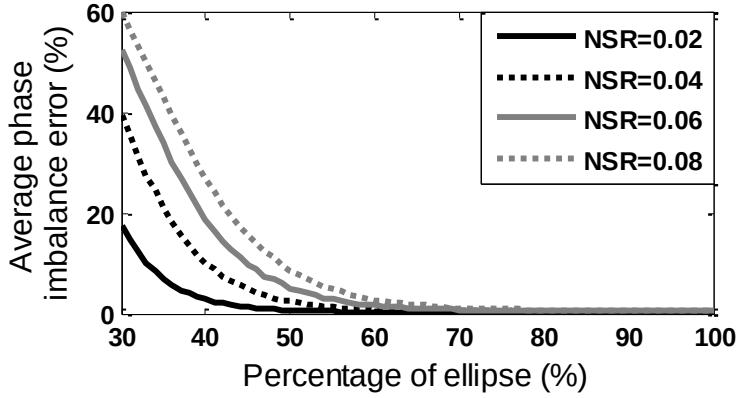

(b)

Fig. 6.4 Percentage of error in computed imbalances as a function of percentage of ellipse available and noise to signal ratio for amplitude imbalance (a) and phase imbalance (b).

6.1.4 Measurements

A measurement was set up to compare the data based imbalance measurement method with an existing method (Park, Yamada, and Lubecke, 2007). The imbalance factors were obtained using a time domain direct measurement method and best fit ellipse method as described below. The imbalance factors were then used to correct the data and estimate the absolute displacement for a known displacement. A 2.4 GHz quadrature Doppler radar system was used for this test. The Doppler radar was assembled using a signal generator, and following off-the-shelf coaxial components: transmit and receive antennas (Antenna Specialist ASPPT2988), two zero-degree power splitters (Mini-circuits ZFC-2-2500), one 90^0 power splitter (Mini-circuits ZX10Q-2-25-S+), and two mixers (Mini-circuits ZFM-4212). Quadrature outputs were dc coupled, pre-conditioned by SR560 low noise amplifiers.

In the first measurement, two external phase shifters were connected in the transmitting signal path, between a 0^0 splitter and the antenna. A metal plate was put in front of the antenna at a fixed distance to simulate a moving target at a constant velocity. Two identical phase shifters were connected in series to create a phase delay of 360° (180° each), and a saw-tooth control voltage of 1.513 V_{pp} was applied. The IQ outputs in time domain are shown in Fig. 6.5. A notch can be observed in each I and Q trace as marked with a grey circle. The notches occur at the same time in both channels and indicate a sudden dc change. However, time domain direct measurement method can still be applied to the raw IQ data since the notches do not affect the positive peaks. A similar notch can also be observed in (Park, Yamada, and Lubecke, 2007). The amplitude imbalance was estimated to be 0.94 as the ratio of Q and I output amplitudes. The phase

imbalance was estimated to be 9.58° from the time difference of the closest two peaks of I and Q outputs. For data based imbalance computation measurement, a precision linear stage (Single-Axis Series CDS-3310) from Galil motion control (Galil, 2012a) with an aluminum foil covered target (a Styrofoam hemisphere of 20-cm diameter) was used to provide motion in front of the radar (Fig. 6.6). The motion was sinusoidal with a frequency of 1 Hz, and measurements were made for different displacements as shown in Table 6.1.

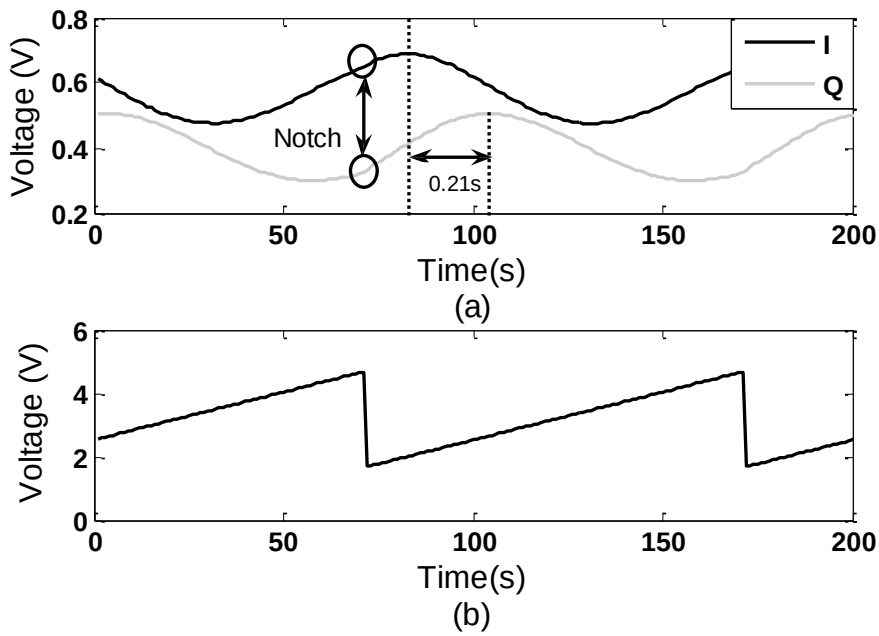

Fig. 6.5 Measurement results using phase shifter method. I and Q data from which amplitude and phase imbalances were estimated (a), and saw-tooth waveform generated to get the required phase shift (b). A notch is always observed with the cycling of sawtooth waveform.

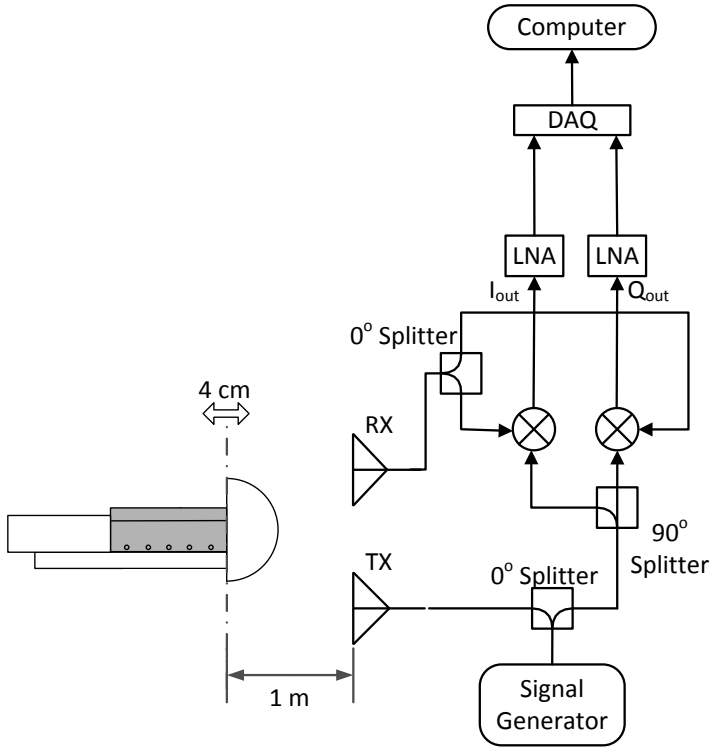

Fig. 6.6 Schematic of radar setup for data based imbalance compensation.

Table 6.1. Imbalance values calculated from phase shifter method and data based ellipse fit method. The imbalance values obtained from 4 cm are highlighted and have been used for GS correction and analysis.

Method	$\mathbf{A_e}$	Φ_e
Phase shifter	0.94	9.58
Data based Ellipse fit Displacement (cm)		
1	0.92	4.40
1.5	0.95	4.91
2	0.95	5.16
2.5	0.88	5.49
3	0.86	6.06
3.5	0.85	7.11
4	**0.83**	**8.62**

Table 6.1 shows the imbalance values obtained from different measurement scenarios. The IQ plot of the measurement for a 4-cm displacement and the best fit ellipse obtained from the proposed method are shown in Fig. 6.7(a), indicating that the best fit ellipse fits the arc very well. When compared to Fig. 6.4, I/Q data in Fig. 6.7(a) could correspond to a noise to signal ratio of 0.08 or more. The best fit ellipse method returns the value of the amplitude imbalance as 0.83 and the phase imbalance as 8.62^{o} for a 4-cm displacement.

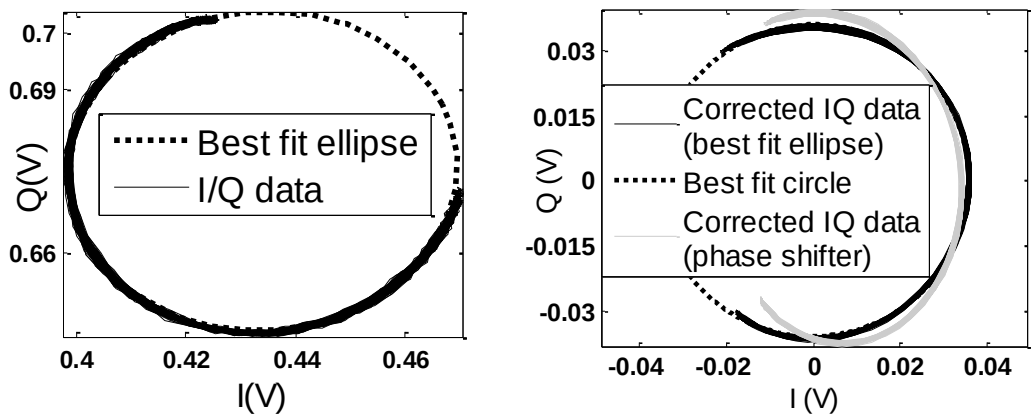

(a) (b)

Fig. 6.7 Plot of I/Q data and the best fit ellipse for 4-cm displacement (a), and corrected 4-cm motion for I/Q data using computed imbalance values from best fit ellipse method and phase shifter method (b). Note that line width for I/Q data in (a) has not been increased.

The imbalance factors were applied in the GS procedure to the experiment data obtained from the mechanical target. The measured data before the correction is shown in Fig. 6.7(a) and data after correction is shown in Fig. 6.7(b). From the figure, it is evident that with the imbalance values obtained by the best fit ellipse method, the GS procedure effectively corrects the imbalance of the original I and Q signals from the 4-cm linear

stage motion measurement, and produces a more circular arc than correction using the phase shifter method. From table 6.1, it can be observed that the data based ellipse fit method yields more consistent values for more than 50% of the transcribed ellipse (3 cm) which is consistent with the simulation results of Fig. 6.4. The imbalance values obtained from the 4-cm measurement were applied for GS correction for all displacements. The data after GS correction were analyzed through arctangent demodulation in order to obtain absolute displacement. Results in the form of displacement estimation, reference, and error are shown in table 6.2. Reference displacement was obtained using Galil motion control software GalilTools (Galil, 2012b). Its motion programming and real-time data capture functions provided precise motion control and reference information.

Table 6.2. Displacement estimation after GS correction using imbalance values obtained from phase shifter method and data based ellipse fit method (4 cm).

Displacement (cm)	**Estimated displacement with correction**			
	Phase shifter		Data-based ellipse fit (4cm)	
	(cm)	Error (cm)	(cm)	Error (cm)
1	0.949	0.051	1.075	0.075
1.5	1.399	0.101	1.578	0.078
2	1.854	0.146	2.080	0.080
2.5	2.322	0.205	2.568	0.068
3	2.826	0.174	3.065	0.065
3.5	3.335	0.165	3.574	0.074
4	3.869	0.131	4.097	0.097

It can be deduced from table 6.2 that correction using the data based ellipse-fit method results in less error than with the phase shifter method. These measurements were repeated in a random manner several times over a period of a couple of weeks. Fig. 6.8

displays a comparison of calculated error rate for 4-cm displacement data given by both methods. The data in table 6.2 corresponds to group number 4 in Fig. 6.8. The transmitted power was changed for some measurements as indicated in Fig. 6.7. It was observed that the data based ellipse fit method results in less variation and more consistent and accurate estimation of imbalance factors than the phase shifter method, and thus leads to more accurate calculation of absolute displacement.

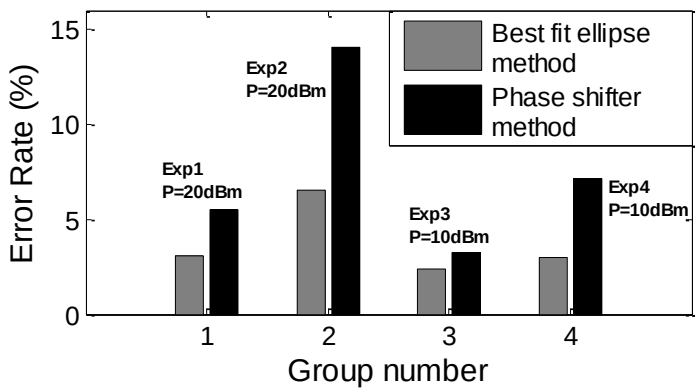

Fig. 6.8 Comparison of accuracy of the two methods by displacement estimation of 4-cm motion for different measurements. In general, imbalance values estimated using the data based best fit ellipse method give more accurate displacement estimation than the phase shifter method.

6.2 Displacement measurement with harmonic tag

6.2.1 Simulation

Displacement information was extracted for simulated baseband signals at 2.45 GHz and 4.9 GHz using arctangent demodulation algorithm (Gao *et al.*, 2012b). The expression for simulated quadrature baseband signals is shown in (6.13):

$$
\begin{aligned}
B_{i1} &= \cos(4\pi x(t) / \lambda_{2.45}) \\
B_{q1} &= \sin(4\pi x(t) / \lambda_{2.45}) \\
B_{i2} &= \cos(4\pi x(t) / \lambda_{4.9}) \\
B_{q2} &= \sin(4\pi x(t) / \lambda_{4.9})
\end{aligned}
\tag{6.13}
$$

where

$$
x(t) = \frac{D}{2}\cos(2\pi ft) \tag{6.14}
$$

B_{i1} and B_{q1} are the baseband signals from conventional 2.45GHz radar receiver, while B_{i2} and B_{q2} represent the counterparts for harmonic 4.9 GHz radar receiver. $x(t)$ is the periodic motion of the target, while D and f are denoting the motion's displacement and frequency. In accordance with the experiment, target motion was simulated with 1.0 cm displacement at 0.3 Hz oscillation, simulating respiratory motion.

Fig. 6.9 compares the ideal baseband signals from both frequencies on I/Q plot in complex plane. It is evident that at harmonic radar frequency of 4.9 GHz, a longer arc is formed. After arctangent demodulation, displacement information was acquired for both cases and plotted in Fig. 6.10 overlapped with the reference displacement generated from Eq. (6.14). From Fig. 6.10 we can see that arctangent demodulation provides perfect estimation for displacement on the ideal baseband signals. The estimation agrees well with its reference of 1.0 cm sinusoidal motion. In the following section, arctangent demodulation algorithm will be applied on the measured baseband signals from two receivers, and displacement estimation results will be compared.

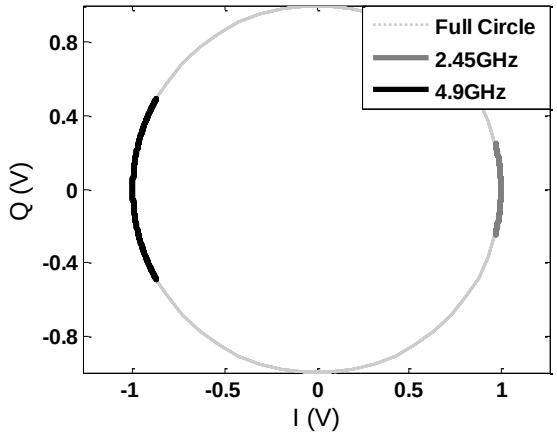

Fig. 6.9 Comparison of ideal I/Q channel baseband signals forming an arc at 2.45 GHz (grey) and 4.9 GHz (black).

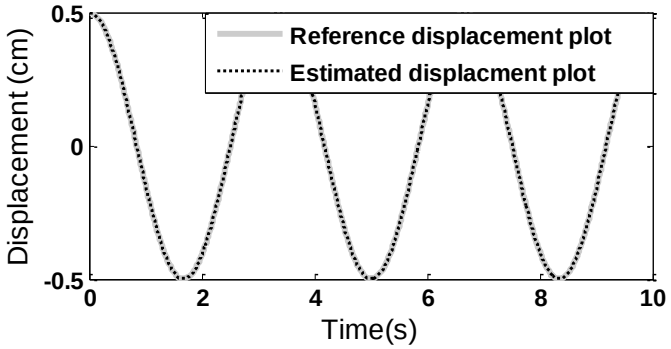

(a)

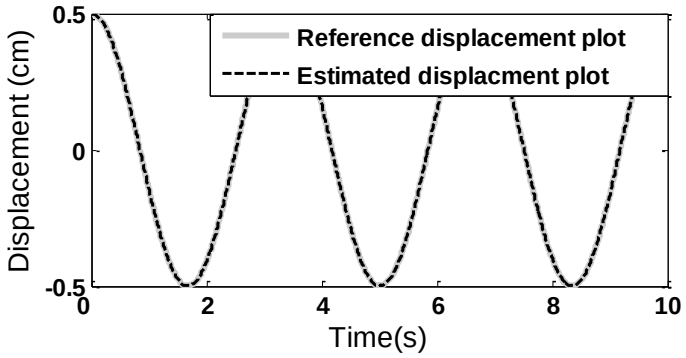

(b)

Fig. 6.10. Displacement estimation results for ideal 2.45 GHz radar baseband signal (a), and ideal 4.9 GHz radar baseband signal (b).

6.2.2 Experiment

Displacement measurement was performed on the 2.45 GHz and 4.9 GHz Doppler radar systems using the designed harmonic tag. Two block diagrams displaying the structure of measurement systems are shown in Fig. 6.11.

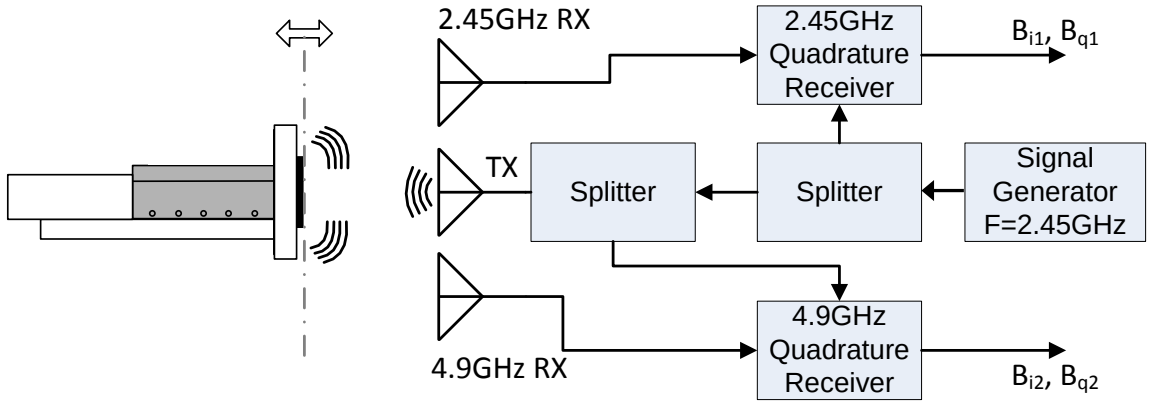

(a)

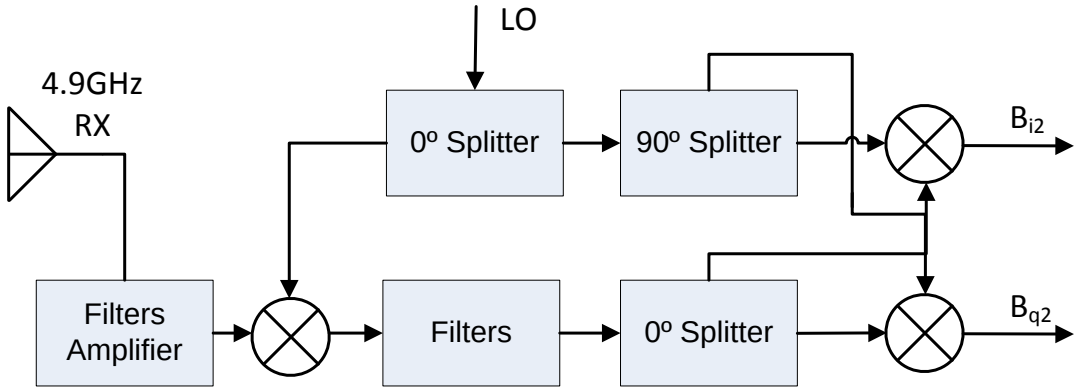

(b)

Fig. 6.11 Block diagram of displacement measurement system with simultaneous operation of both receivers (a), and receiver architecture for 4.9 GHz radar receiver (b).

The two quadrature Doppler radar systems were connected to operate together. One transmitting antenna and two receiving antennas; one for each radar system were connected. The heterodyne architecture discussed in chapter 5 was used for receiving 4.9 GHz signal. The linear stage was programmed using GalilTools, for displacement values from 5mm to 50 mm, with increments of 5 mm. A harmonic tag was placed over a Styrofoam mounted on linear stage, which was put 95 cm away from the antenna. The harmonic tag acted as a backscatter for 2.45 GHz as well. Each experiment lasted 60 seconds, and data was acquired at a rate of 100 Samples/s using a DAQ (NI-USB 6259).

The baseband signals from Doppler radar were digitally processed with arctangent demodulation algorithm for extracting displacement information. According to Park *et al.* (Park, Yamada, and Lubecke, 2007), imbalance compensation technique should be taken into account for both sets of raw data. However, considering the fact that short displacements forming small arcs may lead to ambiguity in estimation, a system calibration technique described in Gao *et al.* (Gao *et al.*, 2012a) was applied. Baseband signals from the motion with displacement of at least 60% of the carrier wavelength were used during calibration to obtain imbalance factors. Specifically, amplitude imbalance and phase imbalance determined from 2 cm target motion were chosen for 4.9 GHz radar calibration, and those of the 4 cm target motion were chosen for 2.45 GHz radar calibration. Plotted in Fig. 6.12 is the I/Q plot comparison between measured 2.45 GHz baseband signals and 4.9 GHz baseband signals. The length difference between the two agrees with the previous simulation in Fig. 6.9.

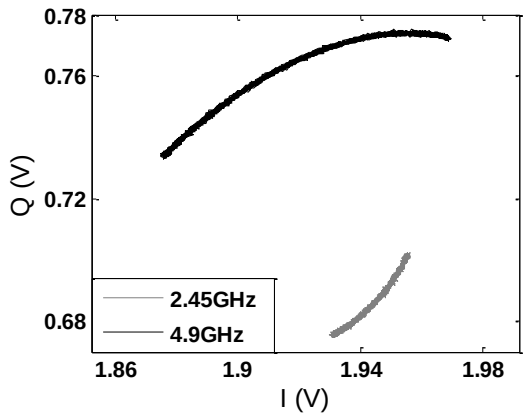

Fig. 6.12 Comparison of measured I and Q channel signals forming an arc at 2.45 GHz (grey) and 4.9 GHz (black).

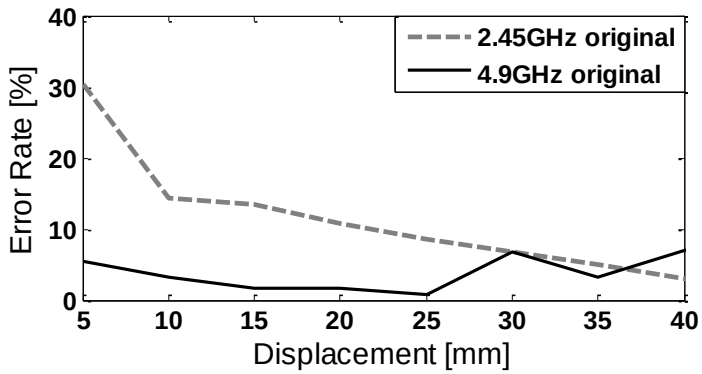

(a)

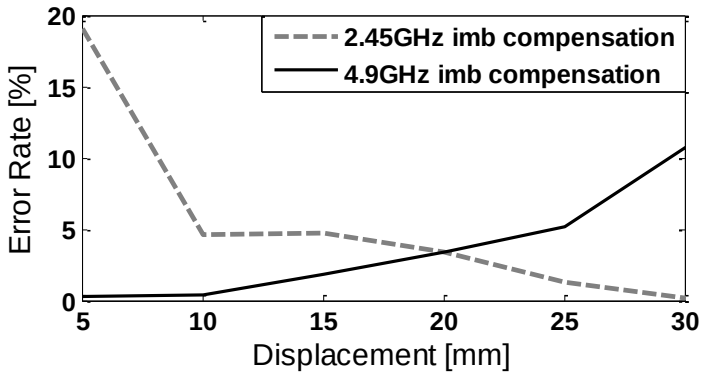

(b)

Fig. 6.13 Comparison of accuracy of displacement estimation results between measured 2.45GHz radar data and 4.9 GHz radar data before imbalance compensation (a), and after imbalance compensation (b).

The estimation results shown in Fig. 6.13(a) and Fig. 6.13(b) compare 2.45 GHz radar data and 4.9 GHz radar data. As illustrated in Fig. 6.9 and Fig. 6.12, reflected signal at 4.9 GHz forms a longer arc than that at the 2.45 GHz radar. This advantage leads to a more accurate estimation for arc center in arctangent demodulation procedure, thus resulting in better displacement accuracy. Fig. 6.13(a) shows displacement error rate for both radars before imbalance compensation. From Fig. 6.13(a), it can be seen that the error rate for 4.9 GHz data, for the motion range of 5mm to 25mm, is significantly lower than that of the 2.45 GHz data. The average error rate within this range for 4.9 GHz radar is below 6%. Fig. 6.13(b) is a plot of error rate after imbalance compensation for both radars. It is evident that within 20 mm, in 4.9 GHz radar data, error rates can be limited to less than 4% after imbalance compensation. To be specific, the estimation on 5 mm target motion using harmonic tag technique gives a result of 4.986 mm, with a deviation of 14 μm. For 10 mm displacement, the estimation yields a 9.965 mm, with a deviation from reference by 35 μm.

However, with the increase of displacement range, accuracy of 4.9 GHz data decreases. For example, at 40 mm displacement, from Fig. 6.13(b), it can be seen that error rate is higher in 4.9 GHz estimation than 2.45 GHz estimation with or without imbalance compensation. This ambiguity in estimation is mainly due to the spiral shape of the arc formed by 4.9 GHz baseband data with the 40 mm target motion (Fig. 6.14). Although after imbalance compensation, the overall oval shape had largely been modified into a circular profile, varying radius value issue still existed in both cases. This is because of the deviation of the received signal power, which causes radius of the arc to

vary with its center unchanged. Advanced signal processing techniques aiming at this radius correction issue are currently under study (Gao *et al.*, 2012a).

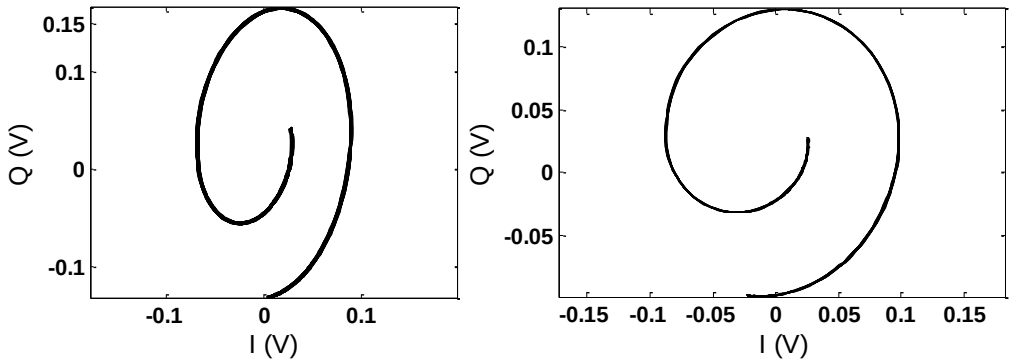

(a) (b)

Fig. 6.14 Effect of large motion on 4.9 GHz radar data. I/Q plot for 40 mm target motion before imbalance compensation (a), and after imbalance compensation (b).

Chapter 7. Multiple motion detection Using Two Frequency Radar

Separating multiple sources of motion using CW Doppler radar has always been a difficult problem. Multiple sources of motion can arise from one lone subject in the form of respiration, heart and other body motion, and from the presence of multiple subjects. While it is conveniently possible to separate sources of motion from one subject due to prior knowledge about such signals (Boric-Lubecke *et al.*, 2002, it is a challenging problem to separate similar forms of motion coming from two different subjects. Various proposed solutions include using MIMO radar systems with blind source separation techniques, Ultra Wide Band (UWB) radar and direction of arrival techniques (DOA) (Boric-Lubecke *et al.*, 2005), (Samardzija *et al.*, 2005), (Lubecke *et al.*, 2007), (Zhou *et al.*, 2006). Although most of these systems can successfully separate motion signatures, they cannot identify the particular source of motion for each signature.

Doppler radar with passive frequency doubling harmonic tags has been shown to be an effective way to isolate desired motion from other motion clutter (Singh and Lubecke, 2012c). Such tags and systems could be useful in situations where the tagged motion is the motion of interest. However, they could also be used in situations where the tagged motion is known and it would be of interest to find other motion that is not tagged. An example of such an application could be a rescue operation where the rescuer is wearing a tag (Fig. 7.1). In such a case, in addition to keeping track of the rescuer, the objective is to find any other person in need of help (casualty). In this case, we can use CW harmonic radar (2.45- 4.9 GHz) and CW Doppler radar (2.45 GHz) to keep track of

both the tagged and non-tagged activity (Fig. 7.2). The harmonic radar receives only the ‘2f’ (4.9 GHz) tag reflected signal, and thus can readily isolate the rescuer motion. The conventional radar receives the ‘1f’ (2.45 GHz) signal which is reflected by both the rescuer and the victim, and thus does not by itself allow isolation of the victim. The ‘1f’ motion caused by the rescuer can be considered noise. However, the signal from the tag that has been isolated by the harmonic ‘2f’ receiver is correlated with this noise in the ‘1f’ system. Subtraction of the non stationary tag signal from the baseband signal of 2.45 GHz radar could facilitate reliable monitoring of the un-tagged source of motion.

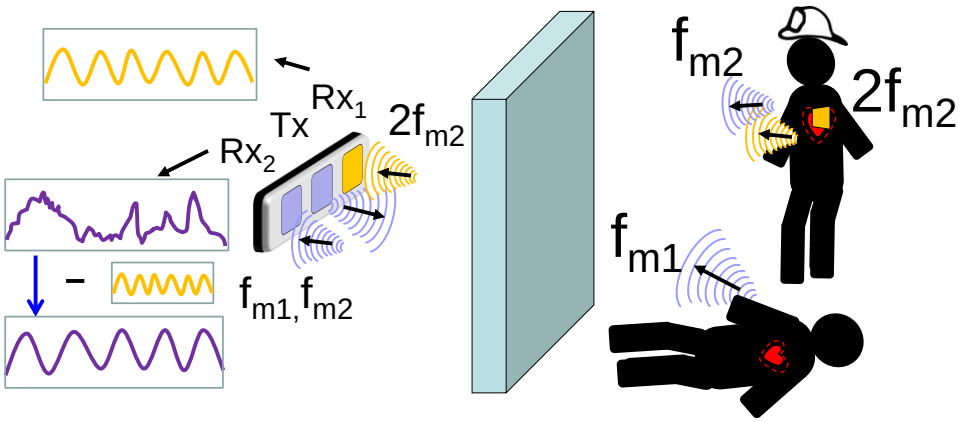

Fig. 7.1 Application of two frequency radar in rescue operation.

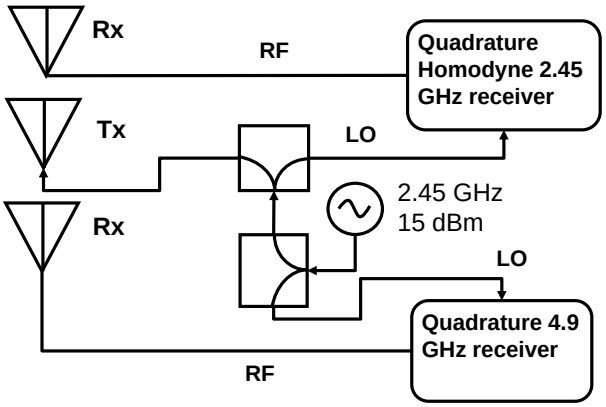

Fig. 7.2 Block diagram showing two frequency radar setup. Tag subtraction algorithms could be used to separate sources of motion.

This chapter explores the feasibility of using various cancellation techniques to reduce or remove the tag motion component from a 2.45 GHz radar baseband (Singh *et al.*, 2012a), (Singh *et al.*, 2012e). The advantages of such a system can be easily extended to any tag based Doppler radar system.

7.1 Tag signal subtraction by mixing

Fixed filters are not an efficient way of reducing tag signal that is dynamic in nature. However, 2.45 GHz and 4.9 GHz baseband signals could be mixed together to cancel out tag information as explained below. Let us assume that baseband signals are

$$\begin{aligned} B_{i1} &= \cos(4\times\pi\times(x+y)/\lambda_{2.45}) \\ B_{q1} &= \sin(4\times\pi\times(x+y)/\lambda_{2.45}) \\ B_{i2} &= \cos(8\times\pi\times y/\lambda_{2.45}) \\ B_{q2} &= \sin(8\times\pi\times y/\lambda_{2.45}) \end{aligned} \quad , \tag{7.1}$$

where B_{i1} and B_{q1} represent the baseband data for 2.45 GHz and B_{i2} and B_{q2} represent the baseband data for harmonic radar. Tag motion is represented by y and untagged motion is represented by x. Using the double angle formula in trigonometry for 2.45 GHz data, we get

$$\begin{aligned} B'_{i1} &= 2\times B_{i1}^{2} - 1 = \cos(8\times\pi\times(x+y)/\lambda_{2.45}) \\ B'_{q1} &= 2\times B_{q1}\times B_{i1} = \sin(8\times\pi\times(x+y)/\lambda_{2.45}) \end{aligned} \tag{7.2}$$

Multiplying B'_{i1} by B_{q2} and B'_{q1} by B_{i2}, we get,

$$\begin{aligned} U &= B'_{i1}\times B_{q2} = 0.5\left[\sin\left(8\times\pi\times(2x+y)/\lambda_{2.45}\right) - \sin\left(8\times\pi\times x/\lambda_{2.45}\right)\right] \\ V &= B'_{q1}\times B_{i2} = 0.5\left[\sin\left(8\times\pi\times(2x+y)/\lambda_{2.45}\right) + \sin\left(8\times\pi\times x/\lambda_{2.45}\right)\right] \end{aligned} \tag{7.3}$$

Subtracting V from U, we get

$$U - V = -\sin\left(\frac{8 \times \pi \times x}{\lambda_{2.45}}\right) \tag{7.4}$$

where *U*-*V* contains information only about untagged motion. Although, the process looks tedious, it is very simple to execute requiring multiplications, additions and subtractions.

The mixing works well for simulated signals but not for real signals because of the presence of amplitude and phase imbalance between I and Q channels. These amplitude imbalances result in different amplitudes for *U* and *V* affecting the subtraction process (7.3). The mixing of signals would also result in generation of some additional undesired signals. Another problem is that double angle formula (7.2) would not scale correctly for the amplitude of 2.45 GHz signals. Let the 2.45 GHz and 4.9 GHz baseband signal amplitudes be A_1 and A_2 respectively. The following manipulation would have to be performed to get to get the double angle

$$\begin{aligned} B'_{i1} &= 2 \times B_{i1}{}^2 - A_1^2 = A_1^2 \cos(8 \times \pi \times (x + y) / \lambda_{2.45}) \\ B'_{q1} &= 2 \times B_{q1} \times B_{i1} = A_1^2 \sin(8 \times \pi \times (x + y) / \lambda_{2.45}) \end{aligned} \tag{7.5}$$

From 7.5, it can be seen that the value of A_1 needs to be calculated, which will make the cancellation process more sophisticated.

As discussed earlier, fixed filters are not a good option to filter out tag signal from 2.45 GHz baseband. Since the tag signal is changing in time, we would need an adaptive filter that changes with the tag signal. The filter transfer function could be generated

using the tag signal as reference and applied to 2.45 GHz baseband signal. Use of adaptive filter to filter out tag signal is similar to principles of adaptive noise cancellation (ANC) and will be discussed in the following sections.

7.2 Adaptive noise cancellation

ANC is based on the principles of adaptive filtering resulting in optimal noise reduction without distorting the signals, as could be the case with direct filtering. It uses a reference signal that contains signal correlated with the noise in the desired signal. This reference signal is used to generate a varying impulse response by the adjustment of filter weights to minimize an error signal by minimizing the total output power of the system. The principles and techniques of adaptive noise cancellation have been adequately described in (Haykin, 1991), (Widrow *et al.*, 1975). ANC can be performed using several algorithms. The two common algorithms are least mean squares (LMS) and recursive least squares (RLS). LMS is used widely due to its simplicity. Normalized LMS (NLMS) is a variant of LMS algorithm that ensures the stability of LMS algorithm by normalizing it with the power of the input (Haykin, 1991). The two important parameters governing the behavior of LMS algorithms are the step-size (μ) and the filter order. Adaptive noise cancellation (ANC) algorithms have been used successfully to cancel out acoustic noise (Boll and Pulispher, 1980). Some other applications include cancellation of 60 Hz from biomedical signals (Haykin, 1991), (Widrow *et al.*, 1975) and cancellation of radar clutter (Palmer, 2012). We use LMS and NLMS algorithms for our application to cancel out the tag component (considered as noise) from 2.45 GHz Doppler radar.

One of the major challenges foreseen in the application of ANC to radar signals is the relative strength of the signal to be cancelled (tag) and its motion content. In some

cases, the tag signal content might be greater than the untagged motion and for some other cases; the rate of movement may be too close to untagged motion. Simulations were performed in MATLAB® in order to study the effectiveness of the algorithms for different signal conditions. The simulations were followed by some experimental results. The simulation and experimental results suggest that it is possible to successfully subtract tag signal and that such cancellation improves the accuracy of a Doppler radar system and provides us with reliable information.

7.2.1 Simulations

The simulations were performed in MATLAB® 7.9.0. Baseband data was generated using the equations for radar as shown below.

$$\begin{aligned} B_{i1} &= \cos(4\times\pi\times(x+y)/\lambda_{2.45}) \\ B_{q1} &= \sin(4\times\pi\times(x+y)/\lambda_{2.45}) \\ B_{i2} &= \cos(8\times\pi\times y/\lambda_{2.45}) \\ B_{q2} &= \sin(8\times\pi\times y/\lambda_{2.45}) \end{aligned} \tag{7.6}$$

B_{i1} and B_{q1} represent the baseband data for 2.45 GHz and B_{i2} and B_{q2} represent the baseband data for harmonic radar. y represents the motion of tag at 1.5 (f_2) Hz and x represents the un-tagged motion at 0.3 (f_1) Hz as shown below:

$$\begin{aligned} x &= \frac{N\times\lambda}{400}\cos(2\times\pi\times f_1\times t) \\ y &= \frac{N\times\lambda}{400}\cos(2\times\pi\times f_2\times t) \end{aligned} \tag{7.7}$$

N denotes the percentage of circle desired (displacement). The baseband data were combined using linear demodulation before performing FFT. Fig. 7.3(a) displays time domain and frequency domain data for the generated baseband signals. Fig. 7.3(b)

indicates the assumed equal signal content of tagged and non-tagged motion for 2.45 GHz radar. Fig. 7.3(a) and Fig. 7.3(c) show magnitude of the tag signal in time and frequency domain respectively.

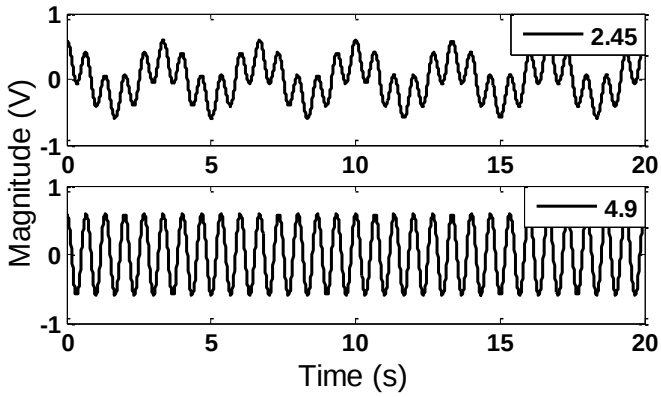

(a)

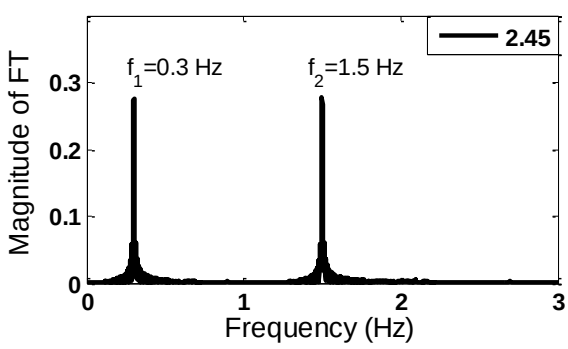

(b)

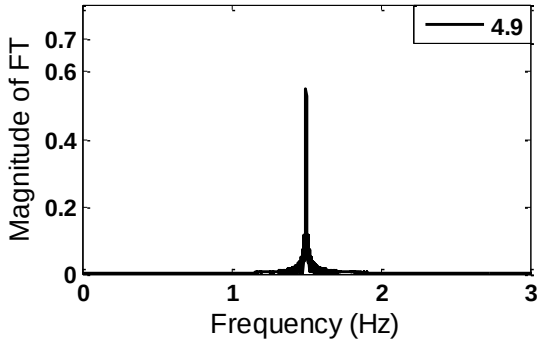

(c)

Fig. 7.3 Simulated baseband signals. Time domain signals showing the 4.9 GHz radar signal as reference, and data as seen by the 2.45 GHz radar (a), FFT of simulated 2.45 GHz radar baseband signal (b) and FFT of simulated 4.9 GHz radar baseband signal (c).

Both LMS and NLMS algorithm were applied for cancellation of the tag signal. The step size (μ) for both algorithms was 0.006 and the order of filter was 16. Fig. 7.4 shows the FFT of the 2.45 GHz after cancellation. Both LMS and NLMS algorithm seem to effectively cancel the tag motion at 1.5 Hz. A residual component can also be clearly

seen at 2.7 Hz ($2\times f_2 - f_1$) in Fig. 7.4(a) but not in Fig. 7.4(b), the implications of which will be discussed after. The simulation results indicate that ANC algorithm could work well for radar data as well. In the simulation, both the signal contents in 2.45 GHz radar data have an equal magnitude that is not true for all situations.

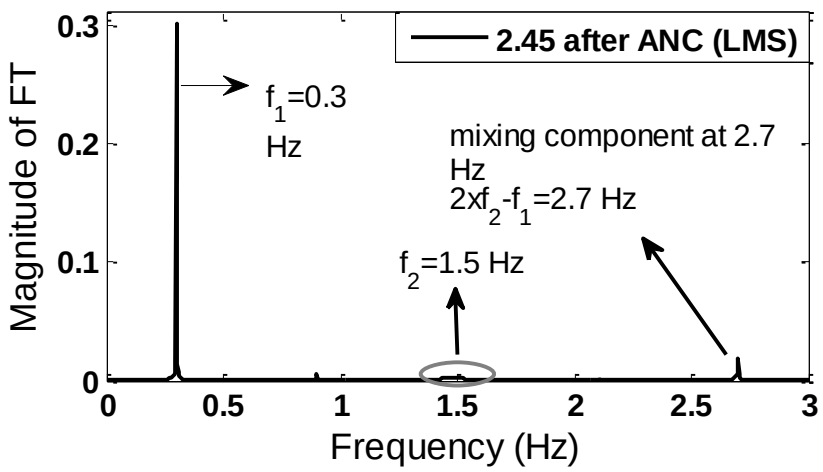

(a)

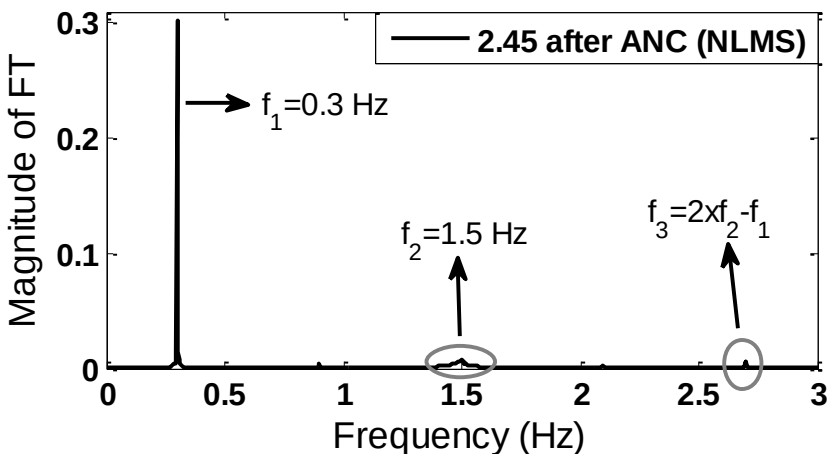

(b)

Fig. 7.4 FFT of filtered 2.45 GHz radar signal after application of LMS algorithm (a), and NLMS algorithm (b).

7.2.1.1 Effect of tag motion frequency

The presence of a residual component indicates that as f_2 approaches f_1, the residual component approaches f_1. This indicates that in addition to cancelling the tag frequency, the ANC algorithm should be capable of suppressing the residual component that would be generated at $2f_2$-f_1 and at $2f_2$+f_1. A parametric study was carried out to study the performance of LMS and NLMS algorithms when the tag motion frequency is varied from 0.4 Hz to 1.5 Hz. The non-tagged motion frequency was kept fixed at 0.3Hz. Both motions were of equal amplitude. For each simulation, FFT was performed on filtered data and the amplitude ratios were calculated for f_1/f_2 and f_1/f_3 the results of which are shown in Fig. 7.5. Fig. 7.5(a) shows that both algorithms perform cancellation very well with LMS outperforming NLMS for same values of μ (0.006) and filter order (16). However, NLMS algorithm proves to be better at suppressing the residual component than LMS (Fig. 7.5(b)). The cancellation efficiency increases as the difference between the tag and non-tagged motion increases.

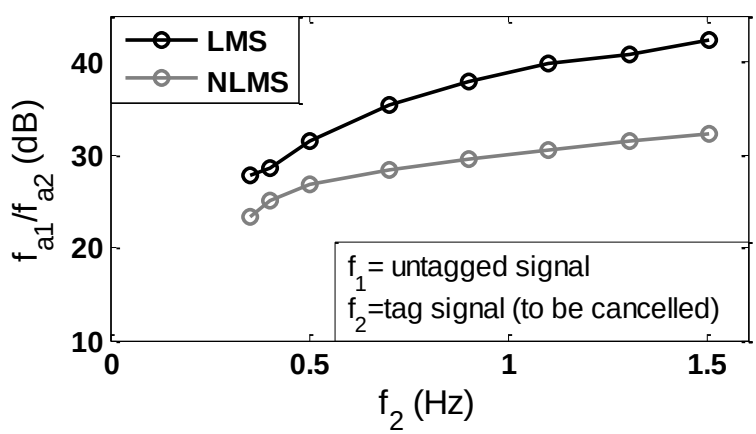

(a)

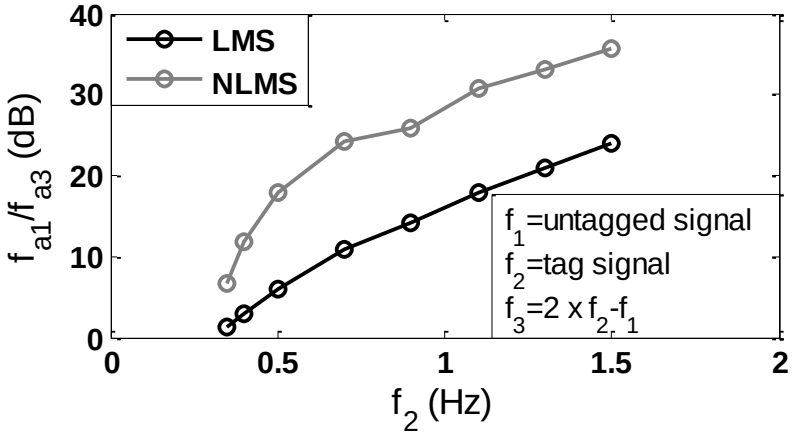

(b)

Fig.7.5. A comparison of performance of LMS and NLMS algorithms as the tag motion frequency (f_2) is varied from 0.4 Hz to 1.5 Hz. SNR was calculated for tag signal cancellation (a), and suppression of residual components (b) . The points of simulation are indicated by markers. f_{a1}, f_{a2} and f_{a3} correspond to the magnitude of FFT at frequency f_1, f_2 and f_3 respectively.

7.2.1.2 Effect of tag displacement

The amount of tag displacement could also affect the cancellation efficiency. It should be noted that linear demodulation is suitable for combining IQ data constituting smaller portions of the arc in the IQ plane. The arc transcribed in the IQ plane is a function of operating frequency of the radar. For a tag motion of x cm, if the arc transcribed for 2.45 GHz radar is y % (of the total circle), then the arc transcribed for 4.9 GHz radar is ($2\times y$%). As the tag displacement increases, the output of linear demodulation will contain harmonics of the fundamental motion frequency. Fig. 7.6 shows an example where the motion constitutes 90% of the arc.

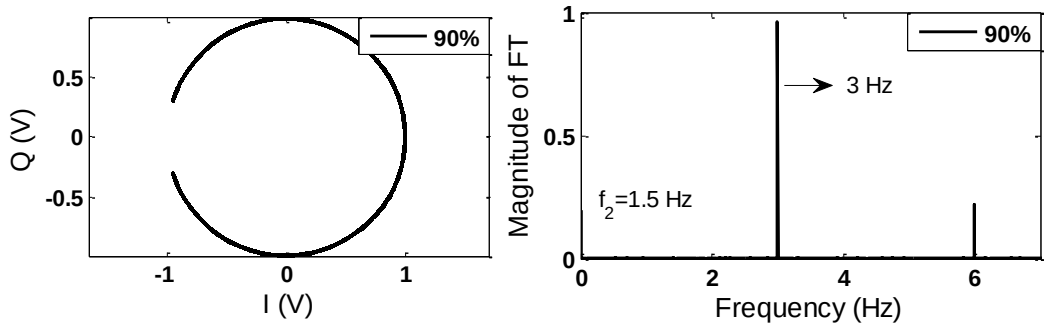

(a) (b)

Fig. 7.6 I/Q plot showing 90% of transcribed arc (a) and FFT of linear demodulated I/Q data (b). Note that the generated frequency of motion at 1.5 Hz is not visible in the frequency spectrum due to harmonics introduced by linear demodulation technique.

To study the effect of tag displacement on cancellation efficiency, a parametric simulation was performed where tag displacement was varied as a multiple of non-tagged object's displacement (x). The resulting baseband signals were combined using linear demodulation and cancellation was performed using NLMS algorithm with a step size (μ) of 0.006 and varying filter order from 8 to 64. Signal to Noise Ratio (SNR) was calculated as the ratio of magnitude of non-tagged motion frequency to tag motion frequency. The combined traces are shown in Fig. 7.7. From Fig. 7.7, it can be observed that increasing tag displacement results in deterioration of SNR as expected. When the tag motion is more than three times the motion of the untagged object (3x), the system is unable to effectively reduce the tag signal which is when SNR becomes negative. It can also be observed that increasing filter order may not necessarily improve adaptive filtering.

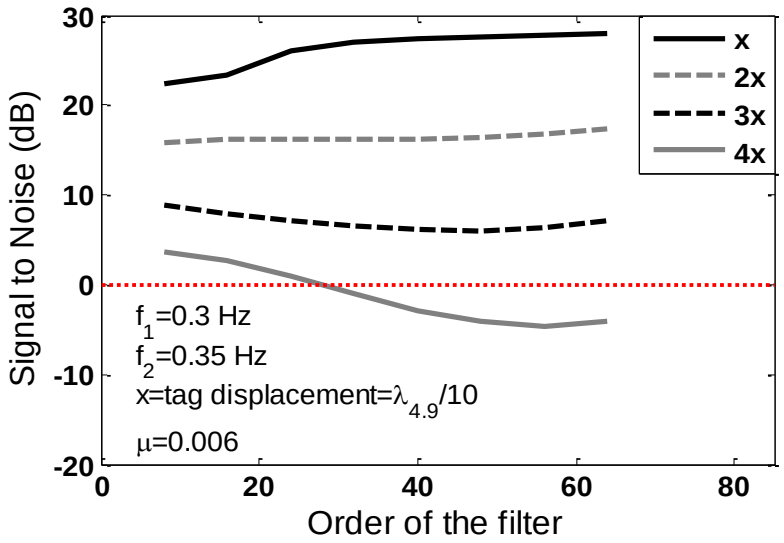

Fig. 7.7 Effect of tag displacement and filter order on cancellation efficiency (linear demodulation). Tag motion frequency of 0.35 Hz was chosen. Displacement 'x' corresponds to 20% of the IQ circle (at 2.45 GHz).

7.2.2 Experiments

The simulation results assuming perfect baseband data show the feasibility of applicability of ANC techniques for subtraction of tag data (f_2). However, harmonic radar does not reject non-tagged motion completely and still detects non-tagged motion (f_1) although its amplitude is significantly less than tagged motion. The presence of non-tagged motion in the reference signal would lower the SNR in the filtered signal. Measurement results were obtained using 2.45 GHz quadrature Doppler radar and heterodyne quadrature harmonic Doppler radar that were set up together using connectorized parts from Mini-Circuits® and Pasternack Enterprises. The transmitting antenna used was ASPPT 2988 from Antenna Specialists having a gain of 8 dBi and an E-plane beam-width of 60^0. Fig. 7.8 (a) shows the block diagram of 2.45 GHz Doppler

radar and Fig. 7.8(b) shows the block diagram of heterodyne harmonic Doppler radar. The concept of heterodyne receiver for Doppler radar employing passive harmonic tags has been discussed in literature (Singh and Lubecke, 2010).

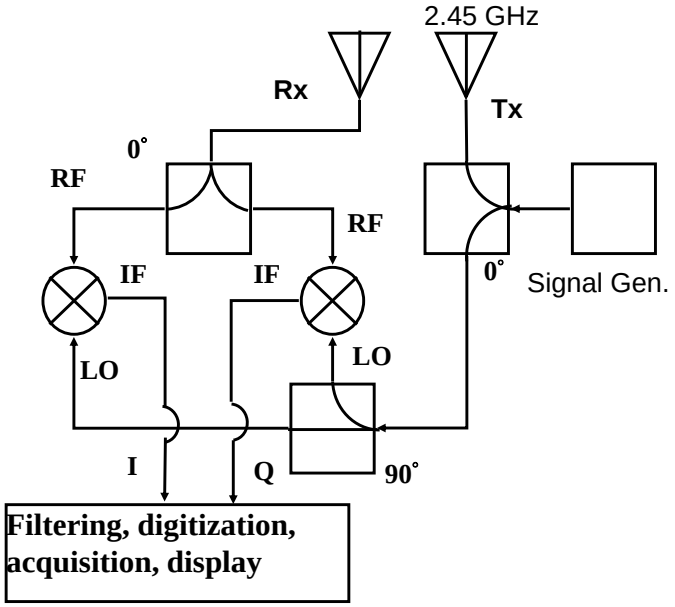

(a)

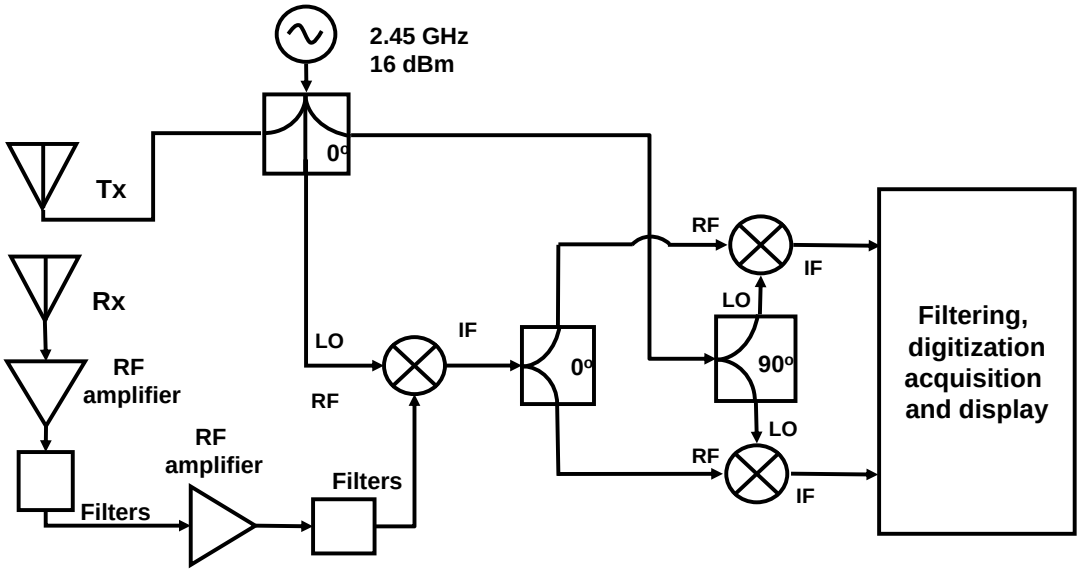

(b)

Fig. 7.8 Block diagram of 2.45 GHz quadrature Doppler radar (a) and 2.45-4.9 GHz quadrature heterodyne harmonic Doppler radar (b).

Mechanical movers were used to move the harmonic tag (htag 2) and a styrofoam ball of 20 cm diameter covered with aluminum foil in front of the two radar systems. The linear stage (Single Axis Series CDS 3310) from Galil was used to move the tag while an L-12 linear servo from Firgelli was used to move the Styrofoam ball. The orientation of targets with radars is shown in Fig. 7.9. For all measurements, power supplied to the transmitting antenna was around 7-8 dBm. The distance between the both targets and antennas was approximately 1m. Low noise amplifiers were used to condition the baseband signal before digitization. MATLAB® was used as the interface for data acquisition and for signal processing. NLMS algorithm was used for ANC for all dataset owing to better suppression of f_3 as shown in Fig. 7.5. Sampling frequency of 100 S/s was used to acquire the data.

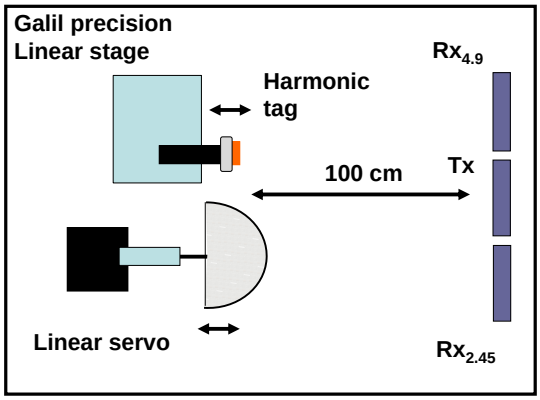

Fig. 7.9 Relative positions of mechanical targets with respect to radar (top-view). For Experiment III, the linear servo was replaced by a human subject.

7.2.2.1 Experiment I

The Styrofoam ball was moved at a frequency of 0.3 Hz with approximately 8 mm of displacement. The harmonic tag was moved at 1.5 Hz with 1 cm displacement. The filter order was increased to 32 keeping μ as 0.006. Fig. 7.10 (a) shows the time

domain data for both radars and the result of adaptive noise cancellation. Fig.7.10 (b) shows the FFT of each radar signal and the filtered signal. The time domain plot (Fig. 7.10(a)) shows successful cancellation of tag signal. The presence of f_1 in 4.9 GHz radar is shown in Fig. 7.10(b). An SNR of around 13 dB is obtained in the filtered signal.

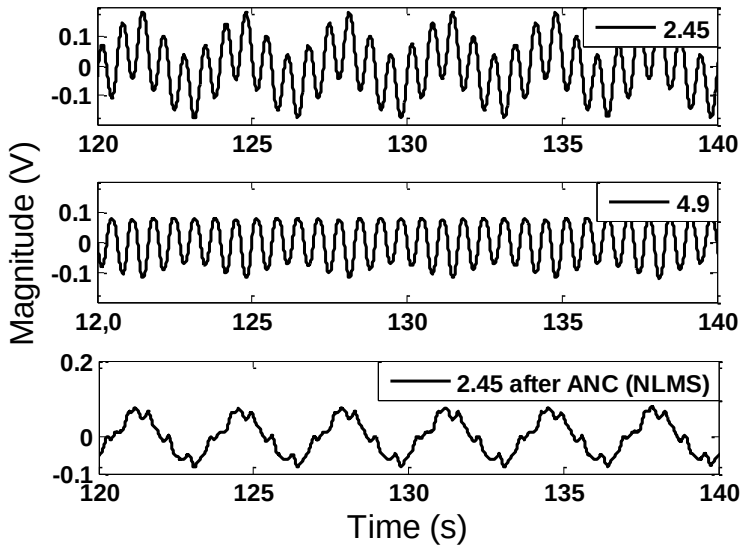

(a)

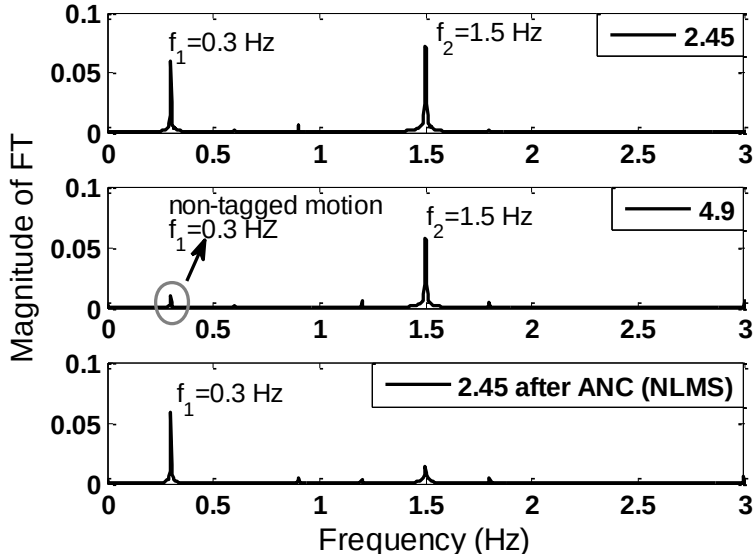

(b)

Fig. 7.10 Results from experiment I. Time domain data from experiment I indicating successful cancellation of tagged motion from 2.45 GHz radar (a), and corresponding

FFT showing relative signal amplitudes (b). Since 4.9 GHz radar has high selectivity, the very small level of detected f_1 does not adversely affect the results of ANC.

7.2.2.2 Experiment II

The effect of larger tag motion on the performance of NLMS ANC algorithm was measured by increasing the tag displacement to 2 cm. All the other conditions were same as experiment I. With a larger tag displacement, we expect to see higher tag signal content in 2.45 GHz baseband signals that should be suppressed in order to get any useful information on the untagged object. Fig. 7.11(a) shows the FFT of both radar signals and the filtered 2.45 GHz radar signal. Windowed FFT was performed on the 2.45 GHz radar data before and after ANC to see any improvement in rate estimation. The effect of larger tag motion on 2.45 GHz radar spectrum can be seen in Fig. 7.11(a). It can also be observed from Fig. 7.11(b) that without the application of noise cancellation procedure, the 2.45 GHz radar would fail to detect the non-tagged motion of Styrofoam ball.

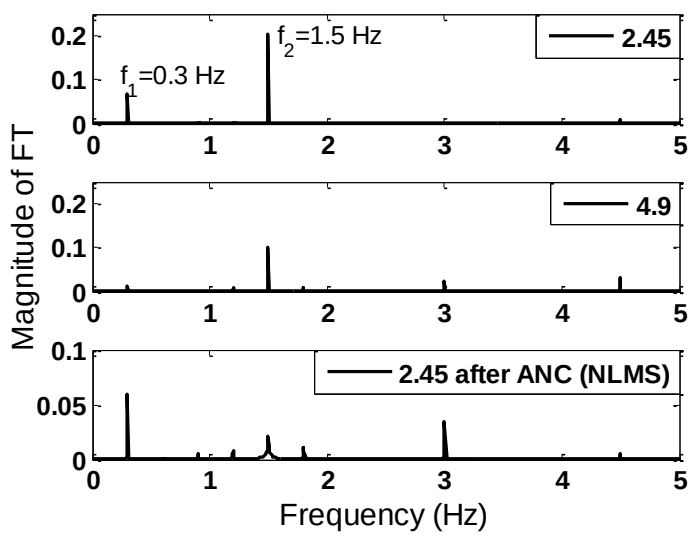

(a)

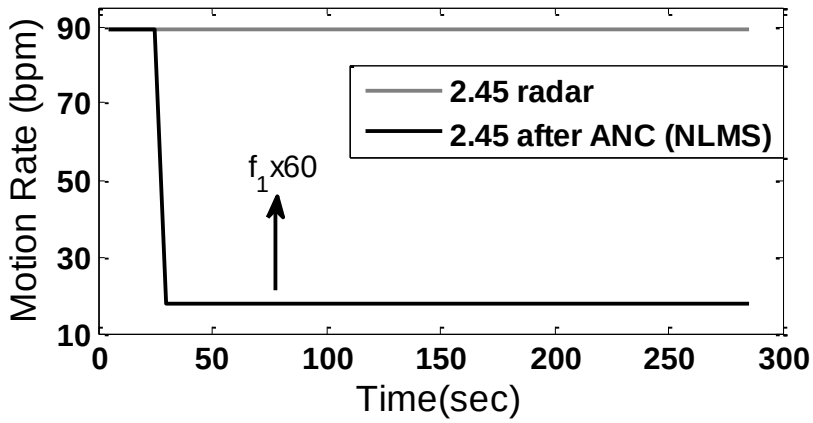

(b)

Fig. 7.11 Results from experiment II. FFT of data obtained from experiment II indicating the larger tag displacement in 2.45 GHz spectrum that is reduced after the application of ANC technique (a) and a plot of detected motion rate with time showing the cancellation of tag signal and successful tracking of non-tagged signal at 18 bpm.

7.2.2.3 Experiment III

After initial validation of ANC techniques with measurement data from mechanical targets, an experiment set up was made to examine the effectiveness of the technique on human respiratory measurement. The measurement set up was similar to Fig. 7.9 with a human subject in front of 2.45 GHz radar instead of the mechanical target. A piezo electric belt (pneumotrace II) from UFI was used as reference chest belt. The linear stage with harmonic tag was moved in front of 4.9 GHz antenna at 0.4 Hz with 1 cm of displacement. NLMS algorithm was applied to the 2.45 receiver data the results of which are shown in Fig. 7.12. FFT was used to analyze the data with a window length of 18 seconds (4-6 respiration cycles) and an overlap of 5 seconds. It is clear from Fig. 7.12 that without application of ANC algorithm, it would be difficult to make any conclusions from analysis of 2.45 GHz receiver data. However, after cancellation of tag signal, the

rate corresponds to respiration rate of human subject as verified by the respiratory belt data.

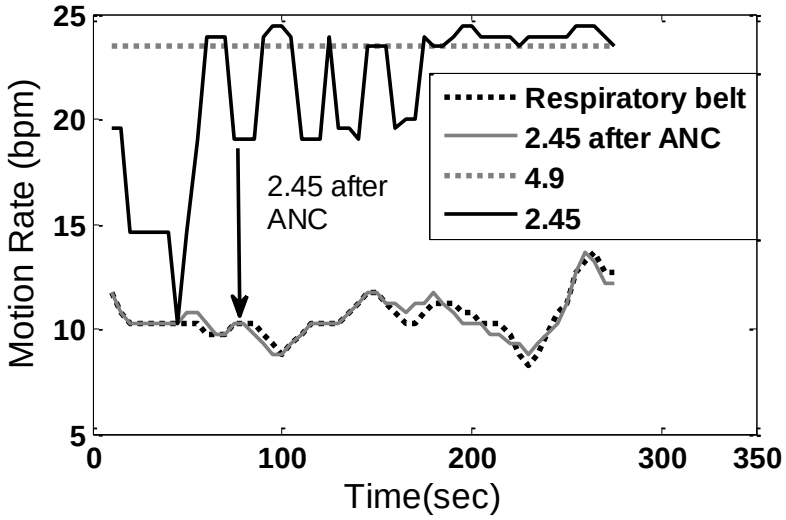

Fig. 7.12 Results from experiment III. Detected motion rate for different signals obtained from experiment III. The 4.9 GHz trace shows the successful detection of the tag motion at 0.4 Hz (24 bpm) exclusively. The trace from 2.45 GHz radar initially fails to track the respiration rate of human subject. After the application of ANC technique, the data from 2.45 GHz radar tracks the respiration of the human subject exclusively as verified by the reference chest belt.

7.3 Discussion

The simulation and experimental results show that simple ANC algorithms can be successfully used to separate tagged and non-tagged motion under various test conditions using two frequency radar systems. From Fig. 7.7, it can be observed that cancellation with linear demodulated signal would work for I and Q data transcribing less than 90% of the arc. When the arc length is more than 90%, linear demodulation results in distortion and loss of information at fundamental frequency. The effect of linear demodulation on

increasing displacement is shown in Fig. 7.13. The simulated motion is at 0.3 Hz. FFT analysis of linear demodulation of arc lengths over 90% indicates the detected signal content at 0.6 Hz, which is second harmonic of the true signal content at 0.3 Hz.

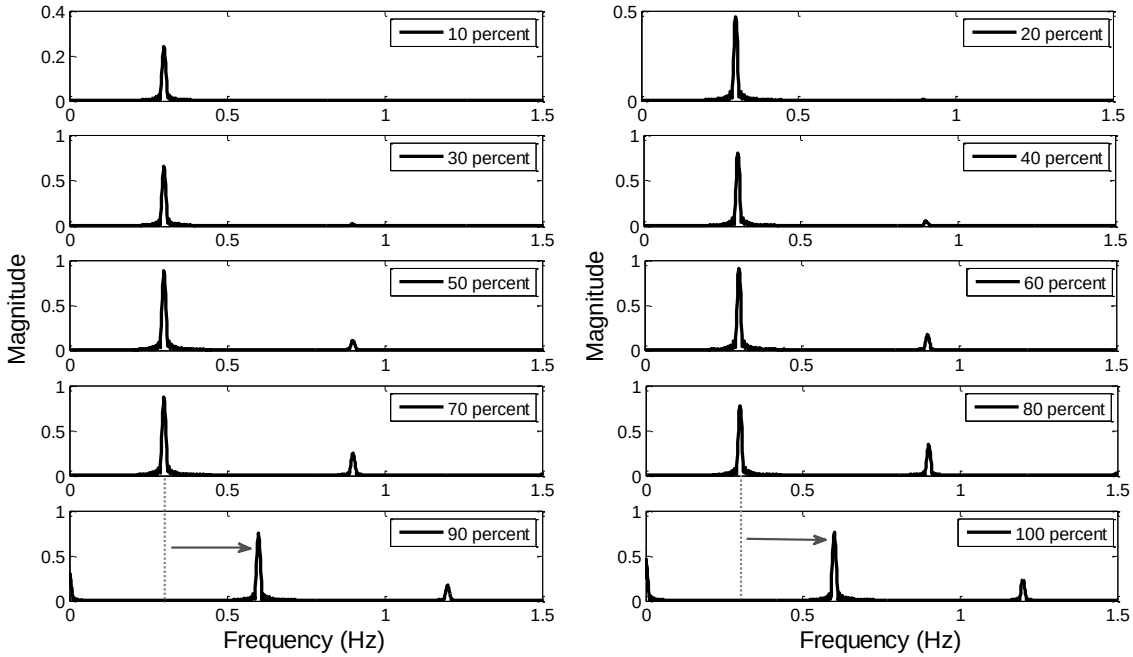

Fig. 7.13 Effect of increasing displacement on linear demodulation. FFT of simulated baseband data combined using linear demodulation for increasing arc length.

A possible solution for successful operation of ANC techniques for larger motion could be the use of arctangent demodulation, as it calculates the arc length. Arctangent demodulation of simulated baseband data indicates that the detected frequency content is never distorted (Fig. 7.14). Adaptive noise cancellation was performed on simulated data at 2.45 GHz and 4.9 GHz, which was combined with arctangent demodulation using NLMS algorithm with a step size (μ) of 0.006 and varying filter order from 8 to 64. Tag displacement at 0.35 Hz was varied as a multiple of untagged object's displacement at 0.3 Hz. Signal to Noise Ratio (SNR) was calculated as the ratio of magnitude of non-tagged motion frequency to tag motion frequency. The combined traces are shown in Fig. 7.15.

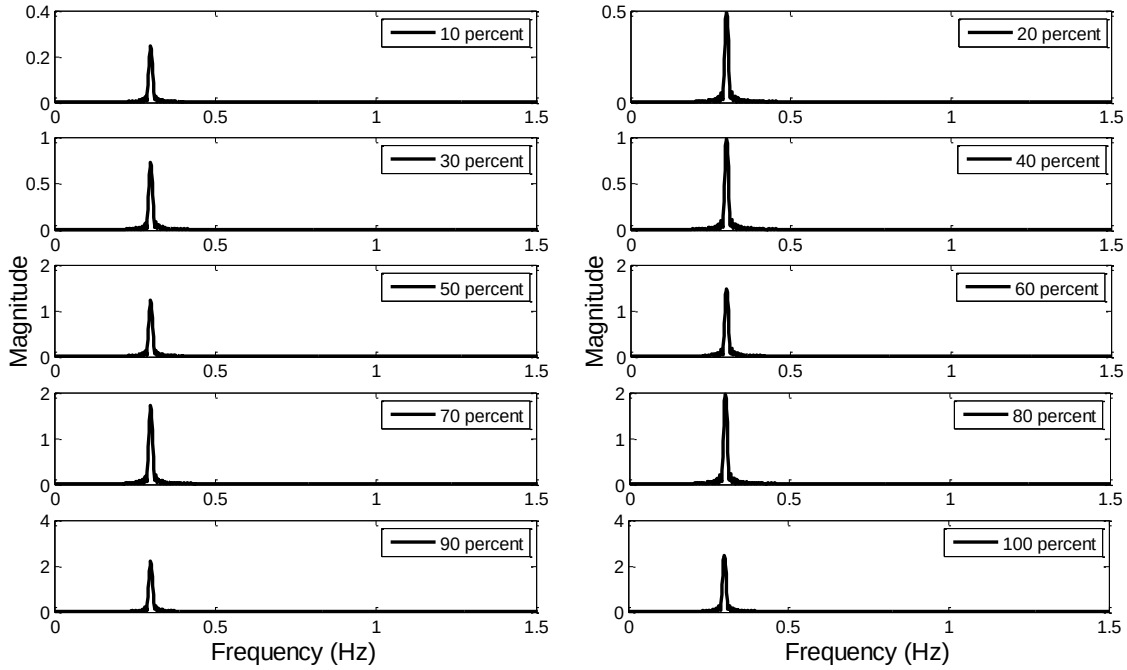

Fig. 7.14 Effect of increasing displacement on arctangent demodulation. FFT of simulated baseband data combined using nonlinear (arctangent) demodulation for increasing arc length does not result in generation of harmonics.

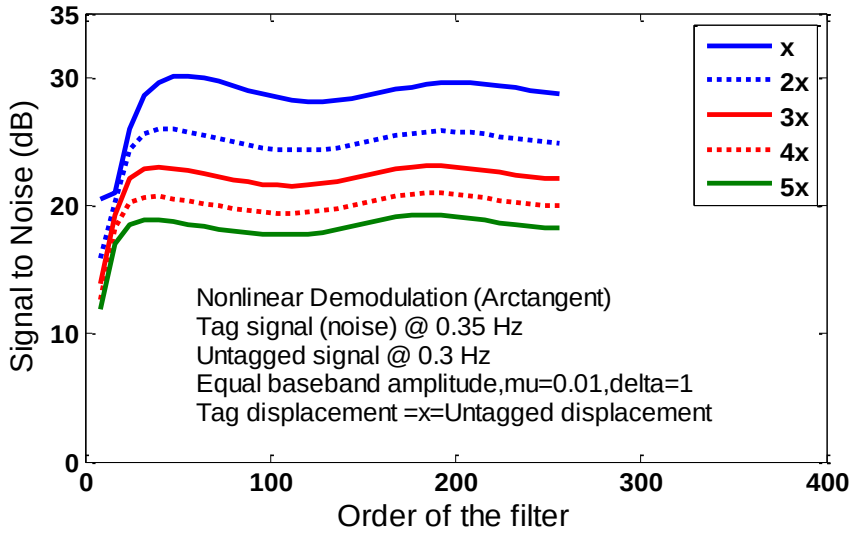

Fig. 7.15 Effect of tag displacement and filter order on cancellation efficiency (arctangent demodulation). Tag motion frequency of 0.35 Hz was chosen. The untagged object's displacement is fixed at 'x' cm and corresponds to 36^0 (10%) arc at 2.45 GHz.

From Fig. 7.15, it can be observed that the SNR remains positive for all displacements, implying that tag signal has been cancelled successfully for all displacements. This behavior is expected after observing the results from Fig. 7.14, which shows the absence of any distortion or harmonics in the demodulated signal, even as the displacement is increased. However, the complexity of arctangent demodulation itself limits its use to generate filter coefficients for adaptive filtering.

An advantage of using adaptive noise cancellation technique is that it is not restricted to the use of harmonic tag and radar, and can be used with any radar system that can uniquely identify a subject and provide its motion signature as a reference. The NLMS algorithm used in this study is simple and can also be conveniently run in real time. The use of ANC techniques has allowed us to accurately track a tagged motion and a non-tagged motion simultaneously. Although harmonic radars may not be able to track multiple harmonic tags at the same time, it can provide us with information to cancel signal from multiple tags to give information about the non-tagged motion.

Chapter 8. Low-IF Tags

To construct a Doppler radar system compatible with some type of RFID system, the problem is not just to find a type of modulation but to find a technique to modulate the return signal in a way that preserves the motion related phase information. Since the signal is already phase modulated, the simpler choice could be amplitude modulation or frequency modulation. If we envision a radar system with amplitude modulated tag, it would contain a programmable microcontroller which could be operated in two ways:

1) The microcontroller would allow the RFID tag to transmit only when it is detecting a particular signal code sent by the transmitter unique to it. Such a system would allow us to monitor different tags but not at the same time. However, this would increase the complexity of the transmitter.
2) The transmitted signal would be the same but the tag will only re-transmit at certain times. This corresponds to using microcontroller as a switch. These times could be made unique for each tag. However, this would complicate the design and even though it will send the id, it would be difficult to decode it in the presence of interfering motion.

Another way to solve the problem is shifting the incident frequency by a little and retransmitting it. The local oscillator frequency would remain the same. The receiver would then generate an intermediate signal (IF) that could be digitized and demodulated in software. If we could generate a unique shift for each tag, we could then detect many tags at the same time just by separating the channels using a band pass filter in software or hardware. This tag would work for continuous wave signals, pulsed signals and

FMCW signals. This chapter proposes the use of such frequency shifting tags to identify subject/s and detect physiological motion. Such tags will be referred to as low intermediate frequency (low-IF) tags in the text.

There are radar receivers that use similar technology known as low-IF receivers. But as the name suggests, they obtain a low-if signal in the receiver and not at the source of motion. This chapter will discuss the low-IF receiver technology, differences between the proposed low-IF tag and low-IF receiver, design of low-IF tags, experimentation and analysis of measurement results.

8.1 Low-IF receivers and low-IF tag

The direct conversion receivers that have been used thus far in this dissertation are also referred to as zero intermediate frequency (zero-IF) receivers (Abidi, 1995) where the demodulated output is termed as baseband. Low intermediate frequency (low-IF) receivers are a class of receivers where the generated intermediate frequency lies near the baseband signals. Low-IF receivers are used in communication systems to combine benefits from both zero-IF and IF systems (Crols and Steyaert, 1998). Since the required signal lies away from DC, it does not suffer from DC offset problems unlike zero-IF receivers and avoids the use of High Q high frequency filters required for IF systems (Skolnik, 2001), (Razavi, 1997). Another advantage of using low-IF receivers is the reduction in flicker noise (Mostafanezhad, Boric-Lubecke and Lubecke, 2010).

Doppler radars require phase correlation between the received signal and the local oscillator to detect the small phase deviations occurring due to motion. The effect that is known as range correlation is the reason why baseband data (mixer output) in homodyne

radar systems are not cluttered with noise (Gillespie *et al.*, 1961), (Droitcour *et al.*, 2004). Application of low-IF receiver for a CW Doppler radar system would require the generation of LO and RF from the same source (for coherence) and has been described as a coherent low-IF receiver shown in Fig. 8.1 (Mostafanezhad, Boric-Lubecke and Lubecke, 2010). In a coherent low-IF receiver, the signal is transmitted and received at the same frequency. The low-IF is generated by up-converting the LO signal to $f_{LO} + f_{IF}$ using the same source used to generate the transmitted signal. Using Doppler radar with a coherent low-IF receiver will increase the SNR of the system considerably and provide many other benefits but cannot still provide the selectivity with respect to subjects since every subject will be detected at the same low-IF frequency.

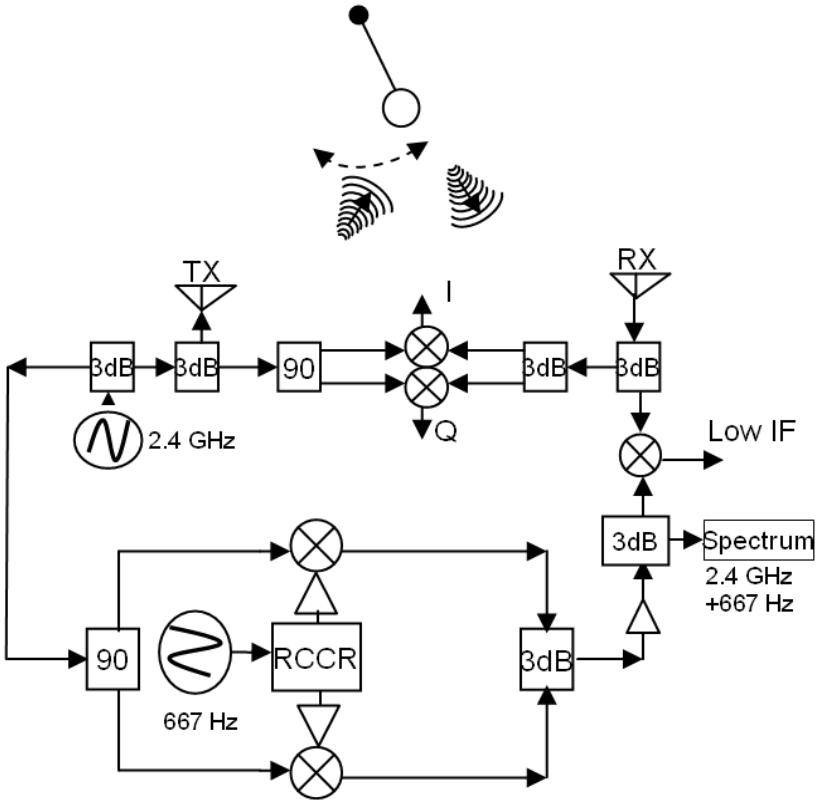

Fig. 8.1 A coherent low-IF receiver (Mostafanezhad, Boric-Lubecke and Lubecke, 2010).

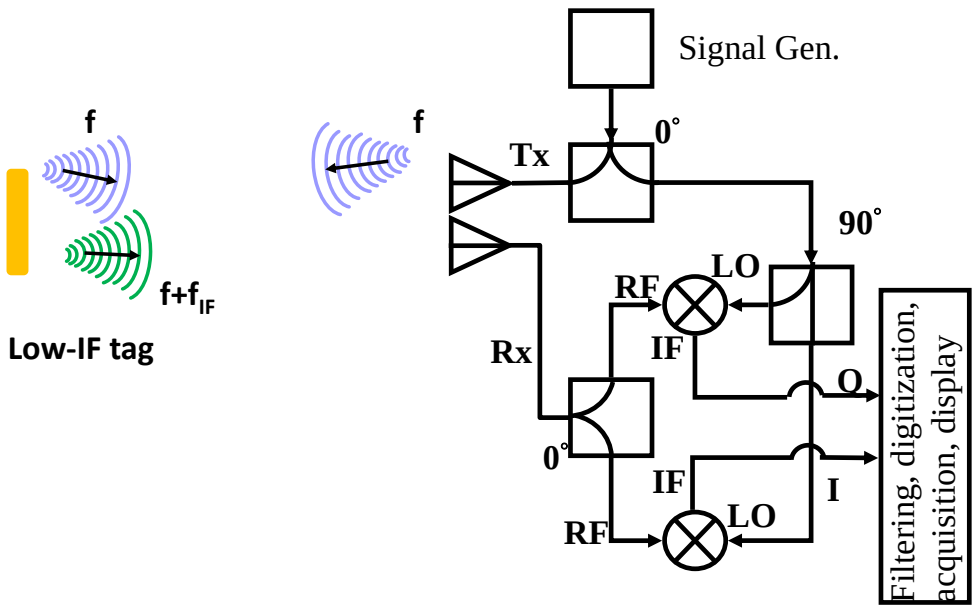

Fig. 8.2 Doppler radar with low-IF tag. Note that the receiver architecture remains the same as quadrature homodyne receiver.

Low-IF tags are different than low-IF receivers as the IF is generated at the source of motion and there is no change in the receiver architecture when compared to a standard homodyne quadrature receiver (Fig. 8.2). This allows us to preset unique IF signal for each tag thereby adding selectivity to the Doppler radar system along with other advantages of the low-IF system. The only trade-off now in using the low-IF system is the use of a high speed data acquisition system.

An important feature to understand for such system is the effect of motion on the low-IF signal. Traditionally, the received CW signal is phase modulated which is demodulated by quadrature mixing with the LO signal. The modeling of CW radar system includes a stationary transmitter and receiver and a moving target with a zero net velocity. However, with a low-IF tag system, the net velocity of the target would be zero only from a frame of reference of an observer. From the point of view from radar, due to

the presence of an IF not close to DC, the radar is effectively looking at an object travelling radially at a speed corresponding to that IF. For example, let us consider the following situation:

$$\text{Tag motion} = x(t),$$

Transmitting frequency = 2.45 GHz, and

Intermediate frequency = 1 kHz

An IF of 1 kHz would correspond to a velocity of 61.22 m/s. The tag can then be considered as lying on the object moving at 61.22 m/s and moving at $x(t)$. This is illustrated in Fig.8.3.

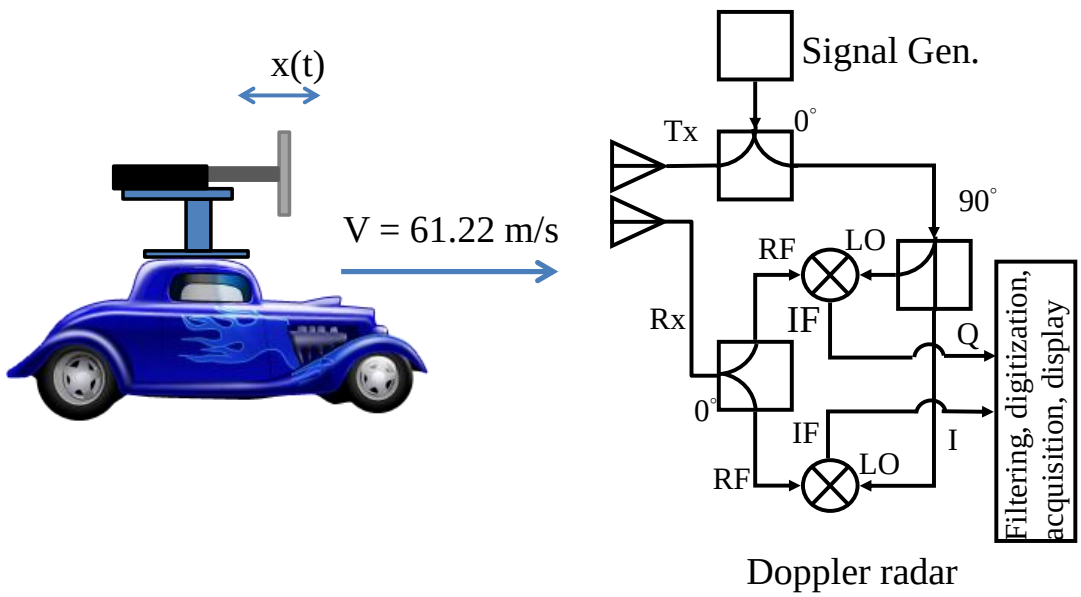

Fig. 8.3 Physical scenario representing signals resulting from a low-IF tag.

The problem then is to correctly model this behavior and predict the resulting signal. Fortunately, this behavior does resemble the radar scattering by flying airplanes that has been studied and referred to as Jet Engine Modulation (U.S Navy, 1999). What it implies

is that moving or rotating surfaces on a moving target will have the same Doppler shift as the moving target, but will also impose amplitude modulation (AM) on the Doppler shifted return (Naval air warfare, 1999). Amplitude demodulation techniques can then be applied to the obtained Doppler shifted return to obtain information about the moving surface.

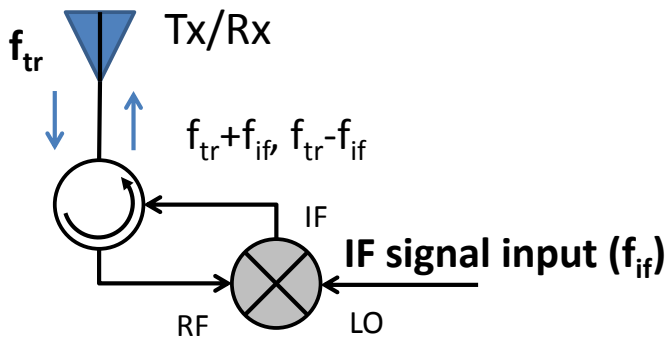

Fig. 8.4 A simple circuit representation of a low-IF tag.

The concept of low-if tag design is shown in Fig.8.4. The tag antenna would receive the transmitted signal (f_{tr}) and mixed with generated IF signal (f_{if}). The output of the mixer will then be transmitted back to the receiver. When tag is stationary, the down-converted signal should contain the IF signal without any information. When the tag is in motion, the IF signal should contain information about the motion. The signal at the receiver would be

$$R = A_R\left[\left(\cos(\omega_{tr}t + \omega_{if} + m(t)\right) + \left(\cos(\omega_{tr}t - \omega_{if} + m(t)\right)\right] \tag{8.1}$$

where $\omega_{tr} = 2\pi f_{tr}$ is the transmitted signal. If the local oscillator signal is represented as

$$LO = A_L \cos\left(\omega_{tr}t\right),$$

After mixing, we would get the IF signal that corresponds to a double sideband amplitude modulated signal.

$$IF = \frac{A_R A_L}{2}\left[\cos\left(\omega_{if} + m(t)\right) + \cos\left(\omega_{if} - m(t)\right)\right] \tag{8.2}$$

8.2 Low-IF tag design

8.2.1 Design

Since the Low-IF signal at the receiver has to be digitized, it would be preferable to keep it under 10 kHz. Any signal above 1 MHz would require expensive data acquisition hardware. At the same time, we need enough bandwidth to include the number of tags we desire for a system. The LO signal in the tag corresponds to the low-IF signal desired at the receiver. An oscillator from Linear technology (LTC6900) was selected to generate LO signal. LTC 6900 is a low power resistor set oscillator that can generate square wave from 1 kHz to 20 MHz. A schematic of the integrated circuit (IC) is shown in Fig. 8.5(a) with its typical application shown in Fig. 8.5(b) (Linear Technology, 2012). The IC runs from 2.7 V to 5.5 V and requires 500 μA of supply current.

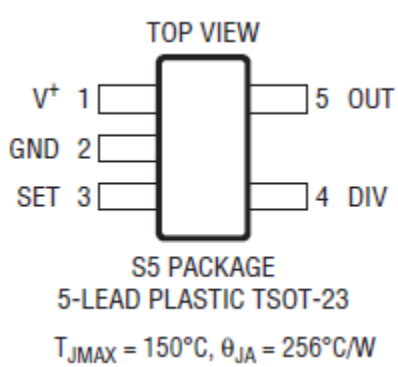

(a)

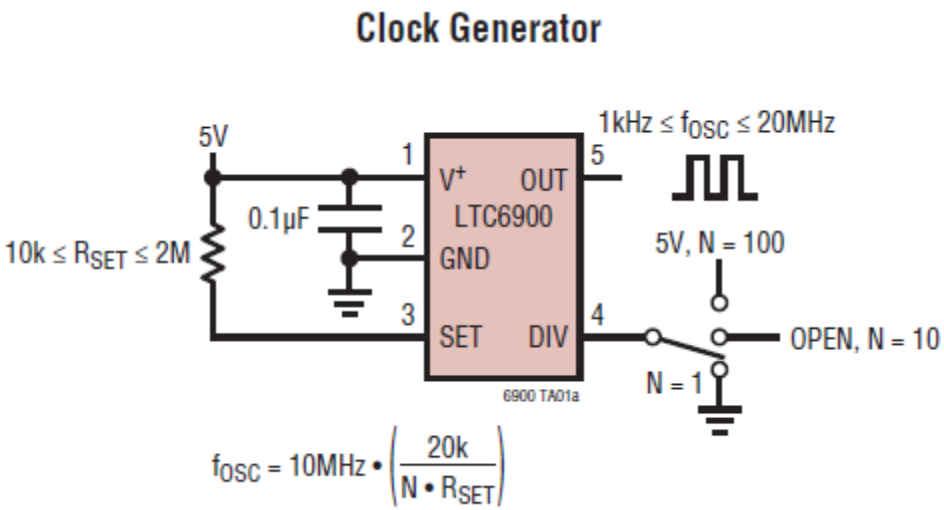

(b)

Fig. 8.5 Pin out of the resistor set oscillator (a) and a typical application circuit (b).

The oscillating frequency for a known resistor R_{set} can be calculated using the equation

$$f_{osc} = 10MHz \times \left(\frac{20000}{N \times R_{set}} \right), \tag{8.3}$$

where N is the value of the divider can be set by connecting to ground (1), leaving it open (10) or connecting to V^+ (100).

It would be ideal to keep the tag passive so that it would remove any dependencies on battery for its operation. But any generation of signal requires some energy that would have to be provided. That energy could be generated from incident EM radiation using an antenna and a rectifier, together termed as rectenna. However, to simplify the design for preliminary system testing, 3V batteries would be used to power the oscillator.

The choice of mixer for low-IF tag demands some consideration. Commercial up-converting mixers are available but seldom in the frequency range of IF that we desire. Some that are available are active mixers. Down-converting mixers can be used as up-converting mixers only if their design permits. Although, we would have power from the battery, the idea is to minimize power consumption so as to relax the design parameters of the rectenna (in the future). Most passive mixers are constructed by using diode pairs and filters. Hence, a single diode could also act as a simple mixer. As such, Schottky diode from Avago Technologies (HSMS-286Y) was used a mixing element in the low-IF tag. Owing to its small size, a 2.45 GHz dielectric antenna from TOKO was chosen (part No. DAC2450CT1T). The parameters of the antenna are shown in Fig. 8.6.

FEATURES

- Miniature footprint: 16mm diameter
- Low profile: 6.5mm max.
- Center Frequency: 2450 MHz
- Bandwidth: ± 50 MHz
- Peak Gain: Less than +2.14 dBi (0 dBi typ.)
- Impedance: 50 Ω
- Weight: 4.3 grams
- Operating temperature: - 10°C to + 60°C
- Storage temperature: - 20°C to + 85°C

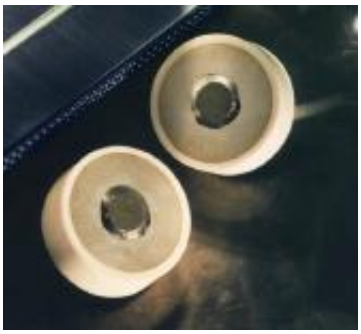

Fig. 8.6 Picture and parameters of the dielectric antenna used for low-IF tag design.

A circuit simulation was set up in Agilent ADS to evaluate the performance of the circuit. The simulation schematic shown in Fig. 8.7(a) and the generated frequency bands and their power levels are shown in Fig. 8.7(b). The input power at the port was kept to -30 dBm and the frequency was 2.45 GHz. An IF of 1 kHz at 500 mV was used for simulation. The results from Fig. 8.7 indicate the feasibility of making a functional tag prototype for quick testing.

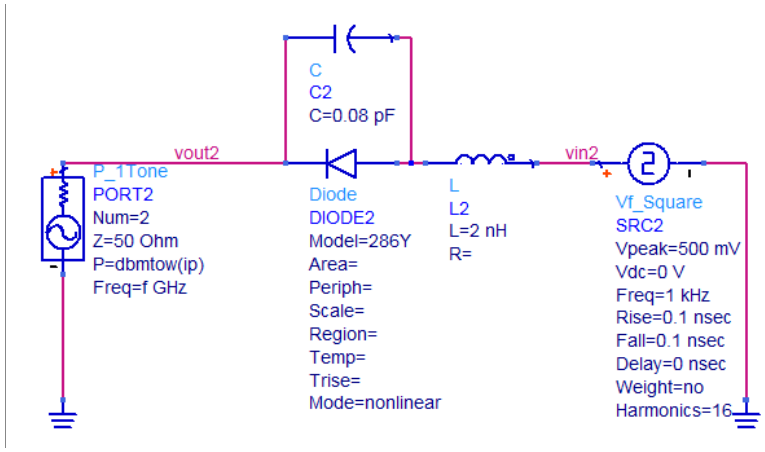

(a)

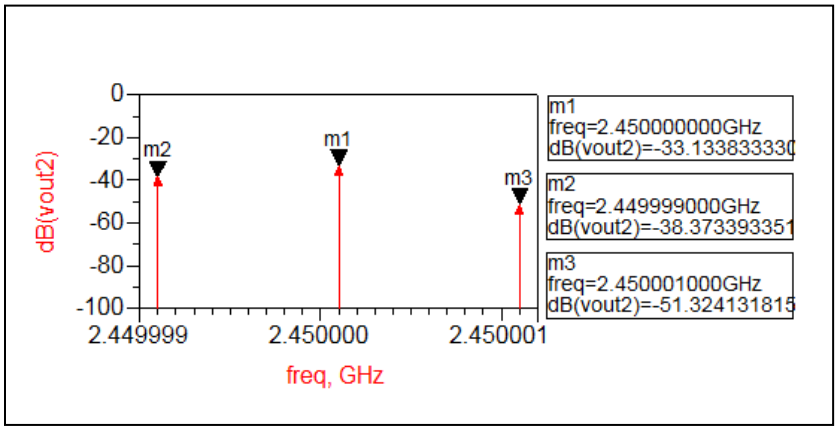

(b)

Fig. 8.7 Simulation results for a simple low-IF tag. Schematic of a low-IF tag (a), and simulation results for input power of -30 dBm and an IF of 1 kHz (b).

8.2.2 Fabrication and testing

Two tags were fabricated on 1 inch diameter through-hole plated prototype board. For one tag (tag 1), the R_{set} was chosen to be 1.82 MΩ which sets the theoretical output frequency at 1098.9 Hz and for tag 2, the R_{set} was chosen to be 1.32 MΩ that results in a theoretical output frequency of 1515.15 Hz. The fabricated tags were tested for correct output frequency before they were connected to the antenna and diode. The output of the

oscillator was connected to an oscilloscope. The measurement results are shown in Fig. 8.8. The output frequencies were 1096 Hz for tag 1 and 1531 Hz for tag 2 which is within the stated tolerance of 2%. After verifying that the generated frequency was as expected, the antenna and diode were soldered in place. The fabricated tags are shown in Fig.8.9. The individual parts of the tag are shown in Fig. 8.10(a) and Fig. 8.10(b).

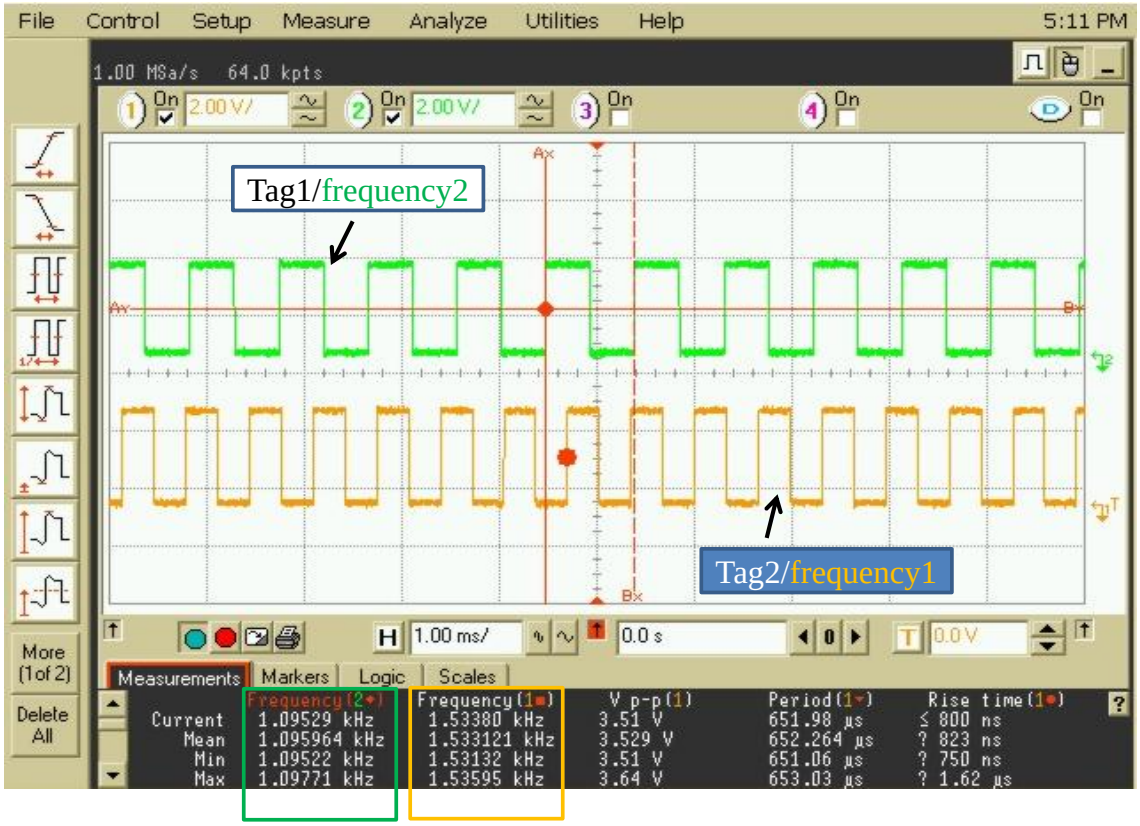

Fig. 8.8 Measured output frequencies from the two tags. A snapshot of oscilloscope output showing the oscillator output for tag 1 (green) and tag 2 (orange). The detected frequencies for each tag are enclosed by boxes with their trace colors.

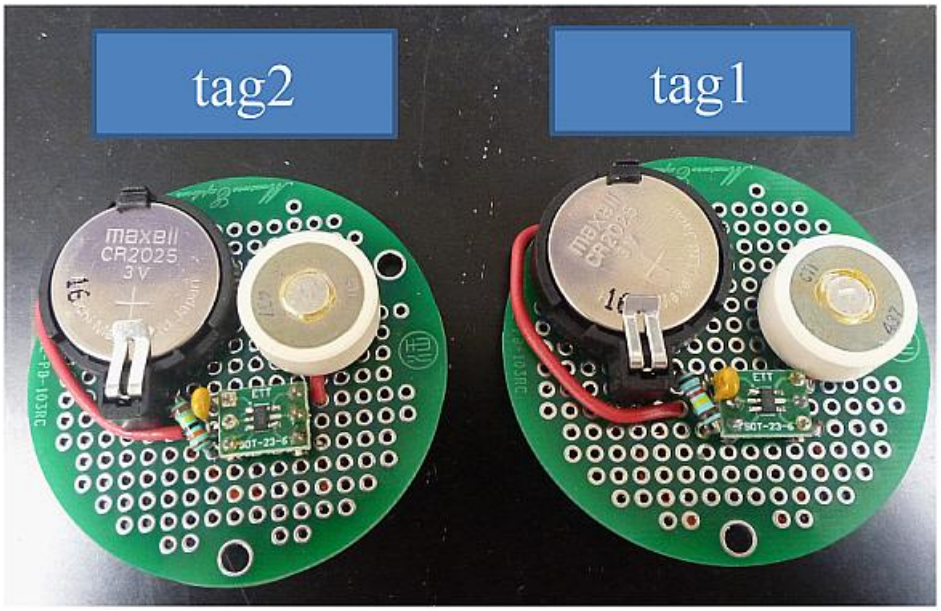

Fig. 8.9 Fabricated low-IF tags.

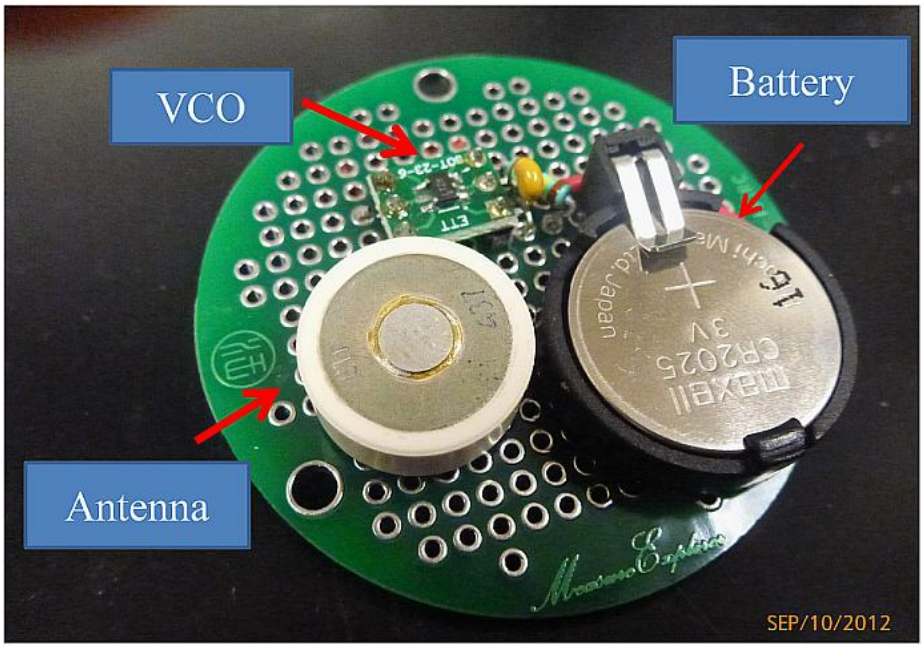

(a)

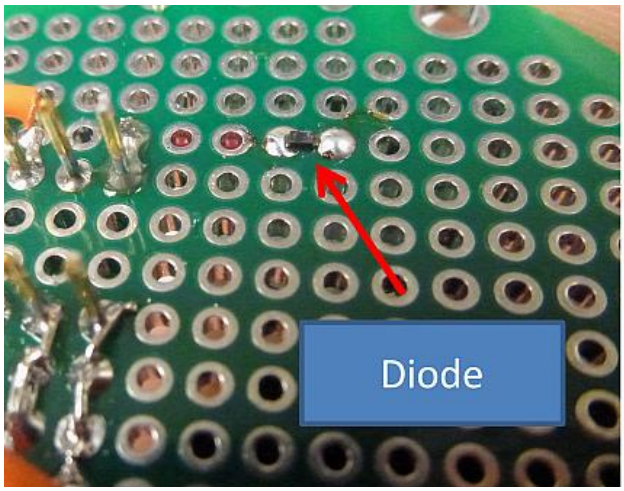

(b)

Fig. 8.10 Components used for low-IF tag circuit. Front (a), and backside of the low-IF tag showing the Schottky diode (b).

8.3 Measurements

8.3.1 Individual tag testing

A quadrature homodyne 2.45 GHz radar receiver was set up to receive signals from low-IF tags individually to test the presence of low-IF signals. A Linear stage from Galil was used to move the tags at a frequency of 0.3 Hz with 1 cm displacement. The power to the transmitting antenna was approximately 10 dBm. The distance between the antennas and the tag was approximately 70 cm. Tag1 was first moved in front of the radar the results of which are shown in Fig. 8.11. A sampling frequency of 20000 S/s was used for data acquisition. The AM data from channel I was demodulated in MATLAB® using envelope detection techniques. Data was first squared and then multiplied by 2 to preserve the amplitude. The signal was then passed through a low pass filter to yield the envelope. FFT (FFT) was then performed on the envelope to extract information on tag

motion. The results are shown in Fig. 8.12. Tag motion of 0.3 Hz can be clearly seen in Fig. 8.13(b) indicating the successful operation of tag 1.

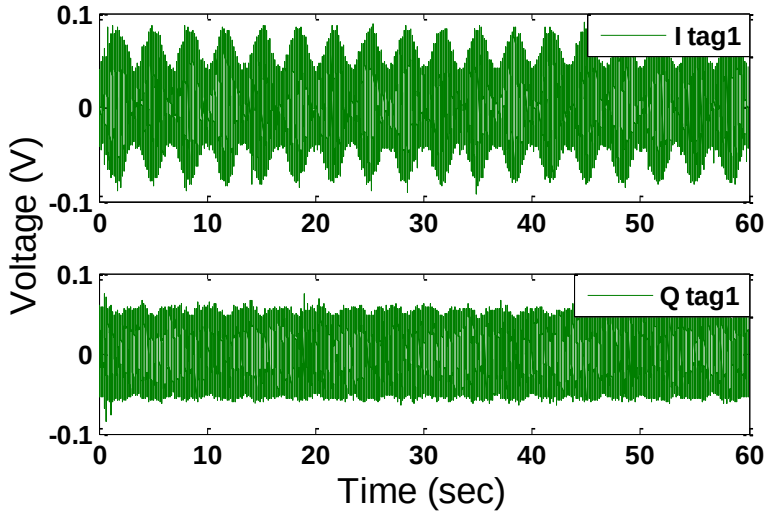

(a)

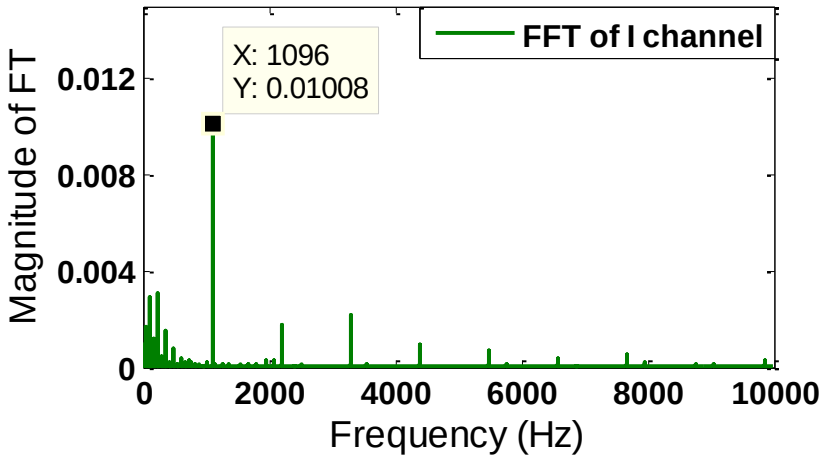

(b)

Fig. 8.11 Measurement results from tag1. Raw data from tag1 showing the amplitude modulated motion data (a) and FFT of I channel showing the presence of 1096 Hz.

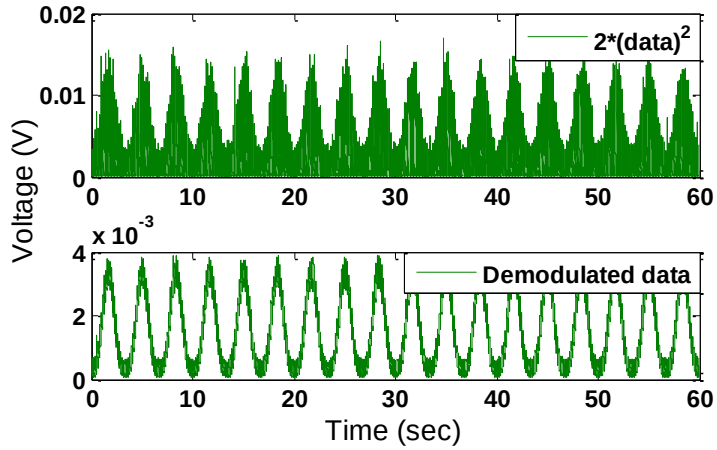

(a)

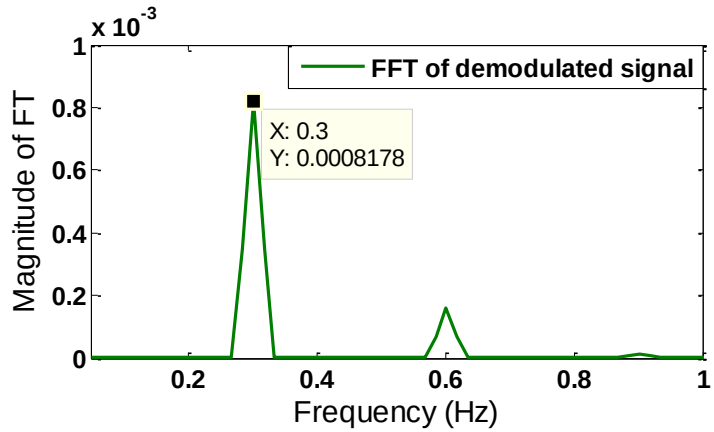

(b)

Fig. 8.12 Demodulated signal from tag 1. Voltage vs. time plots showing the extraction of envelope from the IF. Tag motion of 0.3 Hz can be clearly seen in the envelope (a), and the FFT of demodulated data from I channel clearly showing the presence of tag motion at 0.3 Hz.

The results for tag 2 for same experiment conditions are shown in Fig. 8.13 and Fig. 8.14. FFT analysis of channel I from tag shown in Fig. 8.13(b) shows the presence of 1531 Hz in the signal. Demodulation and FFT analysis of envelope in Fig. 8.14 indicates that tag 2 is moving at 0.3 Hz or 18 beats per minute (bpm). The experiment validates that both the low-IF tags are operational. Since the output of the tags is not filtered,

harmonics are also generated. To avoid interference, it is best to avoid assigning integer multiples of a frequency to a low-IF tag.

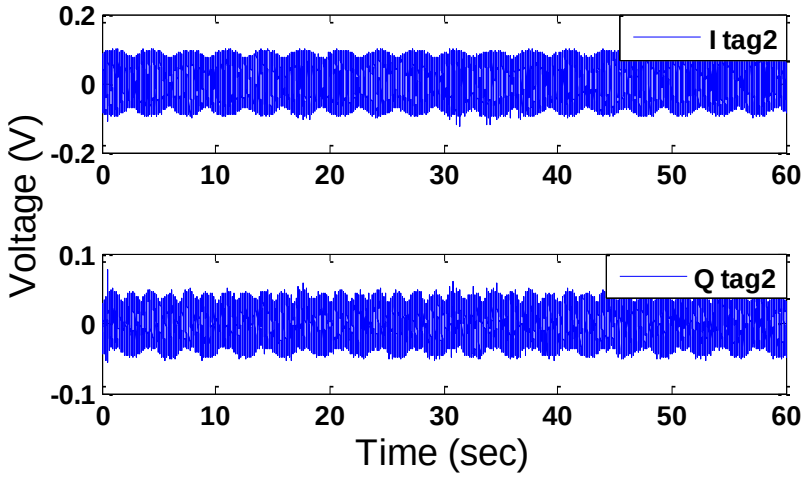

(a)

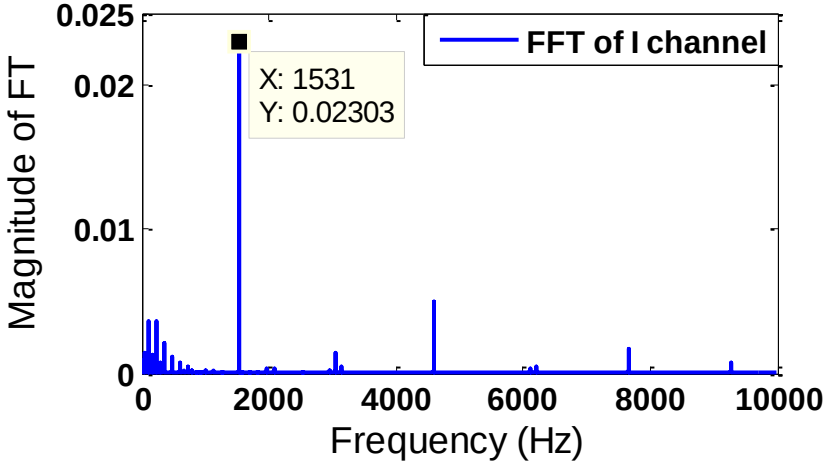

(b)

Fig. 8.13 Measurement results from tag 2. Raw data from tag 2 showing the amplitude modulated motion data (a), and FFT of I channel showing the presence of 1531 Hz. The generation of harmonics of IF can also be seen suggesting the need to define non-overlapping frequency for each tag in the system.

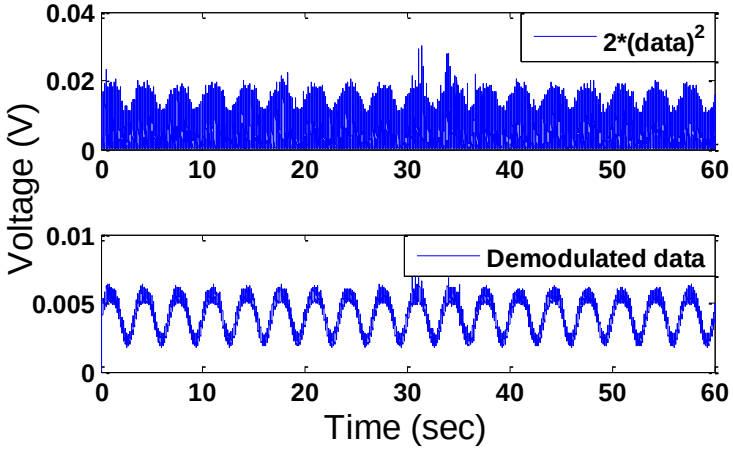

(a)

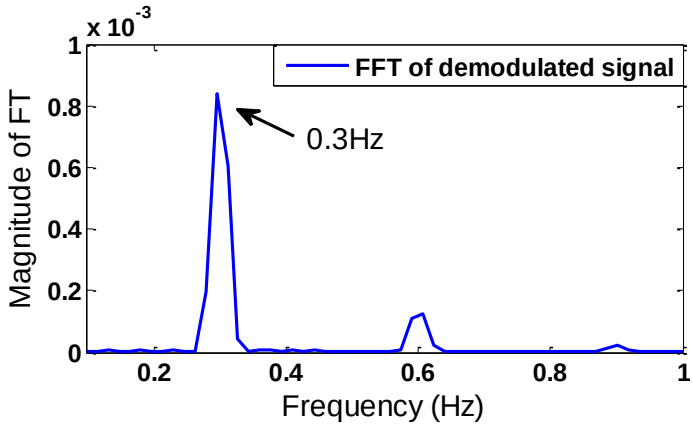

(b)

Fig. 8.14 Demodulated signal for tag 2. Voltage vs. time plots showing the extraction of envelope from the IF. Tag motion of 0.3 Hz can be clearly seen in the envelope (a), and the FFT of demodulated data from I channel clearly showing the presence of tag motion at 0.3 Hz.

8.3.2 Two tags together

After successful testing the operation of the tags individually, a test was set-up to see if the radar can detect the motion of both tags simultaneously. Both the tags were moved at 0.3 Hz with 1cm motion using the same linear mover. The distance between the

tags and the antennas was approximately 75 cm. The gain of the low noise amplifiers was set to 2000. The sampling frequency was reduced to 10000 Samples/s. The configuration of tags attached to the linear mover is shown in Fig. 8.15. The raw data from the measurement is shown in Fig. 8.16. From visual inspection, channel Q was selected for further analysis. Looking at the low-If data obtained from radar in Fig. 8.16, it is difficult to tell the presence of two tags. Since, the frequencies of the tags are known; band-pass filtering can be performed separating the intermediate frequencies.

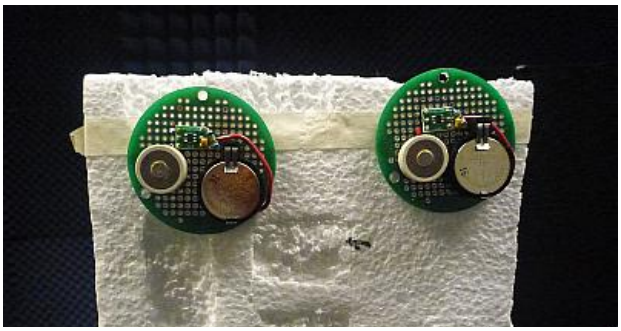

Fig. 8.15 Low-IF tags attached to the same mover.

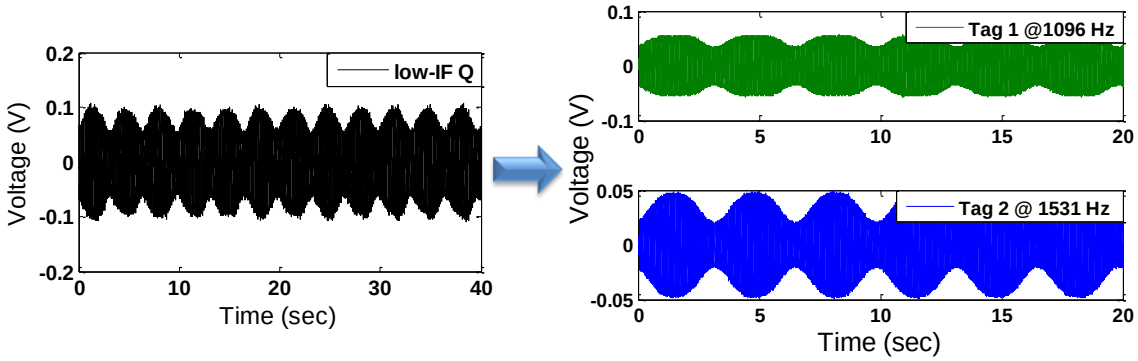

Fig. 8.16 Low-IF data from radar for simultaneous movement of tag 1 and tag 2 showing their presence after band-pass filtering.

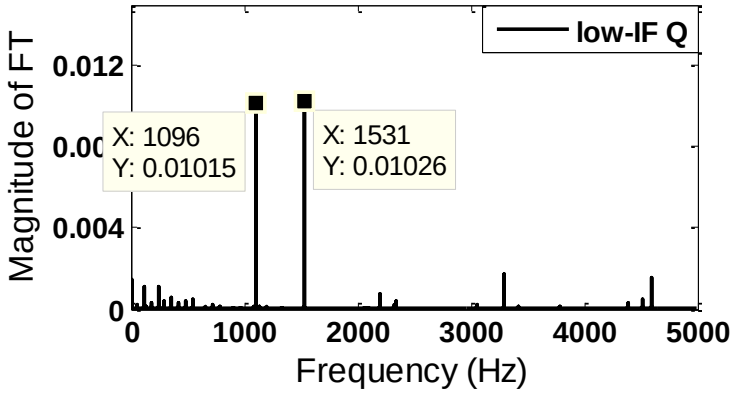

Fig. 8.17 FFT of low-IF data (channel Q) for simultaneous movement of tag 1 and tag 2 .

The FFT of low-IF data shown in Fig. 8.17 also indicates the presence of two frequencies at near-equal magnitudes. The band-pass filtered signals were demodulated and FFT was performed to obtain motion information for each tag. Fig. 8.18 shows the demodulated signals for each tag and Fig.8.19 shows the FFT of demodulated signals. The results prove that it is possible to use a radar system with one transmitting and one receiving antenna to detect two moving objects simultaneously by using low-IF tags. It also proves that the tags can be detected even if they all are moving at the same rate. It is important to note that the theory can be extended to multiple tags.

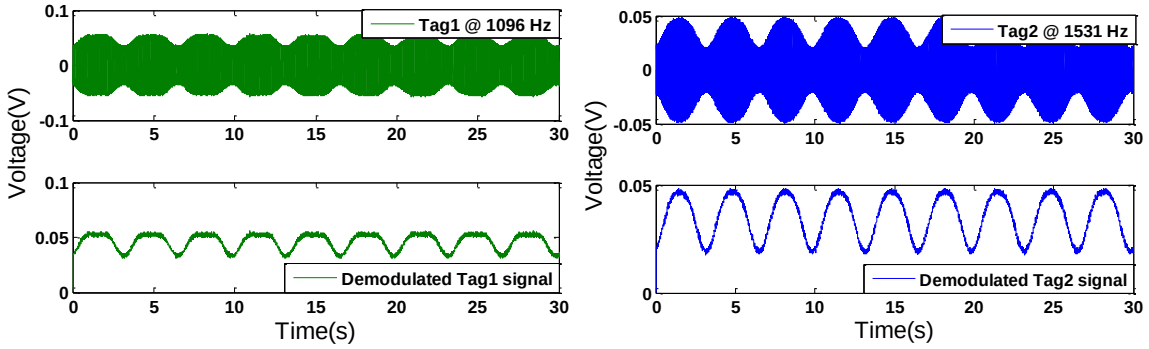

(a) (b)

Fig. 8.18 Demodulated signal for tag 1 (a), and tag 2 (b).

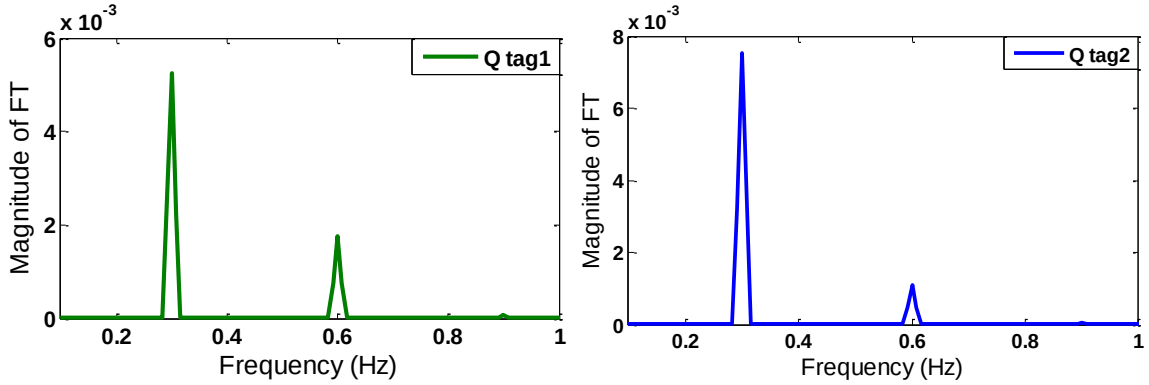

(a) (b)

Fig. 8.19 FFT of demodulated signal for tag 1 and tag 2. The detected motion rate of 0.3 Hz for tag 1 (a), and tag 2 (b) indicates the successful detection of two objects moving at the same rate.

8.3.3 Two tags and an untagged object

We now have a radar system that can distinguish and track two targets simultaneously. In a field operation such as a rescue operation as discussed in chapter x, we also want to know the presence of motion that is not tagged. Adaptive noise cancellation algorithms were applied to two frequency radar operation to cancel out harmonic tag motion from the baseband of quadrature 2.45 GHz radar to give information about the non-tagged motion. In this case, two radar receivers had to be used. We also receive baseband signal from low-IF tag radar. However, this baseband signal is corrupted due to the presence of multiple motion sources .This section would explore the use of adaptive noise cancellation technique to cancel out the demodulated low-IF tag signal from baseband data. The principles of adaptive noise cancellation for radar application have been discussed in chapter 7.

Before we could perform adaptive noise cancellation, another problem needs to be solved. So far, the tag signals were visually inspected to make decisions on optimal channel selection. It would be more appropriate to combine I and Q signals instead of processing individual channel. The channels could be combined immediately after they are acquired which would be computationally more expensive due to high sampling rate. In addition, it is not certain if linear demodulation of IF signals would give the correct signal. Another possibility is to combine the channels after demodulating and down sampling each channel. A comparison between the options for linear combination is shown in Fig. 8.20 and Fig. 8.21.

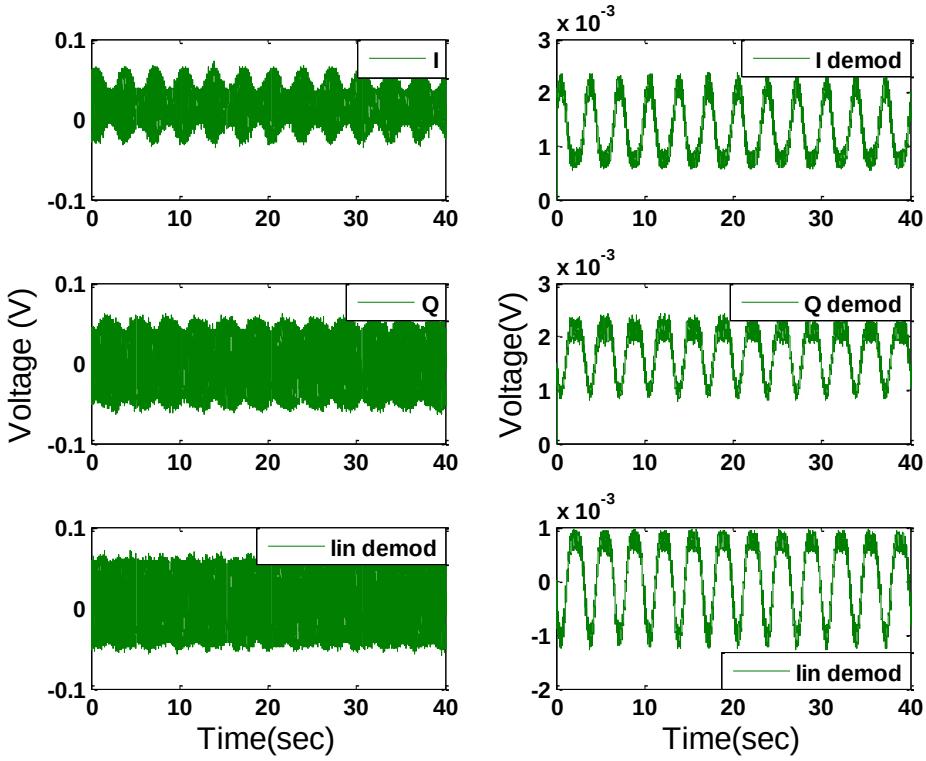

Fig. 8.20 Comparison of two methods for linear demodulation of low-IF data. Left side represents linear demodulation of low-IF signals and right side represents linear demodulation following independent demodulation of amplitude modulated I and Q channels.

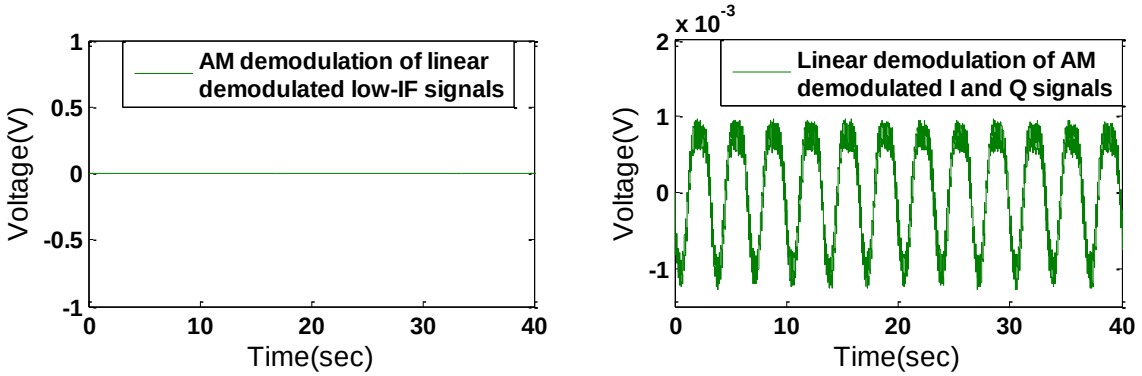

Fig. 8.21 Results from two methods for linear demodulation of low-IF data. Left side shows demodulation of AM signal following linear combination of low-IF I and Q signals. Right side shows linear combination of AM demodulated I and Q channels.

Results from Fig. 8.21 indicate the absence of any motion in the linear demodulated low-IF signals which is incorrect as shown by the second method where the linear demodulation was performed after the AM demodulation of I and Q channels separately. It can be concluded from this experiment that it is best to combine the signals after their envelope has been extracted.

An experiment was set up using three targets and three movers. The low-IF tags were put in front of the antennas at a distance of 60 cm. A Styrofoam hemisphere having a diameter of 20 cm represented an untagged motion source. The Styrofoam hemisphere was covered with aluminum foil to increase scattering. Since the physical cross section of hemisphere was very big compared to the low-IF tags, it was placed at a distance of 90 cm. The untagged object was placed at an angle to the receiving antenna but within its E plane beam-width of 60^0 owing to limited space in front of the antenna. The motion characteristics of each target are listed below and the orientation of targets with respect to radar is shown in Fig. 8.22.

Tag1: 0.3 Hz, 7-8 mm

Tag2: 0.4 Hz, 10 mm

Untagged object: ~0.2 Hz, maximum angular displacement between 5-10mm.

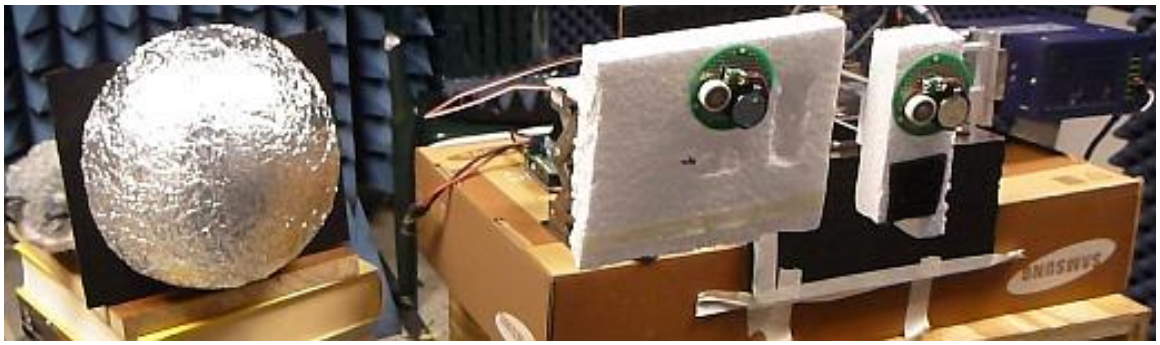

(a)

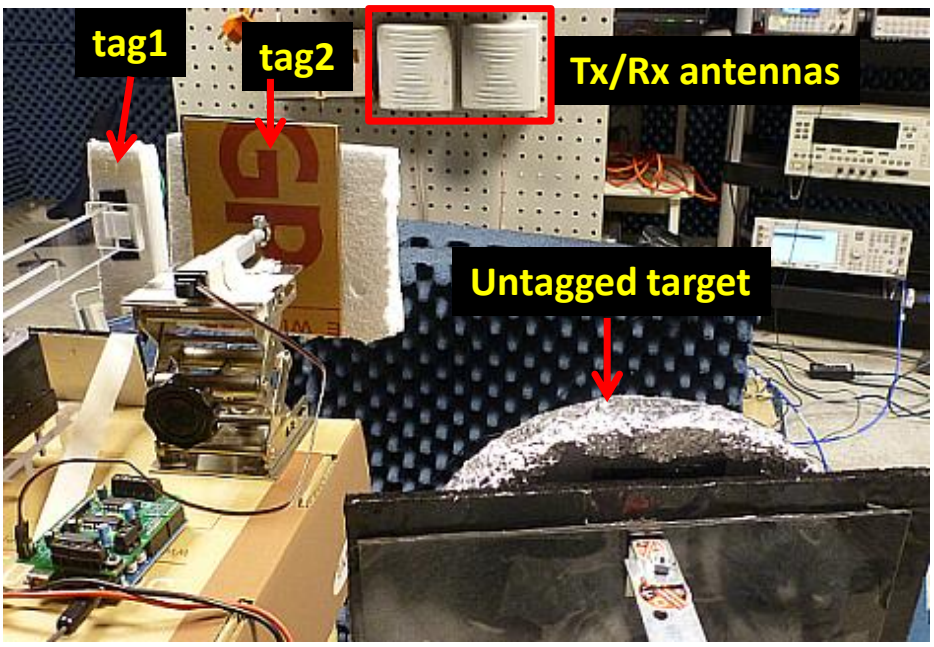

(b)

Fig. 8.22 Measurement setup for three targets. Positions of target with low-IF tags directly in front of the antenna (a), and setup showing the antennas along with the positions of the targets (b).

The mixer output was fed to low noise amplifier having a band-pass filter setting of 0.03 Hz – 3 kHz. The recorded low-IF data was separated into three frequency bands corresponding to tag 1, tag 2 and baseband respectively. The envelopes for I and Q channels for each tag were extracted and then combined using linear demodulation to yield one signal. The baseband data was obtained by passing the low-IF channels through a low pass filter and then combining the signals using linear demodulation. Signals are shown in Fig. 8.23. Offsets and a gain of 50 were deliberately added to tag 1 and tag 2 signals for display clarity.

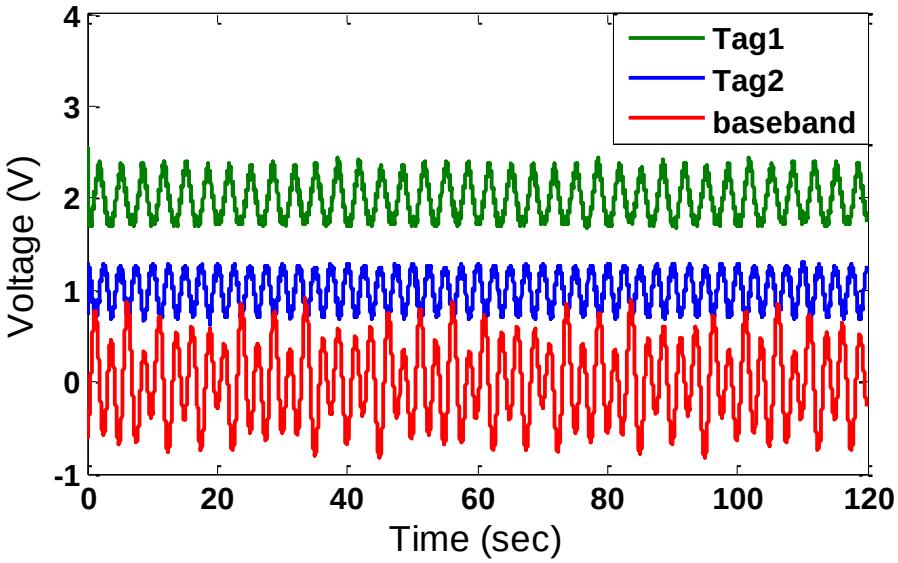

Fig. 8.23 Measurement results from three target motion. Signals from the two tags after envelope extraction and linear demodulation of I and Q channels. Baseband signal was obtained after low-pass filtering and subsequent linear demodulation of low-IF signals.

FFT was performed on signals in Fig. 8.23 and are shown in Fig. 8.24. FFT analysis of tag 1 data (Fig. 8.24(a)) shows its motion at 0.3 Hz and analysis of tag 2 data shows its motion at 0.4 Hz in Fig. 8.24(b). Analysis of baseband data reveals the presence of three distinct frequencies at 0.21, 0.3 and 0.4 Hz. While the FFT data displays the

different frequency components present in the signal, it is a very difficult proposition to track all the three detected frequencies using one radar system without employing MIMO techniques. Even so, it would be even more difficult to identify the source of motion with absolute certainty as MIMO techniques identify the signal from the angle of arrival. A change in the rate of the signal can also be interpreted as a change in the position of the source of that signal which brings ambiguity to the system.

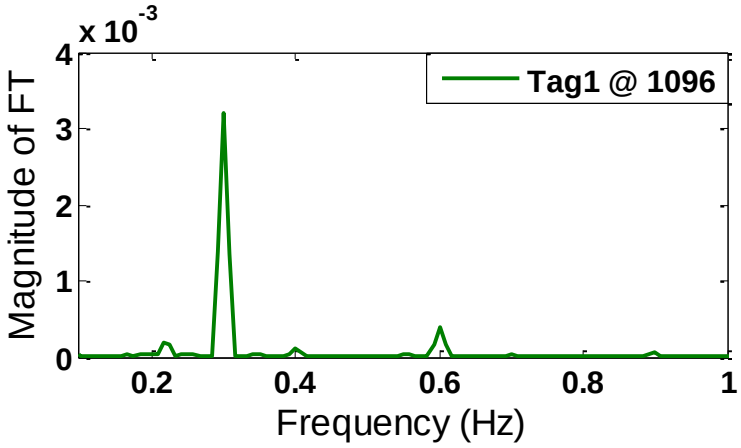

(a)

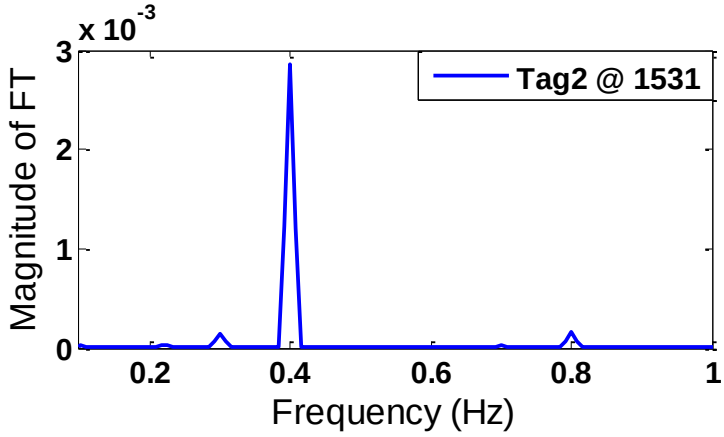

(b)

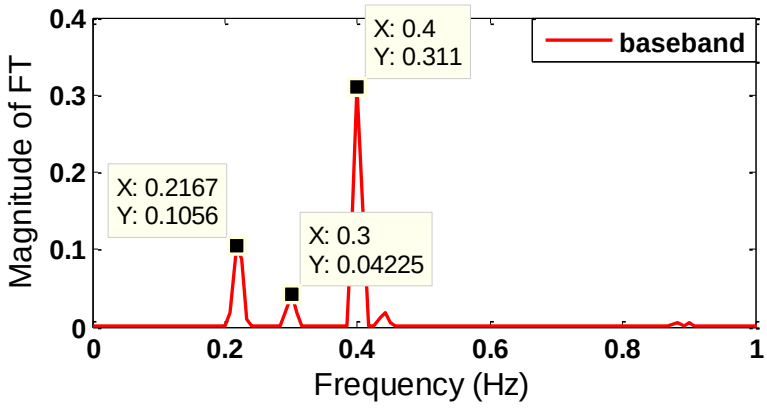

(c)

Fig. 8.24 FFT of signals obtained in Fig. 8.23 for tag 1 (a), tag 2 (b) and baseband (c).

For low-IF tag system, this ambiguity is removed as the information at 0.3 Hz and 0.4 Hz can be attributed to tag 1 and tag 2 respectively. Subtraction of tag signals from baseband can then provide us with motion content from any untagged object. However, this subtraction would have to be carried out twice to cancel information from each tag. From Fig. 8.23, it could also be observed that the baseband signal magnitude is an order higher than the extracted signal from the tag. Hence, the tag signals that were amplified by 50 in Fig. 8.23 were used for application of ANC algorithm. All the signals were down sampled to 100 Hz to ease the computational cost for performing adaptive noise cancellation. Normalized Least Mean Squares (NLMS) algorithm with a step size of 0.006 and a filter order of 32 was employed to cancel out the tag signals from baseband. The baseband signal after application of ANC is shown in Fig. 8.25 and its FFT analysis shown in Fig. 8.26.

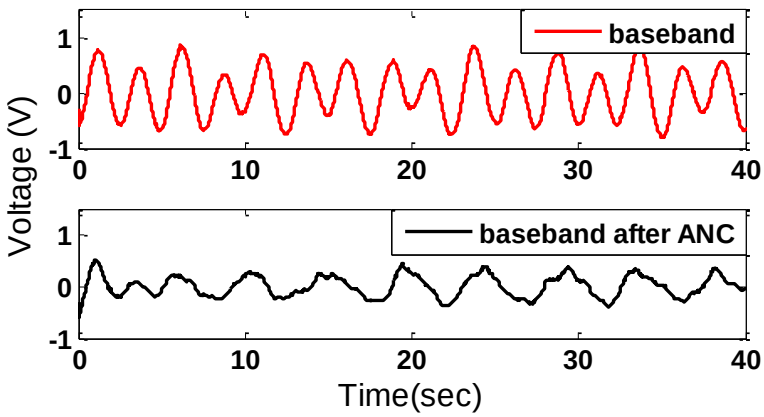

Fig. 8.25 Comparison of baseband signal before and after application of ANC algorithm. Cancellation of some components is evident in the signal.

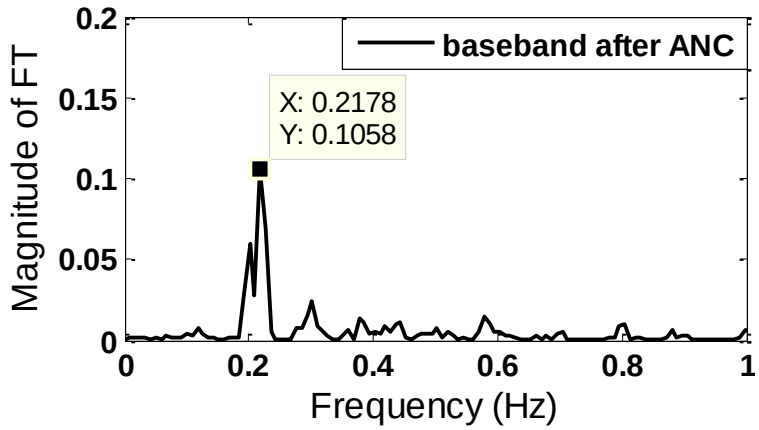

Fig. 8.26 FFT of baseband signal after ANC showing successful cancellation of 0.3 Hz and 0.4 Hz signal content that relate to the low-IF tags.

As discussed previously, although it is convenient to detect the presence of various non-overlapping motion content using CW quadrature Doppler radar, it is almost impossible to identify and track all of them without the use of additional markers (physical or biometric). After application of rate tracking algorithm on the acquired data, it is shown in Fig. 8.27 that the low-IF tag radar system is able to track two tags and an untagged source of motion without the use of MIMO techniques or sophisticated signal

processing algorithms. Short time Fourier transform (STFT) was used to determine the rate. A data window of 30 seconds with an overlap of 10 seconds was applied to estimate the rate. The estimated rates are within 3% of actual rate owing to poor frequency resolution due to small window length and low sampling frequency (100 Samples/s). From Fig. 8.27, it can be seen that baseband signal is tracking 0.4 Hz (24 bpm) corresponding to tag 2 frequency before the application of ANC algorithm. After cancellation of the two tag signals, baseband signals is shown to correctly track the untagged motion at approximately 14 bpm.

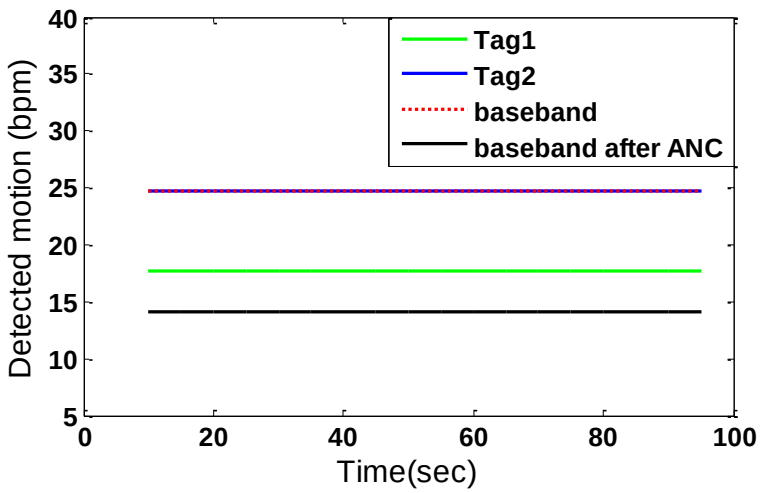

Fig. 8.27 Tracking of multiple targets using a low-IF tag radar system. Application of ANC algorithm improves the baseband tracking accuracy to 100%.

To show the ability of the radar to track the tags as they change their motion, another experiment was performed where the conditions were same as Fig.8.22 but the positions of tag 1 and tag 2 were interchanged. This was done as it was technically not feasible to dynamically change the motion of the linear movers without interfering with the experiment. Now, tag 1 was moving at 0.4 Hz and tag 2 was moving at 0.3 Hz. The motion of untagged object remained the same. The obtained data was processed in a

similar manner as described above and the obtained rate data was appended to previous data set. What it implied was that we now have a data set where for the first 95 seconds, tag 1 will move at 0.3 Hz and tag 2 at 0.4 Hz. After 95 seconds, tag 1 would start moving at 0.4 Hz and tag 2 would start moving at 0.3 Hz. Using MIMO and blind source separation techniques, it would be difficult to attribute this change to a change of rate for individual targets or swapping of location. The low-IF tag radar should conveniently be able to determine this change in the motion of the tags owing to their unique low-IF. The results are shown in Fig. 8.28.

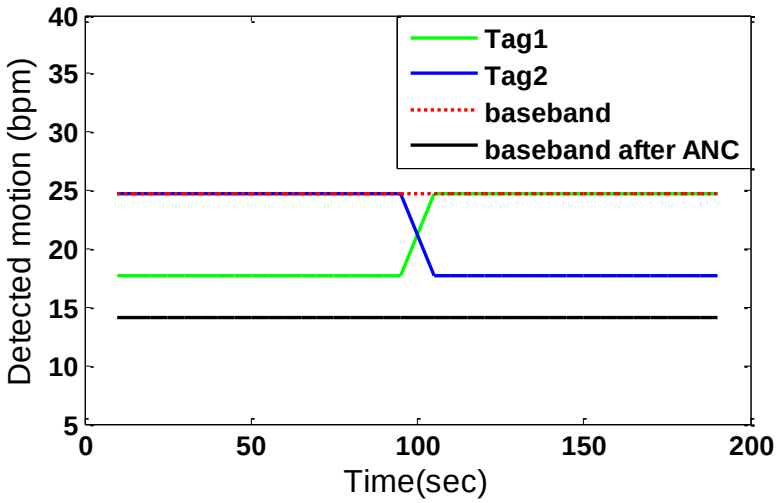

Fig. 8.28 Tracking results for simulated data where the rate of motion of low-if tags is swapped during the measurement. Plot displaying correct tracking of motion sources due to the use of low-IF tags. It is interesting to note that the baseband signal tracks the 0.4 Hz motion irrespective of the low-IF tag that is attached to it. This could be attributed to the larger displacement of the linear mover moving at 0.4 Hz.

Fig.8.28 presents three interesting results:

1) It can correctly identify the source of motion for low-IF tags.

2) Baseband signal tracks 0.4 Hz irrespective of the tag attached to it. This could be attributed to the larger displacement of the corresponding linear mover. However, this can change for different situations and corresponds to the location of the three targets with respect to the transmitting and receiving antennas.
3) The change in tag frequency does not affect the ANC algorithm and rate estimation of adaptively filtered baseband signal.

Chapter 9. Summary and Conclusions

The ability to detect the desired motion and reject the undesired motion is very important, especially for applications of radar in physiological monitoring of humans or animals. Selectivity for Doppler radar was defined as a two-level problem. An important aspect of the problem was to obtain this selectivity without completely changing the current Doppler radar architecture. Two types of radio frequency tags and systems compatible with existing Doppler radar system were introduced in this work. Both of these system work on similar principle, i.e., modifying the frequency that is scattered back by placing the tag on the desired motion. While harmonic tag enables us to distinguish a tagged object from an untagged object and clutter, low-IF tags allow us to monitor multiple sources of motion using multiple tags. Both of these systems were used to monitor untagged motion by cancelling the signal from the tag/tags using adaptive noise cancellation principles. Since low-IF tags are superior in performance and provides both levels of selectivity, the need for harmonic tags becomes doubtful. However, harmonic radar system would still be useful where small displacements need to be measured as they increase the resolution of the radar system by doubling the operating frequency. They are also useful in applications where objects of same type do not need to be distinguished. Harmonic tags are passive and very inexpensive to fabricate. Studies with harmonic radar and low-IF tag radar provided a comprehensive understanding of challenges involved with designing a robust Doppler radar system. The measurement results from these systems prove the feasibility of using Doppler radar for home health monitoring application, field operations and for animal monitoring. The studies also

provided a direction that could be taken to perfect the system. The following sections would talk about ideas that merit further research and develop on this research.

9.1 Harmonic tag and radar

The idea of clutter rejection and subject isolation led to the development of ‘f-2f’ Doppler radar systems that employ passive harmonic tags. These harmonic tags employ non linear Schottky diodes and the tag antenna and diode are matched at second harmonic of the incident frequency. The received system was modified to detect the backscatter from the tag at second harmonic (‘2f’) and reject any fundamental frequency (‘f’). The harmonic tag designed was functional and good albeit not optimum.

9.1.1 Effect of inductor stub width on tag antenna

The performance of the tag relies strongly on the matching between the tag antenna and the diode. The received incident power depends on the resonant frequency of the tag and the impedance match between the tag antenna and the diode. An inductive stub was used in chapter 3 to match the tag antenna with the capacitive impedance of the Schottky diode. During simulation, it was observed that the width of the inductive stub on the tag plays an important role in deciding the impedance of the tag at 2.45 GHz. As the stub width was increased, the impedance of tag antenna at 2.45 GHz was decreasing resulting in closer match to diode impedance that increased the power transfer. The stub was simulated with different widths from 0.5 to 2 mm and the antenna and system simulations were carried out for different widths. The system simulations were carried out for a distance of 1 meter and a transmitted power of 10 dBm. The results are shown in table 9.1. The simulation results also indicate that the tag antenna impedance does not

change significantly for 4.9 GHz. For comparison, for an input power of -12 dBm, the diode impedance at 2.45 GHz and 4.9 GHz was 6.01 – j 218 Ω and 5.64 - j62.79 Ω respectively.

Table 9.1. Calculation of generated harmonic power as a function of inductor stub width

Width of stub (mm)	**$Z_{2.45\ GHz}$**	**$Z_{4.9\ GHz}$**	**Generated harmonic (dBm)**	**Assumed retransmitted harmonic (-3dB)**	**Received power @ analyzer (dBm)**
0.5	243.25 + j414		-66.024	-69.0	-104.23
0.75	152.25 + j362		-62.040	-65.0	-100.23
1	104.45 + j319		-60.285	-63.3	-93.34
1.25	75.3 + j283		-52.149	-55.1	-90.33
1.5	56.1 + j 253	146 + j 223.2	-46.830	-49.8	-85.03
1.75	42.7 + j228	131.05 + j 220	-43.763	-46.7	-81.93
2	33.3 + j 207	119.05 + j 217	-43.478	-46.4	-81.63

With proper tools, it is also possible to design more sophisticated tag antennas such as microstrip fractal antennas (Gianvittorio and Rahmat-Samii, 2002). An application of fractal antenna structure for harmonic tag design has been shown by Psychoudakis *et al.* (Psychoudakis *et al.*, 2008). Fractal antennas allow longer electric length to be fitted in a smaller physical area by using fractal geometry, allowing us to fabricate smaller antennas for the same resonant frequency.

9.1.2 Other harmonic radars

Perfect isolation was not achieved using ‘f-2f’ radar system due to the transmission of small signal levels of 4.9 GHz that were getting detected and subsequently amplified. One way to improve the performance of the harmonic radar

system would be by using ‘f-3f’ radar. The transmission of third harmonics from the transmitting antenna would be very low and allow the system to have even better SNR. Tag design would also be easy as diode pairs could be used to generate odd harmonics of the incident frequency. However, more power would be needed to turn on the tags due to the use of two diodes. Homodyne receiver for ‘f-3f’ systems would require a frequency Tripler that are conveniently available and heterodyne systems would require the addition of another mixing stage.

9.2 Low-IF tags

In addition to separating the subject from non stationary clutter low-IF tags allow the encoding of unique frequency shifts to each tag by simply changing a resistor. These frequency shifts can be uniquely detected using band-pass filters in software, allowing us to monitor several tagged motion sources at a time. The number of tags for a system will be limited by the data acquisition hardware and the frequency bandwidth. The maximum sampling rate of the data acquisition hardware will limit the maximum frequency shift that could be used for the tags. For example, to detect a frequency shift of 10 kHz, the system should be able to sample at 20 KS/s or more. For optimum operation of the tags, it would be beneficial to avoid using the second harmonic of a frequency. For example, if an IF of 1 kHz is used for one tag, the use of 2 kHz as IF for another tag should be avoided. Since the frequencies are resistor set, that have standard values, a combination of resistors might be required to achieve the exact frequency that is desired.

Improvements in low-IF tag design could be made by matching the mixer diode with the output of the oscillator and the antenna. The oscillator output in this case can drive 10pF

loads as well. A rectenna circuit could power the circuit using incident radiation and eliminate the use of a battery. The feasibility of using a very low power microcontroller as an oscillator was also considered. The use of microcontroller was found unsuitable owing to programming hardware and software requirements whereas the VCO could be run and tuned by a resistor. Even with a battery, the low-IF tag has some advantages over using wearable wireless sensors. Wearable wireless sensors still need contact sensors that undergo wear and tear and are personalized. Wearable sensors tend to be more expensive and not a cost effective solution for large systems.

Another interesting addition to the current low-IF tags would be temperature sensing. Temperature sensing could be incorporated in the low-IF tags by using a thermistor to set the operating frequency. Changes in temperature could then be detected by detecting the changes in the IF.

9.3 Conclusion

Most of the work in the dissertation focused on applications of tag with respect to human physiological monitoring. However, the work can easily be extended to any application that requires selective monitoring. Small animal monitoring is one such example. The requirements for this application would be different in terms of tag size and the radar frequency but could be achieved using the knowledge and tools presented in this work.

This dissertation contributes to the field of electrical engineering by solving one of the bigger problems of selectivity associated with the Doppler radar. In doing so, techniques were developed that can be applied to any radar. Simulations and

measurement results for harmonic tags indicate that selective monitoring of a subject could be done simply by placing a harmonic tag on that subject. Harmonic tag and radar could also be used with a conventional radar system to detect both tagged and untagged motion. The displacement measurements also indicate the advantages of using harmonic tags for measuring small displacements. The use of low-IF tags allowed us to monitor and track more than one tagged motion source. Adaptive noise cancellation algorithms were used to show the feasibility of cancelling tagged motion to track an untagged motion source. The use of ANC algorithm would work for any RF tag and radar system. To summarize, the work presented in this dissertation provides selectivity to a radar system, thereby making it more robust and reliable, and bringing it one step closer to practical applications.

References

Abidi, A. A., 1995, "Direct-conversion radio transceivers for digital communications". *IEEE Journal of Solid State Circuits*, vol. 30, no. 12, pp. 1399-1410.

Agilent EEs of EDA design software, 2012."Advanced Design System". [online] Available at < http://www.home.agilent.com/en/pc-1475688/agilent-eesof-eda-design-software?nid=-34360.0&cc=US&lc=eng>. [Accessed December 4 2012].

Arai, I., 2001. "Survivor search radar system for persons trapped under earthquake rubble". *Proceedings of the Asia Pacific Microwave Conference*, Taipei, Taiwan, 3-6 Dec 2001, pp. 663-668.

Avago technologies, 2012. "HSMS-286Y: microwave Schottky detector diode in SOD-523 package". [online] Available at http://www.avagotech.com/pages/en/rf_microwave/diodes/schottky/hsms-286y/>. [Accessed November 26, 2012].

Bache, R. J., Harley, A., and Greenfield, J. C., Jr., 1969. "Evaluation of thoracic impedance plethysmography as an indicator of stroke volume in man". *American Journal of Medical Sciences*, 258:(2), 1969, pp. 100-113.

Balanis, C., 1997. "Antenna theory: analysis and design, 2nd edition". *John Wiley and Sons, Inc.*, 1997.

Behbahani, F., Leete, J. C., Kishigami, Y., Roithmeier, A., Hoshino, K., and Abidi, A. A., 2000. "A 2.4 GHz low-IF receiver for wideband WLAN in 0.6-um CMOS - architecture and front end". *IEEE Journal of Solid State Circuits*, vol. 35 no. 12, pp. 1908-1916.

Bjorklund, S., Petersson, H., Nezirovic, A., Guldogan, M. B., and Gustafsson, F., 2011. "Millimeter-wave radar micro-Doppler signatures of human motion". *International Radar Symposium*, Leipzig, 7-9 Sept. 2011, pp. 167-174.

Boll, S., and D. Pulsipher, D., 1980. "Suppression of acoustic noise in speech using two microphone adaptive noise cancellation". *IEEE Transactions on Acoustic, Speech and Signal Processing*, vol. 28 issue 6, pp. 752-753.

Boric-Lubecke, O., Ong, P. -W., and Lubecke, V. M., 2002. "10 GHz Doppler radar sensing of respiration and heart movement". *Bioengineering Conference, 2002. Proceedings of the IEEE 28th Annual Northeast*, Philadelphia, PA, USA, 20-21 April 2002, pp. 55-56.

Boric-Lubecke, O., Lubecke, V. M., Host-Madsen, A., Samardzija, D., and Cheung, K., 2005. "Doppler radar sensing of multiple subjects in single and multiple antenna systems". *7th international conference on Telecommunication in modern satellite, cable and broadcasting services*, vol.1, 28-30 Sept. 2005, pp.7-11.

Braunwald, E., and Perlkoff, J. K., 2001. “Physical examination of the heart and circulation”. in Heart Disease: A textbook of cardiovascular medicine, (E. Braunwals, D. P. Zipes, and P. Libby, Eds.), New York: *W. B. Saunders Company*, pp. 45-81.

Brazee, R. D., Miller, E. S., Reding, M. E., Klein, M. G., Nudd, B., and Zhu, H., 2005. “A transponder for harmonic radar tracking of the Black Vine Weevil in behavioral research”. *American Society of Agriculture Engineers Trans.*, vol. 48(2), pp. 831–838.

Budge, M. C., Jr., and Burt, M. P., 1993a. “Range correlation effects in radars”. *IEEE Radar Conference*, Lynnfield, MA, USA, 20-22 April 1993, pp. 212-216.

Budge, M. C., Jr., and Burt, M. P., 1993b. “Range correlation effects on phase noise spectra”. *Proceedings of Twenty-Fifth Southeastern Symposium on System Theory*, Tuscaloosa, AL, USA, 7-9 March 1993, pp. 492-496.

Butler, P. J., Frappell, P. B., Wang, T., and Wikelski, M., 2002. “The Relationship Between Heart Rate and Rate of Oxygen Consumption in Galapagos Marine Iguanas (*Amblyrhynchus cristatus*) at two different temperatures”. *Journal of Experimental Biology*, vol. 205, pp. 1917-1924.

Cao, H., Soltani, A. T., Fager, C., Eriksson, T., and Zirath, H., 2009. “I/Q imbalance compensation using a nonlinear modeling approach”. *IEEE Transactions on Microwave Theory and Techniques*, vol. 57, no. 3, pp. 513-518.

Chan, K. H., and J. C. Lin, J. C., 1987. “Microprocessor based Cardiopulmonary rate monitor”. *Med Biol Eng. Comput.*, vol.25, issue 1, pp. 41-44.

Chang, S. H., Chung, H. S., and Kim, K., 2009. “Impact of quadrature imbalance in optical coherent QPSK receiver”. *Photonics Technology Letters, IEEE*, vol.21, no.11, pp. 709-711.

Chen, K. –M., Huang, Y., Zhang, J., and Norman, A., 2000. “Microwave life-detection systems for searching human subjects under earthquake rubble or behind barrier”. *IEEE Transactions on Biomedical Engineering*, vol. 47, no. 1, pp. 105-114.

Chuang, H. R., Chen, Y. F., and Chen, K. M., 1990. “Microprocessor-controlled automatic clutter-cancellation circuits for microwave systems to sense physiological movements remotely through the rubble”. *Proceedings of the Instrumentation and Measurement Technology Conference*, 13-15 Feb 1990, pp. 177-181.

Churchill, F. E., Ogar, G. W., and Thompson, B. J., 1981. “The correction of I and Q errors in a coherent processor”. *IEEE Transactions on Aerospace and Electronic Systems*, vol. AES-17, no.1, pp. 131-137.

Colpitts, B., Luke, D., Boiteau, G., and Doyle, M., 1999. “Harmonic radar identification tag for insect tracking”. *Proceedings of 1999 IEEE Canadian conference on Electrical and Computer Engineering*, Alberta, Canada, 9-12 May 1999, pp. 602-605.

Colpitts, B. G., and Boiteau, G., 2004. “Harmonic radar transceiver design: miniature tags for insect tracking”. *IEEE Transactions on Antennas and Propagation*, vol. 52, no. 11, pp. 2825-2832.

Crols, J., and Steyaert, M. S. J., 1998. “Low-IF topologies for high-performance analog front ends of fully integrated receivers”. *IEEE Trans. on Circuits and Systems II: Analog and Digital Signal Processing*, vol. 45, no. 3, pp. 269-282.

Dobkin, D. M., 2008. “The RF in RFID: Passive UHF RFID in Practice”. *Publisher Newnes (Elsevier)*, Oxford, UK. 2008.

Droitcour, A., Lubecke, V., Lin, J., and Boric-Lubecke, O., 2001. “A microwave radio for Doppler radar sensing of vital signs”. *2001 IEEE MTT-S International Microwave Symposium Digest*, Phoenix, AZ, USA, 20-25 May 2001, vol.1 pp. 175-178.

Droitcour, A., Boric-Lubecke, O., Lubecke, V. M., and Lin, J., 2002. “0.25 μm CMOS and BiCMOS single chip direct conversion Doppler radars for remote sensing of vital signs”. *IEEE ISSCC Digest of Technical Papers*, Feb, pp. 348-349.

Droitcour, A. D., Boric-Lubecke, O., Lubecke, V. M., Lin, J., and Kovacs, G. T. A., 2004. “Range correlation and I/Q performance benefits in single-chip silicon Doppler radars for noncontact Cardiopulmonary monitoring”. *IEEE Transactions on Microwave Theory and Techniques*, vol. 52 no. 3, pp. 838-848.

Droitcour, A. D., 2006. “Non contact measurement of heart and respiration rates with a single chip microwave Doppler radar”. *Department of Electrical Engineering, Stanford university*, California, USA, 2006.

Fatadin, I., Savory, S. J., and Ives, D., 2008. “Compensation of quadrature imbalance in an optical QPSK coherent receiver”. *Photonics Technology Letters, IEEE* , vol. 20, no. 20, pp. 1733-1735.

Fearnley, S. J., 1995. “Pulse Oximetry”. *in Update in Anaesthesia*, issue 5, article 2, World Federation of Anaesthesiologists, n.p.

Galil, 2012a. [online] Available at <http://www.galilmc.com/products/single-axis.php>. [Accessed November 26, 2012].

Galil, 2012b. [online] Available at <http://www.galilmc.com/products/galiltools.php>. [Accessed November 26, 2012].

Gao, X. M., Singh, A., Yavari, E., Lubecke, V. M., and Boric-Lubecke, O., 2012a. “Non-contact Displacement Estimation Using Doppler Radar”. *Engineering in Medicine and Biology Society, (EMBC 2012), Annual International Conference of the IEEE*, San Diego, CA, USA, Aug 28-Sept.1 2012, pp. 1602-1605.

Gao, X. M., Singh, A., Boric-Lubecke, O., and Lubecke, V., 2012b. “Small scale displacement measurement with passive harmonic RF tag using Doppler radar”. [Accepted] *IEEE International Wireless Symposium*, Beijing, China, 14 -18 April 2013, n.p.

Garg, R., Bhartia, P., Bahl, I., and Ittipiboon, A., 2001. “Microstrip antenna design handbook”. *Artech House, Inc.*, 685 Canton street, Norwood, MA, 02062, 2001.

Gianvittorio, J. P., and Rahmat-Samii, Y., 2002. “Fractal antennas: a novel antenna miniatureization technique and applications”. *IEEE Antennas and Propagation Magazine*, vol. 44, issue 1, 2002, pp. 20-36.

Gillespie, N. R., Higley, J. B., and MacKinnon, N., 1961. “*The evolution and application of coherent radar systems*”. IRE Transactions on Military Electronics, vol. Mil-5, no. 2, 1961, pp. 132-139.

Hafner, N., and Lubecke, V., 2009. “Performance assessment techniques for Doppler radar Physiological sensors”. 31st *Annual International conference of the IEEE EMBS*, Minneapolis, MN, USA, 2-6 Sept. 2009, USA.

Haykin, S., 1991. “Adaptive filter theory, second edition”. *Prentice hall*, Englewood Cliffs, NJ, 1991.

Heal, J. W., 1975. “An animal acitivty monitor using a microwave Doppler system”. *Medical Biological Engineering*, vol. 13, issue 2, p. 317.

Kamarudin, M. R., Nechayev, Y. I., and Hall, P. S., 2005 “Antennas for On-body communication systems.” *IEEE International Workshop on Antenna Technology: small antenna and novel metamaterials*, 7-9 March 2005, pp. 17-20.

Kiriazi, J., Nakamura, J., Hall K., and Lubecke, V., 2007. “Low profile Harmonic radar transponder for tracking small endangered species”. *Engineering in Medicine and Biology Society (EMBC 2007), 29th Annual International Conference of the IEEE*. Lyon, France, 22-26 Aug, 2007, pp. 2338 – 2341.

Li, C., Lin, J., 2007. “Non-Contact measurement of periodic movements by a 22-40GHz radar sensor using nonlinear phase modulation”. *IEEE MTT-S International Microwave Symposium Digest*, Honolulu, HI, USA, 3-8 June 2007, pp. 579-582.

Li, C., and Lin, J., 2008a. “Random body movement cancellation in Doppler radar vital sign detection”. *IEEE Transactions on Microwave Theory and Techniques*, vol. 56, no. 12, pp. 3143-3152.

Li, C., and Lin, J., 2008b. “Complex signal demodulation and random body movement cancellation techniques for non-contact vital sign detection”. *IEEE MTT-S International Microwave Symposium Digest*, Atlanta, GA, 15-20 June, pp. 567-570.

Lin, J. C., 1975. “Non-invasive microwave measurement of respiration”. *Proceedings of the IEEE*, vol. 63, issue 10, p. 1530.

Lin, J. C., 1992. “Microwave sensing of Physiological movement and volume change: A review”. *Bioelectromagnetics*, vol.13, pp. 557-565.

Linear Technology, 2012. [online] Available at <http://cds.linear.com/docs/Datasheet/6900fa.pdf>. Last accessed: November 26, 2012.

Lubecke, V. M., Boric-Lubecke, O., Host-Madsen, A., and Fathy, A. E., 2007. "Through the wall radar life detection and monitoring". *IEEE MTT-S International Microwave Symposium*, Honolulu, HI, USA, 3-8 June 2007, pp. 769-772.

Martin, P. H., and Unwin, D. M., 1980. "A microwave Doppler radar activity monitor". *Behavior Research Methods Instrumentation*, vol. 12, issue 5, pp. 517-520.

Madsen, S. N., and Skou, N., 1990. "Review of the homodyne technique for coherent radar". *IEEE Radar Conference*, Arlington, VA, USA, 7-10 May 1990, pp. 159-163.

Mascanzoni, D., and Wallin, H., 1986. "The harmonic radar: a new method of tracing insects in the field". *Ecological Entomology*, vol. 11, issue 4, pp. 387–390.

Massagram, W., Lubecke, V. M., Host-Madsten, A., and Boric-Lubecke, O., 2009. "Assessment of heart rate variability and respiratory sinus arrythmia via Doppler radar". *IEEE Transactions on Microwave Theory and Techniques*, vol. 57, no. 10, pp. 2542-2549.

Massagram, W., Lubecke, V. M., and Boric-Lubecke, O., 2009. "Microwave non-invasive sensing of respiratory tidal volume". *Engineering in Medicine and Biology Society 2009 (EMBC 2009), Annual International Conference of the IEEE*, Minneapolis, MN, USA, 3-6 Sept. 2009, pp. 4832 – 4835.

Massagram, W., 2008. "A study of feasibility in long term cardiopulmonary monitoring via Doppler radar". PhD dissertation, *Department of Electrical Engineering, University of Hawai'i at Mānoa*, Honolulu, USA, 2008.

Miller, M. R., *et al.*, 2005. "Standardization of spirometry". *European Respiratory Journal*, vol. 26, no. 2, pp. 319-338.

Mostafanezhad, I., Boric-Lubecke, O., Lubecke, V., and Host-Madsen, A., 2008. "Cancellation of Unwanted Motion in a Handheld Doppler Radar Used for Life Sign Monitoring". *IEEE MTT-S International Microwave Symposium Digest*, Atlanta, GA, USA, 15-20 June 2008, pp. 1171-1174.

Mostafanezhad, I., Boric-Lubecke, O., and Lubecke, V., 2010. "A low IF receiver architecture for Doppler radar motion detector". *IEEE Radio and Wireless Symposium*, New Orleans, LA, USA, 10-14 Jan 2010, pp. 571-574.

Nagy, K. A., Girard, I. A., and Brown, T. K., 1999. "Energetics of free-ranging mammals, reptiles, and birds". *Annual Review of Nutrition*, vol. 19, pp. 247-277.

U.S Navy, 1999. "Electronic Warfare and Radar Systems Engineering Handbook". *Naval air warfare center weapons division*, point mugu CA, USA. [online] Available at http://www.microwaves101.com/encyclopedia/navy_handbook.cfm. [Accessed Dec 4, 2012].

Occhiuzzi, C., Cippitelli, S., and Marrocco, G., 2010. "Modeling, design and experimentation of wearable RFID sensor tag". *IEEE Transactions on Antennas and Propagation*, vol. 58, no. 8, pp. 2490-2498.

Oppenheim, A. V., and Schafer, R. W., 2009. “Discrete-time signal processing”. *Third edition, Pearson Higher Education Inc.*, Upper Saddle river, NJ 07458, USA.

Palmer, J. E., 2012. “Evaluation of adaptive filter algorithms for clutter cancellation in passive bistatic radar”. *IEEE Radar Conference*, Atlanta, GA, USA, 7-11 May 2012, pp. 493-498.

Park, B.-K., S. Yamada, S., Boric-Lubecke, O., and Lubecke, V. M., 2006. “Single-channel receiver limitations in Doppler radar measurements of periodic motion”. *IEEE Radio and Wireless Symposium*, 17-19 Jan 2006, pp. 99-102.

Park, B. K., Boric Lubecke, O., and Lubecke, V., 2007. “Arctangent demodulation with dc offset compensation in quadrature Doppler radar receiver systems”. *IEEE Transactions on Microwave Theory and Techniques*, vol. 55, no. 5, pp. 1073-1079.

Park, B.-K., 2007. “Design and development of a Doppler radar system for robust cardiopulmonary monitoring”. PhD dissertation, *Department of Electrical Engineering, University of Hawai‘i at Mānoa*, Honolulu, Hawaii, 2007.

Park, B. K., Yamada, S., and Lubecke, V., 2007. “Measurement method for imbalance factors in direct-conversion quadrature radar systems”. *IEEE Microwave and Wireless Components Letters*, vol. 17, no. 5, pp. 403-405.

Pozar, D. M., 2005. “Microwave Engineering, Third edition”. *John Wiley and Sons, Inc.*, New York.

Proakis, J. G., and Manolakis, D. G., 1996. “Digital signal processing: principles, algorithms and applications, Third edition”. *Prentice-Hall Inc. (Pearson Education Inc.)*, Upper Saddle River, New Jersey 07458, U.S.A.

Psychoudakis, D., Moulder, W., Chen, C. –C., Zhu, H., and Volakis, J. L., 2008. “A Portable low-power harmonic radar system and conformal tag for insect tracking”. *IEEE Antennas and Wireless Propagation Letters*, vol. 7, pp. 444-447.

Rajagopalan, H., and Samii, Y. –R., 2010. “On-body RFID tag design for human monitoring applications”. *IEEE Antennas and Propagation Society International Symposium*, Toronto, ON, Canada, 11-17 July 2010, pp. 1-4.

Rao, K. V. S., Nikitin, P. V., and Lam, S. F., 2005. “Antenna Design for UHF RFID Tags: A Review and a Practical Application”. *IEEE Transactions on Antennas and Propagation*, vol. 53, no. 12, pp. 3870-3876.

Razavi, B., 1997. “Design consideration for direct-conversion receivers”. *IEEE Transactions on Circuits and Systems-II Analog and Digital Signal Processing*, vol. 44, no. 6, June 1997, pp. 428-435.

Razavi, B., 1998. “Architectures and circuits for RF CMOS receivers”. *IEEE Custom Iintegrated Circuits Conference*, Santa Clara, CA, USA, 11-14 May 1998, pp. 383- 400.

Riley, J. R., Smith, A. D., Reynolds, D. R., Edwards, A. S., Osborne, J. L., Williams, I. H., Carreck, N. L., and Poppy, G. M., 1996. "Tracking bees with harmonic radar". *Nature*, vol. 379, pp. 29-30.

Riley, J. R., and Smith, A.D., 2002. "Design considerations for an harmonic radar to investigate the flight of insects at low altitude". *Computers and Electronics in Agriculture*, vol. 35, issue 2-3, pp. 151-169.

Rudell, J. C., Ou, J. –J., Cho, T. B., Chien, G., Brianti, F., Weldon, J. A., and Gray, P. R., 1997. "A 1.9 GHz wide-band IF double conversion CMOS integrated receiver for cordless telephone applications". *ISSCC Digest of Technical Papers*, pp. 304–305.

Rykaczewski, P., Pienkowski, D., Circa, R., and Steinke, B., 2005. "Signal Path optimization in software-defined radio systems". *IEEE transactions on Microwave Theory and Techniques*, vol. 53, no. 3, pp. 1056-1064.

Safar, M. E., 2000, "Pulse pressure, arterial stiffness, and cardiovascular risk". *Current Opinion in Cardiology*, vol. 15, issue 4, pp. 258-263.

Safar, M. E., 2001. "Systolic blood pressure, Pulse pressure and arterial stiffness as cardiovascular risk factors". *Current opinion in Nephrology and Hypertension*, vol. 15, issue 4, pp. 257-261.

Samardzija, D., Boric-Lubecke, O., Host Madsen, A., V. M. Lubecke, Sizer, T., Droitcour, A. D., and Kovacs, G. T. A., 2005. "Applications of MIMO techniques to sensing of cardiopulmonary activity," *IEEE/ACES International Conference on Wireless Communications and Applied Computational Electromagnetics*, 3-7 April, 2005, pp. 618-621.

Samardzija, D., Park, B. -K., Boric-Lubecke, O., Lubecke, V. M., Host-Madsen, A., and Sizer, T., 2007. "Experimental evaluation of multiple antenna techniques for remote sensing of Physiological Motion". *IEEE MTT-S International Microwave Symposium*, Honolulu, HI, USA, 3-8 June 2007, pp. 1735-1738.

Sanad, M., 1994. "Effect of human body on microstrip antennas". *Antennas and Propagation Society International Symposium, AP-S Digest*, 20-24 June 1994, Seattle, WA, USA, vol.1, pp. 298-301.

Singh, A., and Lubecke, V., 2009. "Respiratory monitoring using a Doppler radar with passive harmonic tags to reduce interference from environmental clutter". *Engineering in Medicine and Biology Society 2009 (EMBC 2009), Annual International Conference of the IEEE*, Minneapolis, MN, USA, 3-6 Sept. 2009, pp. 3837-3840.

Singh, A., and Lubecke, V. M., 2010. "A heterodyne receiver for harmonic doppler radar cardiopulmonary monitoring with body-worn passive RF tags," *IEEE MTT-S International Microwave Symposium*, Anaheim, CA, USA, 23-28 May 2010, pp. 1600-1603.

Singh, A., and Lubecke, V., 2011. “Body-Worn passive planar harmonic tag design for use with Doppler radar”. *Biomedical Wireless Technologies, Networks, and Sensing Systems (BioWireleSS), 2011 IEEE Topical Conference on*, Phoenix, AZ, USA, 16-19 Jan 2011, pp. 51-54.

Singh, A., Lubecke, V. M., and Boric-Lubecke, O., 2011. “Pulse Pressure Monitoring Through Non-Contact Cardiac Motion Detection Using 2.45 GHz Microwave Doppler Radar”. *Engineering in Medicine and Biology Society 2011* (*EMBC 2011), Annual International Conference of the IEEE*, Boston, MA, USA, Aug 30-Sept.3 2011, pp. 4336-4339.

Singh, A., and Lubecke, V., 2012a. “Adaptive noise cancellation for two frequency radars using frequency doubling passive RF tags,” *IEEE MTT-S International Microwave Symposium*, Montreal, QC, Canada, 17-22 June 2012, pp. 1-3.

Singh, A., Lee, S. SK., Butler, M., and Lubecke, V., 2012b. “Activity monitoring and motion classification of the lizard *Chamaeleo jacksonii* using multiple doppler radars”. *Engineering in Medicine and Biology Society* (*EMBC 2012), Annual International Conference of the IEEE*, San Diego, CA, USA, Aug 28-Sept.1 2011, pp. 4525-4528.

Singh, A., and Lubecke, V., 2012c. “Respiratory monitoring and clutter rejection using a CW radar with passive RF tags”. *IEEE sensors*, vol. 12 issue: 3, pp. 558-565.

Singh, A., Gao X., Yavari, E., Zakrzewski, M., Lubecke, V., and Boric-Lubecke, O., 2012d. “Data based quadrature imbalance compensation for a CW Doppler radar system”. *IEEE Transactions in Microwave Theory and Techniques*, (submitted in 2012).

Singh, A., and Lubecke, V., 2012e. “Adaptive noise cancellation for two frequency radar using frequency doubling passive RF tags”. *IEEE Transactions in Microwave Theory and Techniques*, (submitted in 2012).

Skolnik, M. I., 2001. “An introduction to Radar”. *in Introduction to Radar Systems*, Third Edition, McGraw- Hill, New York, pp. 1-27.

Strang, G., 2003. “*Introduction to Linear Algebra* (3rd ed.)”. Boston, MA: Wellesley-Cambridge.

Stuchly, S. S., Smith, A., Goldberg, M., Thansandote, A., and Menard, A., 1980. “A microwave device for arterial wall motion analysis”. *Proc. 33rd Annual Conference Eng. Med. Biol.*, vol. 22, no. 47, 1980, pp. 22-57.

Svitek, R., and Raman, S., 2005. “DC offsets in direct-conversion receivers: characterization and implications”. *IEEE Microwave Magazine*, vol. 6, issue 3, pp. 76-86.

Umstattd, R., 1993. “Operating and evaluating quadrature modulators for personal communication systems”. *National Semiconductor Application Note 899*, n.p.

Valkama, M., Renfors, M., and Koivunen, V., 2001. “Advanced methods for I/Q imbalance compensation in communication receivers”. *IEEE Transactions on Signal Processing*, vol. 49, issue 10, pp. 2335-2344.

Vergara, A., and Lubecke, V. M., 2007. “Data acquisition system for Doppler radar vital-sign monitor”. *Engineering in Medicine and Biology Society (EMBC 2007), Annual International Conference of the IEEE*, France, Lyon, France, 22-26 Aug 2007, pp. 2269 - 2272.

Vergara, A., Petrochilos, N., Boric-Lubecke, O., Host-Madsen, A., and Lubecke, V., 2008. “Blind Source Separation using human body motion using Direct conversion Doppler radar”. *IEEE MTT-S International Microwave Symposium 2008*, Atlanta, GA, USA, 15-20 June 2008, pp. 1321-1324.

Want, R., 2006. “An introduction to RFID technology”. *IEEE Pervasive Computing*, vol. 5, issue 1, pp. 25-33.

Widrow, B., Glover, J. R., Jr., McCool, J. M., Kaunitz, J., Williams, C. S., Hearn, R. H., Zeidler, J. R., Eugene, D., Jr., and Goodlin, R. C., 1975. “Adaptive noise cancelling: principles and applications,” *Proceedings of the IEEE*, vol. 63, no. 12, pp. 1692-1716.

Wikelski, M., and Cooke, S. J., 2006. “Conservation Physiology”. *Trends in Ecology and Evolution*, vol. 21, pp. 38-46.

Wildemeersch, M., Petit, J., and Fortuny-Guasch, J., 2009. “Doppler radar and post processing techniques for small area surveillance”. *IEEE 10th Workshop on Signal Processing Advances in Wireless Communications*, Perugia, 21-24 June 2009, pp. 549-553.

World Health Organization, 2011. “ Factsheet No 317, September 2011”.[online] Available at <http://www.who.int/mediacentre/factsheets/fs317/en/index.html>. [Accessed December 6 2012].

Yan, Y., Li, C., and Lin, J., 2010. “Effects of I/Q mismatch on measurement of periodic movement using a Doppler radar sensor”. *IEEE Radio and Wireless Symposium 2010*, New Orleans, LA, 10-14 Jan 2010, pp. 196-199.

Yu, X., Li, C., and Lin, J., 2011. “Two-dimensional Noncontact Vital Sign Detection Using Doppler Radar Array Approach,” *Microwave Sysmposium digest (MTT), IEEE MTT-S International Microwave Symposium*, Baltimore, MD, USA, 5-10 June 2011, pp. 1-4.

Zakrzewski, M., Raittinen, H., and Vanhala, J., 2012. “Comparison of Center Estimation Algorithms for Heart and Respiration Monitoring with Microwave Doppler Radar”. *IEEE Sensors*, vol. 12, issue 3, pp. 627-634.

Zhou, Q., Liu, J., Host-Madsen, A., Boric-Lubecke, O., and Lubecke, V., 2006. “Detection of multiple heartbeats using doppler radar”. *IEEE International Conference on Acoustics, Speech and Signal Processing*, vol. II, Toulouse, 14-19 May 2006, pp. 1160-1163.